The Henryk Niewodniczański
INSTITUTE OF NUCLEAR PHYSICS
Polish Academy of Sciences
ul. Radzikowskiego 152, 31-342 Kraków, Poland

`www.ifj.edu.pl/publ/hab/`

Kraków, July, 2017

Commissioning, operations and monitoring of the large scale tracking system for the ATLAS experiment

Ewa Stanecka

Habilitation Thesis

This work was supported in part by the Polish Ministry of Science and Higher Education
under grant no DIR/WK/2016/13.

Wydrukowano nakładem Instytutu Fizyki Jądrowej
Polskiej Akademii Nauk
Kraków, 2017

Recenzent: Prof. dr hab. Michał Turała
ISBN 978-83-63542-80-1

I would like to dedicate this thesis to my loving parents.

Abstract

This monograph describes the control, operation and performance aspects of the ATLAS Inner Detector at the Large Hadron Collider at CERN. The Inner Detector is a large system with almost 90 million readout channels. It combines semiconductor devices (pixels and silicon strip) and straw gaseous detectors to measure trajectories of the charged particles emerging from proton-proton collisions and to reconstruct vertices of the interactions. A specialised Detector Control System designed to allow robust and safe operations of the Inner Detector is described. The details of the environmental management projects as well as the tools for monitoring of the radiation levels inside the Inner Detector volume and protection against beam induced accidents are given. The improvements done in the Inner Detector during the long technical stop at the LHC to prepare for proton bunches collisions every 25 ns, with the energy $\sqrt{s}$ =14 TeV and instantaneous luminosity $\sim 1 \times 10^{34} cm^{-2} s^{-1}$ are mentioned. Finally, the combined Inner Detector tracking performance at the beginning of the second season of data taking at LHC is presented.

Contents

Acronyms

ADC Analogue-to-Digital Converter. 26, 72, 73, 110

ALICE A Large Ion Collider Experiment. 2, 8

API Application User Interface. 24

ASIC Application-Specific Integrated Circuit. 14

ATLAS A Toroidal LHC ApparatuS. 2–13, 15, 17–20, 25–34, 37–41, 45–47, 49–52, 56, 57, 59, 63–65, 69, 71, 73, 76–79, 81–85, 87–89, 91–93, 95, 96, 101–103, 105, 106, 108, 110, 111

BCM Beam Conditions Monitor. 5, 46–49, 51, 57, 72–79, 103, 110

BE Back-End. 30

BIS Beam Interlock System. 75

BLM Beam Loss Monitor. 5, 46, 51, 57, 78, 79, 103

CAN Controller Area Network. 25–27, 57, 63, 64, 71, 91, 102

CERN European Organization for Nuclear Research. 1, 2, 6, 8, 20, 25–27, 90

CMS Compact Muon Solenoid. 2, 8

CSCs Cathode Strip Chambers. 17

CTP Central Trigger Processor. 19

CTRL Control Manager. 24

CU Control Unit. 27

D Driver Manager. 23

DAQ Data AcQuision system. 5, 20, 22, 30, 31, 73, 82, 90, 91, 111

DCS Detector Control System. 4–7, 18, 20, 22, 25–32, 44, 49, 56–64, 66, 67, 69–74, 76–80, 83, 84, 90, 93, 101–105, 108–110

DDC DAQ-DCS-Communication. 30

DIM Distributed Information Management System. 30

DIP Data Interchange Protocol. 32

DM Database Manager. 23, 24

DQM Data Quality Monitoring. 84

DQMF Data Quality Monitoring Framework. 83, 84

DSS Detector Safety System. 22, 64, 65, 74

DU Device Unit. 27

ECAL Electromagnetic Calorimeter. 16

EF Event Filter. 19

ELMB Embedded Local Monitor Board. 6, 25–27, 63, 64, 66, 68, 71, 72, 102, 104, 110

ELMB-DAC ELMB Digital-to-Analog Converter. 71, 73

EV Event Manager. 23

FE Front-End. 30, 57

FPGA Field-Programmable Gate Array. 50, 64, 67

FSM Finite State Machine. 27, 28, 31, 57, 59–63, 66, 68, 69, 73, 74, 76, 104, 109

GCS Global Control Station. 30

HCAL Hadronic Calorimeter. 16

HEX Heat Exchangers. 38

IBL Insertable B layer. 11–13, 45, 69, 70, 89, 92, 105, 108

ID Inner Detector. 2–6, 11, 13, 18, 33, 34, 36–38, 40–43, 45, 47, 51, 52, 54, 58, 59, 62, 63, 72, 73, 79, 92, 95, 98, 102–106, 109, 110

IDE Inner Detector Environment. 6, 56, 57, 59, 62, 75, 77–80, 103–105, 110

IDEP Inner Detector Endplate. 68

ITk Inner Tracker. 7, 106

JCOP Joint Controls Project. 22, 23, 25, 90, 102

LAr calorimeter Liquid Argon calorimeter. 16

LCS Local Control Station. 30, 56, 57

LHC Large Hadron Collider. 2–9, 11, 12, 14, 18, 20, 22, 24–26, 29, 32, 45, 46, 50, 52, 57, 75–79, 81, 82, 85–89, 94, 95, 101–106, 110, 111

LHCb LHC beauty experiment. 2, 8

LTS1 Long Technical Stop 1. 4, 23, 81, 89–92, 94, 95, 104, 105

LU Logical Unit. 27

LUCID LUminosity Cherenkov Integrating Detector. 47

LVL1 Level-1. 19, 50, 73

LVL2 Level-2. 19

MDTs Monitored Drift Tubes. 17

MS Muon Spectrometer. 10, 17, 18

NIEL Non-ionising energy loss. 51–53, 72, 103

NTC Negative Temperature Coefficient. 43, 54

OPC UA Object Linking and Embedding for Process Control Unified Architecture. 25, 26, 102

pCVD polycrystalline Chemical Vapour Deposition. 48, 51

PID Proportional-Integral-Derivative. 58, 64, 65, 104

Pixel Detector Pixel Detector. 11, 15

PLC Programmable Logic Controller. 25, 58–62, 104

PST Pixel Support Tube. 66, 68

PSU Power Supply Unit. 27, 71

PVSS Prozessvisualisierungs und Steuerungs System. 23

RADFET Radiation Field Effect Transistors. 52, 54

RADMON Radiation Monitor System. 5, 57

RBAC Role Based Access Control. 29

REM Radiation Experiments and Monitors. 52

RMSB Radiation Monitor Sensor Board. 52, 54

ROD ReadOut Driver. 73, 74, 76, 90, 91, 111

ROI Regions-of-Interest. 19

RPCs Resistive Plate Chambers. 17, 19

SCADA Supervisory Control And Data Acquisition. 23, 25

SCS Sub-detector Control Station. 30, 56, 57, 78

SCT Semiconductor Tracker. 5, 11, 14, 15, 33–38, 41, 42, 45, 51, 53, 56, 59, 60, 62, 63, 68–70, 73, 77–79, 84, 85, 89–96, 102–105, 108–111

SEU Single Event Upsets. 86

SMI++ State Machine Interface. 27, 28

SPI Serial Peripheral Interface. 26

SPS Super Proton Synchrotron. 75

TAS Target Absorber Secondaries. 46

TEH Thermal Enclosure Heaters. 66–68, 109

TGCs Thin Gap Chambers. 19

TID Total Ionising Dose. 51, 52, 72, 103

TOT Time-Over-Threshold. 50

TPG Thermal Pyrolytic Graphite. 14

TRT Transition Radiation Tracker. 11, 15, 33–37, 41, 53, 56, 68, 96, 102, 103, 105, 108

TTC Timing, Trigger and Command. 19, 30, 59

UDP User Datagram Protocol. 73

UI User Interface. 24

UPS Uninterruptible Power Supply. 58

WinCC OA SIMATIC WinCC Open Architecture. 23–25, 27, 30, 73, 102, 108

Chapter 1

Introduction

1.1 A word from the author

People often imagine a scientist as a person wearing a white coat and making discoveries in a secret laboratory. When J.J. Thompson discovered the first elementary particle of matter - the electron - in 1897, all the equipment he needed for his cathode ray tube experiment was vacuum tubes, magnets and wires.

Over a century a huge technological and scientific development has been done, and scientists have reached the frontiers in many disciplines of science. Contemporary particle physics (high energy physics) experiments hunting for new particles such as the Higgs boson use very complex and technologically advanced particle accelerators. The resources needed to perform these experiments exceed the capabilities of single laboratories or even countries. Thus “the traditional” way of doing science was replaced by collaborations among many contributing nations and academic groups. Typically, one of the collaborators acts as a host. The infrastructure of the experiments is built and run through the mutual decision of the members of a project on the host site. The research programme and technical design of experiments are also defined by the collaborators. The advantage of such an organisation is that the costs and risks are shared by many partners. The price is that the results are freely and equally available to all those who contribute.

A great example of a world-wide collaboration is the European Organization for Nuclear Research (CERN) laboratory and its flagship - Large Hadron Collider (LHC) [1], together with four experiments: A Toroidal LHC ApparatuS (ATLAS) [2], Compact Muon Solenoid (CMS) [3], A Large Ion Collider Experiment (ALICE) [4] and LHC beauty experiment (LHCb) [5].

I consider myself lucky to be part of such a big international cooperation for the ATLAS experiment, which unites over 3000 scientists, engineers and technicians from over 177 institutions and 38 countries. I joined the Inner Detector (ID) [6] group in the very exciting moment when all sub-components of the detector were being installed in their final destination - an underground cavern at CERN. After decades of design, development and tests on assembly sites in various laboratories, we put all the puzzles together to get combined physics measurements at the LHC.

1.2 The ATLAS Inner Detector as a large scale system

The ATLAS experiment is one of the largest and most complex particle collider experiments built so far. It has a cylindrical shape, is 46 m long and has 25 m in diameter, and is placed in a cavern 100 m below the ground. The ATLAS experiment weighs $\sim$ 7000 tonnes, has around 100 million electronic channels and 3000 km of cables [7]. The ID is the central part of the ATLAS experiment. Although it is only a small part of the total volume, over 80% of the ATLAS readout channels are located there. The Inner Detector expands to a large scale also in the sense of the amount of hardware modules, cables, lines of source code, volumes of data processed and stored, number of developers etc. Many challenges arise from the scale of the ID system:

- The ID development and operations have spanned over decades. It took around 20 years from the first experiment concept to first data taking with the Large Hadron Collider. Moreover, the experiment lifetime is planned for few decades, when it has to be fully operational and robust. Thus the development process must be conducted in a flexible way to be able to solve unpredicted problems and to adopt new technological solutions as they appear with time.

- The ID is a very complex detector comprising three tracking sub-systems developed in different technologies and requiring different (sometimes competing) operation conditions. These subsystems are independently managed and developed, but eventually they are integrated into a unified apparatus for physics studies.
- The ID evolves continuously while it is operating, with different capabilities being added and adjusted to new working conditions. The evolution of the LHC luminosity alone challenges the tracking systems, as they have to adjust constantly to harsher radiation working conditions.
- The ID is developed by a collaboration of multidisciplinary and multicultural teams (over 1000 participants in total). This aspect is not a direct concern of the present monograph. Nevertheless, it is worth mentioning that a large international collaboration requires appropriate work organisation and motivation methods based on a mutual understanding.

The unprecedented scale and complexity of the ATLAS Inner Detector places high demands on the control systems and services that are essential for the efficient and safe detector operation and physics data taking.

1.3 Aim and scope of the document

This document describes the commissioning, operations and performance of the large scale tracking detector in the ATLAS experiment. The emphasis is put on the aspects of the detector control. The ATLAS inner tracking system is designed to reconstruct charged particles tracks and interaction vertices produced in proton-proton collisions. The ID is composed of three independent detectors built in different technologies: two innermost detectors are semiconductor devices, while the outer part uses gaseous detection techniques. All the three systems were designed and developed by separate teams of scientists to provide complementary measurements of charged particle trajectories. Although these detector work in an autonomous way, they share a common environmental volume, and a certain amount of additional hardware and software is necessary to ensure their correct and safe operation.

In Chapter 2 a brief introduction to the ATLAS detector is given to provide a context for detailed descriptions of the ID controls, services and performance that follow in further Chapters.

Chapter 3 contains an extended discussion concerning the design and development of the ATLAS Detector Control System (DCS), which plays a vital role in the detector's operation and safety. The solutions implemented in the hardware and software layers of the DCS as well as strategies for the system development are presented.

Chapter 4 includes an overview of the hardware services installed inside the Inner Detector volume: temperature, humidity and pressure sensors for environmental monitoring, cooling system for semiconductor devices, radiation dose sensors, environmental gas monitoring, cooling system and beam condition monitoring. All these services have hardware and software control layers which ensure correct and safe equipment operations, described in detail in Chapter 5.

Chapter 6 describes aspects of operations, data taking and performance of the whole ATLAS Inner Detector. It covers two seasons of data taking at the LHC and a technical break for luminosity upgrade. The so-called Run-1, which started in 2010 and spanned over more than two years, delivered over 28 fb^{-1} of data. After that the LHC entered the phase of the Long Technical Stop 1 (LTS1) dedicated to upgrades necessary for increasing the beam energy from 8 TeV to 14 TeV and instantaneous luminosity to $\sim 1 \times 10^{34} cm^{-2} s^{-1}$. The Inner Detector subsystems took advantage of the LTS1 to prepare for higher luminosity and harsher radiation conditions during Run-2 of the LHC and to repair faults that had occurred so far. In March 2015 the LHC restarted operations and the Inner Detector was re-commissioned after its modernisation. Chapter 6 mentions the most important consolidation works carried out during LTS1.

1.4 Statement on author's contribution

It must be clearly stated that the work presented in this monograph has been carried out with efforts of many people involved in the ATLAS and Inner Detector collaborations. However, I have made key contributions into a few experiment aspects described here. The main areas of my activities were: Detector Control System for the ATLAS Inner Detector, the ID commissioning and operations with beams at the LHC and preparation of the new ATLAS tracker for the planned LHC upgrades.

I joined the Inner Detector group during the last phase of the detector installation and commissioning to work on the Inner Detector project. In the years 2008-2010 I was primarily involved in the subjects related to monitoring of the beam quality and radiation levels inside the ID volume. I coordinated the team working on the design and development of the control systems for the Beam Conditions Monitor (BCM), Beam Loss Monitor (BLM) and Radiation Monitor System (RADMON). My contribution, also as a developer and an expert, includes design and development of the core part of the BCM detector control project, the control hierarchy and expert functions for configuring the BCM readout electronics from the DCS level. I consulted the implementation of readout firmware for the radiation monitor project. The above-mentioned control systems have been deployed into the ATLAS experiment infrastructure and have been serving the collaboration since the detector commissioning through data taking. As a member of the ID and BCM sub-detector teams, I participated in the BCM detector fine tuning with cosmic rays and with the first LHC beams [8] and in the ID commissioning [9]. Solving the detector issues that appeared during data taking at the LHC was my daily routine when I served as a BCM/BLM/RADMON DCS and Data AcQuision system (DAQ) on-call expert.

Between 2008-2014 I was also appointed as a Semiconductor Tracker (SCT) detector control system and operations expert. Thanks to the efforts of the operations team I belonged to at that time, the SCT's performance during data taking was excellent [10].

First experiences with the whole Inner Detector installed in the ATLAS cavern showed the need for major improvements of the heater pad system, which ensures a thermal barrier between the components of the ID described in Chapter 4. I joined the task force formed to address the safety issues in the existing control heater pad system. As a result of our efforts, a new hardware and software control system was developed and produced. I was the author of the control firmware, based on the Embedded Local Monitor Board (ELMB) board, for the custom-made hardware cards in this system [11]. I was also responsible for preparing a review process for the new heater pad control system within the collaboration [12]. This new heater pad control system was installed under my supervision in the experiment during the first long LHC technical stop (2013-2015), and has been fulfiling its tasks since then.

In autumn 2010 I started a three-year break in my professional career due to family reasons. I returned to the Inner Detector group in 2013 when the LHC was entering a two-year long technical stop. The collaboration appointed me as the coordinator of the Inner Detector Environment (IDE) DCS, covering aspects of combined operations of the whole ID and its services described in Chapters 4 and 5 of this monograph. I joined the Inner Detector technical coordination team, responsible for planning interventions and upgrades to be done during the technical stop. One of my tasks during the long technical stop was to conduct the migration campaign of the ID DCS to new hardware and software standards. It is worth mentioning that all the control systems described in this monograph have been installed in the experiment and have been efficiently working to ensure the ID safety and its healthy operations. The systems are used on a daily basis by the ATLAS operation team and experts.

After the technical stop I helped with the ID re-commissioning for operations at the LHC. The detector's performance proved to be excellent; it ensured correct data quality suitable for physics analysis from the very first collisions after the LHC beams restart [13]. I was delegated to present the Inner Detector performance and data taking topics at international conferences [14]. My work to keep the detector in the best possible condition for measurement of the charged particle tracks for physics analysis was recognised by the ATLAS collaboration, and I was assigned to give overview talks on Standard Model physics measurements at international conferences [15]. In 2015 the ATLAS Outstanding Achievement Award was presented to me for my contribution to the Inner Detector control systems [16].

As a member of the ATLAS DCS team I had a substantial influence on the strategy for the common tools development. I represented the ATLAS experiment at the CERN wide workshop [17], which aimed at defining the mid- and long-term plans for the Joint Controls Project in view of the future ATLAS and LHC upgrades. My role was to collect and present feedback and requests for the future developments and strategy for the control system from the whole ATLAS DCS collaboration.

Owing to my hands-on detector experience I gained during the preparation and operations of the current experiment, in 2015 the ATLAS Collaboration invited me to join the ATLAS Upgrade project. In the ATLAS Upgrade I am involved in the preparation of the new Inner Tracker (ITk) designed for operation at the Super LHC. I was a "chaser" and co-editor of one chapter of the ITk Technical Design Report [18]. As a "chaser" I was responsible for collecting and providing material for a particular topic, which required interactions with several working groups to conclude on findings of the on-going studies. Currently I am a member of an expert panel for designing and installation of new services for ITk.

Chapter 2

The Large Hadron Collider and the ATLAS experiment

2.1 The Large Hadron Collider

The Large Hadron Collider [1] together with the accelerator complex at CERN is the most powerful currently functioning particle accelerator in the world. The LHC consists of thousands of superconducting magnet elements, connected together to form a 27-kilometre-long ring in an underground tunnel. Inside the superconducting ring, two beams of hadrons (protons p or lead ions Pb) are accelerated in opposite directions in two separate pipes with high vacuum. When the hadrons reach the required energy, the beams are bent to collide in four points around the ring where the particle detectors, ATLAS, CMS, ALICE and LHCb, are placed.

The LHC is designed to make 40 million collisions of hadron bunches per second (one bunch contains $\sim 10^{11}$ of protons), with the energy in the interaction point of $\sqrt{s}$ =14 TeV. The design luminosity is $\sim 5-7\times 10^{34} cm^{-2}s^{-1}$. Reaching the nominal parameters of the LHC is a huge technological and logistic challenge, thus it was divided into several stages. In the first data taking period of the LHC (Run-1: from 2010 to 2013), the maximal luminosity measured by the ATLAS experiment was $\sim 8\times 10^{33} cm^{-2}s^{-1}$, with the bunch crossing every 50 ns and the energy of proton-proton (pp) collisions of $\sqrt{s}$ =7 TeV and 8 TeV. The first two-year long technical shut-down, during which the LHC underwent several upgrades to increase the instantaneous luminosity and beam energy, started in spring 2013. The LHC was restarted in May 2015 and the second season of the data taking, Run-2, commenced. In Run-2 the proton bunches are collided every 25 ns, with the centre of mass energy $\sqrt{s}$ =13 TeV. In the course of the run, the energy in the interaction point is expected to reach the nominal value of 14 TeV and the instantaneous luminosity $\sim 1 \times 10^{34} cm^{-2}s^{-1}$.

There are two more upgrades of the LHC foreseen to increase the instantaneous luminosity to $\sim 2 \times 10^{34} cm^{-2}s^{-1}$ and $\sim 5 - 7 \times 10^{34} cm^{-2}s^{-1}$. The operational roadmap of the LHC is summarised in Figure 2.1.

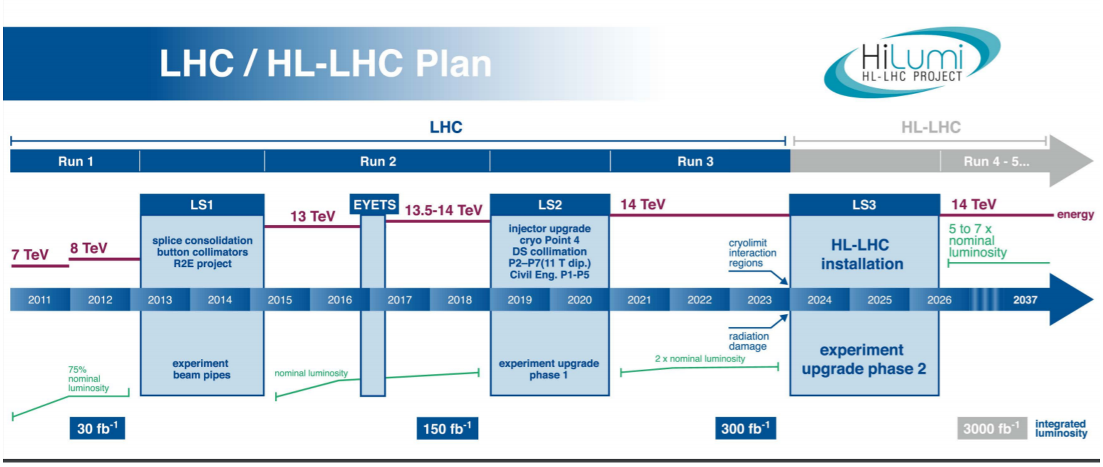

Figure 2.1: The Large Hadron Collider operations plans [19].

At the end of each year of data taking, just before winter technical breaks, the accelerator is tuned to make $PbPb$ collisions. The energy of the heavy ion beams is lower than that of the proton beams. So far, lead nuclei have been collided with the energies of $\sqrt{s}$ =2.76 TeV and $\sqrt{s}$ =5.02 TeV, per nucleon.

2.2 The ATLAS experiment

2.2.1 Introduction

ATLAS is a general purpose experiment built to explore physics phenomena created in pp and $PbPb$ collisions at the LHC. The research scope of the ATLAS experiment is very large, from precision measurements of the Standard Model, Higgs boson, through searches for supersymmetry, new and exotic physics, to the quark-gluon plasma probing.

ATLAS has a layout typical of contemporary particle physics detectors, as shown in Figure 2.2. It consists of several different subsystems organised in layers around the interaction point to provide nearly full coverage in a solid angle. The closest to collision point is the Inner Detector. It provides precise measurements of the tracks of charged particles created in collisions and vertex reconstruction. The next layers are dedicated to particle energy measurement, and these are Electromagnetic and Hadron Calorimeters. The Muon Spectrometer (MS) with its extremely large toroidal magnets is placed outside the calorimeters. All the sub-detectors are described in more detail in Sections 2.2.3.1 - 2.2.5.

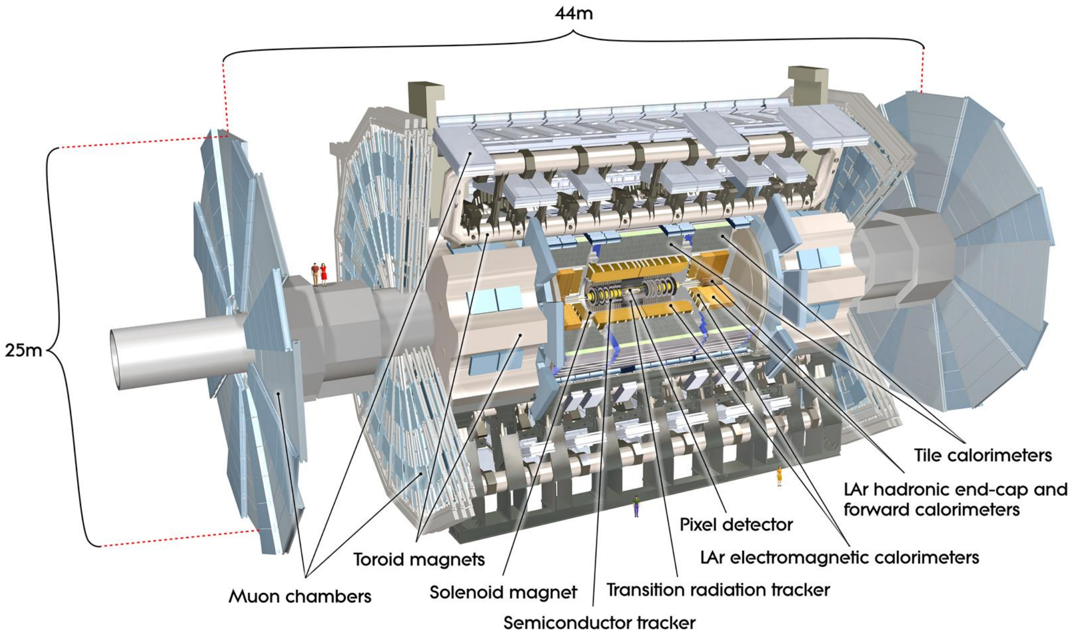

Figure 2.2: Schematic view of the ATLAS detector and its subsystems. Taken from [20].

2.2.2 ATLAS coordinate system and conventions

The right-handed coordinate system with the origin located in the point of interactions of two beams is conventionally used in ATLAS. The x-axis points to the centre of the LHC ring, the y-axis is perpendicular to the LHC plane and points up, and the z-axis is nearly collinear to the beam line. The half of the detector having the positive z coordinate is often refereed to as "side A", and the other side is called "side C". The polar angle θ is measured w.r.t. the positive z-axis and $\theta \in [0, \pi]$. The azimuthal angle ϕ is measured in the $(x - y)$ plane, so that the positive x-axis has an azimuthal angle of $\phi = 0$, and the positive y-axis - an angle of $\phi = \pi/2$, $\phi \in [-\pi, \pi]$. The azimuthal and polar angles can be expressed using the momentum components p_x, p_y, p_z:

$$\tan\phi = p_y/p_x \quad \cot\theta = p_z/p_T \tag{2.1}$$

where $p_T = \sqrt{p_x^2 + p_y^2}$ is the transverse momentum with respect to the beam axis.

The pseudorapidity $\eta = -\log\tan\theta/2$ is often used to describe the angle of the particle momentum with respect to the beam axis for calculation convenience. The differences in η are Lorentz invariant under boosts along the longitudinal axis: they transform additively.

2.2.3 The ATLAS inner tracking system

The task of the ID is to reconstruct the charged particle trajectories and vertices in an event with high efficiency, contributing together with the calorimeter and muon systems to the electron, photon and muon recognition, and supplying an important extra signature for short-lived particle decay vertices [21].

The ATLAS tracking system, the ID, is enclosed in a cylindrical thermal enclosure of a length of ± 3.4 m and a radius of 1.15 m. It is immersed in a magnetic field of 2 T produced by a superconducting solenoid magnet. The ID is composed of three separate and independent sub-detectors built using different technologies. The closest to the interaction point are high precision semiconductor instruments - the Insertable B layer (IBL), the Pixel Detector and the SCT. The

Table 2.1: Basic parameters of the ID subsystems; for the spacial resolution average values are given, as it varies with η.

Detector	Resolution $r - \phi \times Z[\mu m]$	№ Channels	Coverage in η
IBL	10×75	6.02 mln	$\|\eta\| < 2.9$
Pixel	10×115	80.4 mln	$\|\eta\| < 2.5$
SCT	17×580	6 mln	$\|\eta\| < 2.5$
TRT	130	400 000	$\|\eta\| < 2.0$

outermost system in the ID is the Transition Radiation Tracker (TRT) - a gaseous straw detector. Mechanically, all the ID subsystems consist of three structures: a central barrel part and two end-caps. The cross section of the Inner Detector is shown in Figure 2.3, and its basic parameters are listed in Table 2.1. The Inner Detector provides:

- tracking at the LHC luminosity over 5 units in pseudorapidity $|\eta| \leqslant 2.5$,
- precise reconstruction of the primary and secondary vertices,
- excellent b-tagging in jets,
- contribution to identification of electron, muon, tau, b and c hadrons.

2.2.3.1 The Pixel Detector and the Insertable B-layer

The Pixel Detector [23] is the closest to the pp interaction point and has the finest granularity, thus it has the biggest impact on the overall precision of charged particle track and vertex reconstruction. During Run-1, the Pixel Detector was composed of 1744 silicon pixel modules assembled on three barrel layers, and of two end-caps, each with three disks. The average radii of the three Pixel barrels from the beam line are 50.5, 88 and 120 mm. The end-caps are located within $495 < |z| < 650$ mm. All the modules of the Pixel Detector are alike. A single module consists of a pixel sensor bump bonded to 16 front-end chips and glued to the so-called flex hybrid, providing signal routing and electrical connection of the module. The ATLAS Pixel sensor has an active area of 16.4×60.8 mm^2, containing the matrix of pixels organised in 144 columns and 328 rows. Most of the pixels have a size of 50×400 μm^2, which allows them to achieve the intrinsic

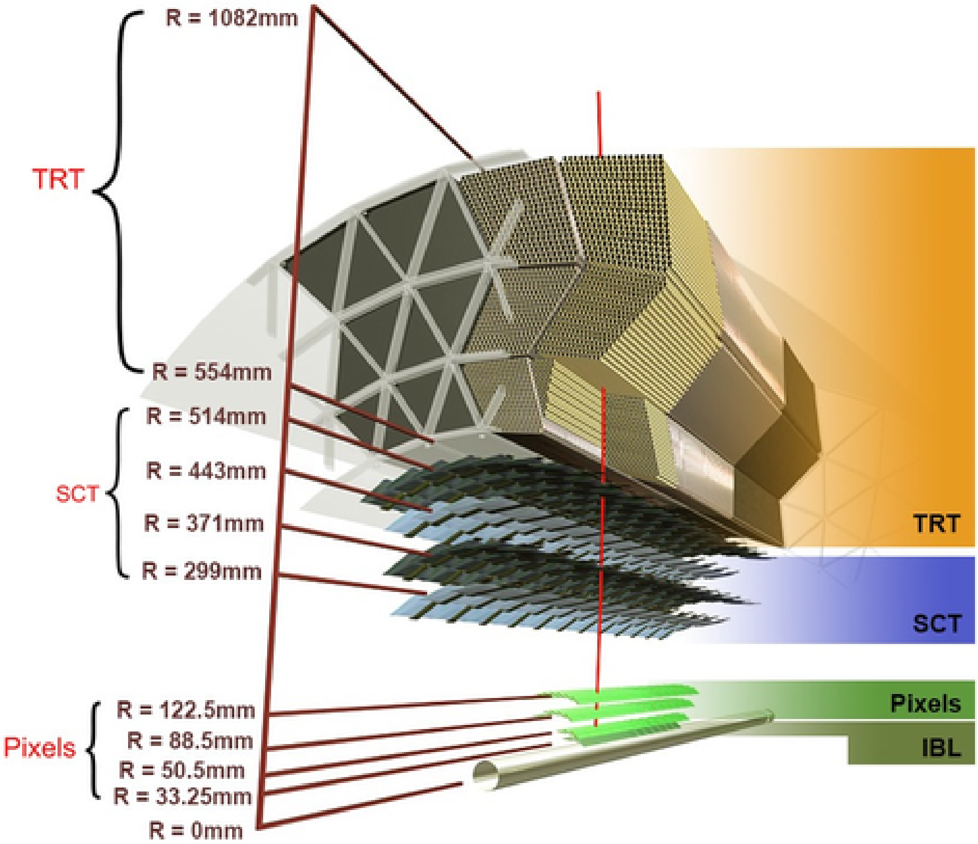

Figure 2.3: Sketch of the ATLAS inner detector showing all its components, including the new IBL. The distances to the interaction point are also shown. Taken from [22].

spacial resolution of 10 μm in $r-\phi$ and 115 μm in z. The performance of the innermost layer of the Pixel Detector is critical for fulfilling the physics analysis requirements for tracking and vertexing. At the same time, this layer suffers from radiation damage effects and inefficiencies especially at high luminosity. To improve the precision of vertexing and tracking and to maintain robust tracking despite the effects arising from luminosity and radiation, the fourth layer of pixel detectors, the IBL, was installed in May 2014 between the existing Pixel Detector and a new smaller radius beam-pipe [24]. The IBL was designed to withstand a high luminosity environment, and it consists of 14 supporting structures - staves mounted around a beryllium beam pipe at a radius of $r = 33.25$ mm from the nominal beam line. Each stave includes 20 modules built in two different technologies. The central part of the stave is populated with 12 planar pixel sensors of the $n^+ - in - n$ type. On each stave side there are four 3D pixel sensors. Each pixel has a size of 50 × 250 μm^2. The intrinsic spacial resolution of the IBL readout is 10 μm in $r - \phi$ and 75 μm in z, respectively.

2.2.3.2 The Semiconductor Tracker

The SCT [25] is a silicon strip detector designed to operate at LHC luminosities and to withstand the fluence up to $\approx 2 \times 10^{14} n_{eq} cm^{-2}$. It is placed after the Pixel Detector and is composed of four coaxial barrels and two end-caps, each containing nine disks. The basic building block of the SCT detector is a module. There are four different shapes of the SCT modules. The barrel part of the SCT is populated with identical rectangular modules, while three different wedge shapes are necessary to cover the end-cap disk geometry. Each of the 2112 SCT barrel modules consists of two layers of 80 μm pitch rectangular micro-strip sensors glued back-to-back onto a stiff, high thermal conductivity baseboard made of the Thermal Pyrolytic Graphite (TPG). The two sensors are rotated with respect to their geometrical centre with a stereo angle of ±20 mrad, to provide required space-point resolution in $r - \phi$ and r. The end-cap modules are designed according to the same principle as the barrel ones. Each of the 1976 end-cap modules has two sets of sensors glued back-to-back around the central TPG spine with a relative rotation of ±20 mrad. The trapezoidal end-cap sensors have radial strips of constant azimuth with a mean pitch of ~80 μm. Each module is equipped with read-out electronics mounted on a wrap-around hybrid. The readout hybrid houses 12 identical 128-channel Application-Specific Integrated Circuit (ASIC) [26] to provide binary readout of 1536 sensor strips per module. The barrel and end-cap sensors are specified to operate at -7^{o}C to reduce the bulk leakage current after radiation damage. However, the SCT modules dissipate a significant amount of power to which contribute the readout chips power $5.5 - 7.5$ W, the sensor load reaching $\sim$ 1W per module after ten years of operation and convective loads of $\sim$ 0.8W per module in the case of elements placed at the top of the barrel cylinders and disks. The heat is extracted by evaporating C_3F_8 at ~-25^{o}C, which circulates in the cooling pipes attached to each module. The SCT provides up to eight space points measurements per charged particle trajectory and a spacial measurement resolution of 16 μm in $r - \phi$, providing excellent tracking up to a radius of 51.4 cm.

2.2.3.3 Transition Radiation Tracker

The TRT [27] is the outermost part of the ATLAS tracker. The TRT is built of thousands of straw gaseous detectors - proportional cylindrical counters with a diameter of 0.4 cm and up to 144 centimetres long. There are about 50000 straws in the barrel mounted in parallel to the beam axis (in the z direction) and 320000 straws in the end-cap regions that run in the r direction (perpendicular to the beam), forming a fan-like structure. The straw wall made of Kapton 70 μm thick constitutes cathodes, and gold-plated tungsten wires running at the centre of each straw are anodes. The straws are filled with a 70/27/3 % $Xe/CO_2/O_2$ gas mixture, with Xenon chosen to absorb the transition radiation (TR). 370,000 TRT straws in total provide typically 36 space points per track. The average uncertainty of the track position measurement $\sigma_{r-\phi}$ for a single straw is 140 μm. However, for higher luminosities and occupancies the resolution diminishes to $\sim$ 250 μm. This resolution is not as precise as the resolutions of the Pixel and SCT detectors, but it was necessary to reduce the cost of covering a larger volume and was required to achieve the transition radiation detection capability for particle identification. The space between the TRT straw layers is filled with stacks of polyethylene fibers (barrel) and foils (end-caps) with different indices of refraction. When a charged ultra-relativistic particle traverses those detector areas, the transition radiation is emitted. The emitted photons, typically within soft X-ray spectrum and collinear to the particle direction, are absorbed in Xenon and much stronger signals in some straws are detected. The intensity of the transition radiation is linearly proportional to the passing particle Lorentz factor, γ. This allows for discrimination between a lighter particle, e.g. an electron which has a large γ, and a heavier particle, such as a hadron (which has a low γ and radiates much less) [28].

2.2.4 Calorimetry

The ATLAS calorimetry system forms a nearly hermetically closed structure. Its purpose is to measure the particle and jet energies as well as to estimate the missing energy. It is situated outside the solenoidal magnet that surrounds the Inner Detector and covers the region up to $|\eta| < 4.9$. The calorimetry system is subdivided into the Electromagnetic Calorimeter (ECAL) [29] and the Hadronic Calorimeter (HCAL) [30]. Both are sampling calorimeters, built of layers of two alternating materials - an absorber and sensing elements. The particles traversing the calorimeter lose the energy by the formation of the electromagnetic or hadronic cascades (particle showers) in the absorber material. The sensing elements are periodically sampling the shape of the resulting particle shower, from which the energy of the original particle is derived.

The relative energy resolution of the calorimetric devices is typically parametrised from experimental measurements, and is given by the formula:

$$\frac{\sigma(E)}{E} = \frac{a}{\sqrt{E}} \oplus b \tag{2.2}$$

where a is the stochastic term and b is the constant term. The constant term represents the instrumental effects causing non-uniformities of the calorimeter response.

2.2.4.1 Electromagnetic Calorimeter

The ECAL uses liquid argon as an ionization medium with lead absorbers organised in an accordion-shaped geometry and is often referred to as the Liquid Argon calorimeter (LAr calorimeter). The LAr calorimeter is further divided into a barrel part covering $|\eta| < 1.475$ and two end-caps that cover $(1.375 < |\eta| < 3.2)$. The segmentation of the calorimeter depends on the detector region. The rapidity segmentation $\triangle\eta$ varies from 0.003 to 0.1, while the azimuthal segmentation $\triangle\phi$ varies from 0.025 to 0.1. The total thickness of the LAr calorimeter exceeds 24 radiation lengths in the barrel region, and 26 radiation lengths in the end-caps. The LAr calorimeter energy resolution is $\frac{\sigma(E)}{E} = \frac{10\%}{\sqrt{E}} \oplus 2\%$.

2.2.4.2 Hadron Calorimeter

The hadron calorimetry system is placed behind the electromagnetic calorimeter and is composed of the Tile Calorimeter, the liquid-argon Hadronic End-cap Calorimeters and the liquid-argon Forward Calorimeter. It absorbs the energy from the hadrons that pass through the Electromagnetic Calorimeter. The tree hadronic calorimetry subsystems cover different pseudorapidity regions, thus they use different techniques and have been adapted to radiation environments.

The Tile Calorimeter is made of modules with alternating tiles of steel and scintillating material. It covers the pseudorapidity range of η <1.7. The radial depth of the tile calorimeter is $\sim$ 7.4 radiation lengths. In the regions of higher pseudorapidity, $1.5 < |\eta| < 3.2$, the liquid-argon end-cap calorimeter is located. It consists of two wheels in each end-cap and is a copper/liquid-argon device. In the very forward region, $3 < |\eta| <4.9$, a dedicated Forward Calorimeter is installed to provide a wide coverage required for a good missing energy estimation. The Forward Calorimeter is installed 4.5 m from the interaction point and it can perform both electromagnetic and hadronic measurements. The forward calorimeter consists of three parts in each end-cap: the first part has copper (to measure electromagnetic interactions), while the two other parts have tungsten as the absorber material.

The Hadronic Calorimeters cover about 10 interaction lengths in order to ensure a good resolution for high-energy jets.

2.2.5 Muon Spectrometer

The MS [31] is a high precision stand-alone tracking system and the outermost part of the ATLAS detector. It detects charged particles (muons) exiting the calorimeters and measures their momentum in pseudorapidity range $|\eta| < 2.4$, with a transverse momentum resolution of approximately 10% for 1 TeV tracks.

For precision measurements within $|\eta| <2$, the MS uses pressurised drift tubes with a diameter of 30 mm, operating with a gas mixture containing 93 % of Argon and 7 % of carbon dioxide at 3 bar, called the Monitored Drift Tubes (MDTs). At the pseudorapidity range from 2 to 2.7 the drift tubes are replaced with the Cathode Strip Chambers (CSCs) that have a finer granularity and better

Table 2.2: Parameters of the four sub-systems of the muon detector. The quoted spatial resolution (columns 3, 4) does not include chamber alignment uncertainties. Column 5 lists the intrinsic time resolution of each chamber type, to which contributions from signal-propagation and electronics contributions need to be added [2]

		Resolution RMS in			Measure/track		№
Type	Function	z/R	ϕ	time	barrel	end-cap	Channels
MDT	tracking	35 μm(z)	-	-	20	20	354k
CSC	tracking	40 μm(R)	5 mm	7 ns	-	4	30.7k
RPC	trigger	10 mm(z)	10 mm	1.5 ns	6	-	373k
TGC	trigger	2-6 mm (R)	3-7 mm	4 ns	-	9	318k

time resolution to cope with high track rates near the beam pipe. Two trigger chamber technologies are used to provide input to the first level trigger logic. The Resistive Plate Chambers (RPCs) and the Thin Gap Chambers (TGCs) provide discrimination on muon transverse momentum in the barrel and end-cap regions.

With its huge toroidal structures - a large barrel toroid and two end-cap toroids - the MS system is the most noticeable part of the ATLAS detector. The air-core toroids generate a magnetic field extending in an area 26 metres long and 20 metres in diameter. This magnetic field is not uniform: the peak field on the toroid coils is about 4 T providing from 2 to 8 Teslameters of bending power.

The combination of all the subsystems of the MS allows momentum measurements to be performed with a precision ranging from 2-3 % for muons between 10 GeV and 200 GeV, and $\sim$ 10 % for 1 TeV muons, exceeding the achieved momentum resolution for high energetic muons in the ID. Table 2.2 summarises the basic parameters of all the subsystems of the Muon Spectrometer.

2.3 Detector Control System

The supervision of the detector hardware (gas systems, power-supply voltages, etc.) is provided by the DCS, which is described in more detail in Chapters 3 and 4.

2.4 Trigger, Data Acquisition and Software Processing

Storing the data from all the pp collisions in the ATLAS detector is technologically impossible and also impractical. If we take the anticipated raw data of the size of about 1.5 Megabyte per event, the 40 MHz recording rate would correspond to writing of 60 terabyte of data per second. However, most events will not reveal any new physics. Most of the events at the LHC are due to inelastic proton-proton interactions with a cross section of 70 mb, whereas the cross sections for the processes ATLAS is hunting for are lower by several orders of magnitude. For example, the cross sections of typical Higgs discovery channels are in the order of 0.1 pb, that is 700 million times less likely than inelastic pp interactions. Therefore, ATLAS uses a complex trigger and data acquisition system to select interesting events and to reduce the event rate from the bunch crossing rate of 40 MHz to around 200 Hz for recording onto mass storage.

2.4.1 Trigger

The ATLAS trigger system [32] consists of three levels:

- Level-1 (LVL1) - a synchronous system of dedicated hardware searching for signatures from high-p_T muons, electron/photons, jets, and τ-leptons decaying into hadrons. It uses the reduced-granularity information from the RPCs and TGCs for high-p_T muons, and all the calorimeter sub-systems for electromagnetic clusters, jets, τ-leptons, E_T^{miss} and large total transverse energy [2]. The LVL1 decision is made by the Central Trigger Processor (CTP) and is distributed to all the detectors in ATLAS at a maximum rate of 100 kHz by the Timing, Trigger and Command (TTC) system. This decision must reach the front-end electronics within 2.5 μs after the bunch-crossing with which it is associated.
- Level-2 (LVL2) - an asynchronous system using programmable processors, analysing data from Regions-of-Interest (ROI). ROI are the regions of the detector where the LVL1 trigger has identified possible trigger objects within

the event. The LVL2 has access to full granularity information and to the tracking systems information and uses custom algorithms optimized for timing performance with an average processing time of 40 ms. The LVL2 trigger reduces the event rate to < 3.5 kHz.

- Event Filter (EF) - uses the off-line analysis procedures on fully-built events to further select events to achieve the rate which can be recorded for subsequent off-line analysis. It reduces the event rate to approximately 200 Hz, with an average event processing time of the order of four seconds [2].

After the final selection with a latency up to many seconds, the entire event data is written to mass storage and the event is available for further physics analysis. The control of the data movement along the trigger chain up to the data storage is performed by the DAQ [32].

2.4.2 Off-line Event Processing

ATHENA [33], a modular software framework, is dedicated to the off-line data analysis. Its main tasks are to reconstruct and analyse data from the ATLAS detector and to simulate the samples of data for the background physics studies and the detector performance validation. For the reconstruction and simulation a lot of information is needed beyond what is provided as the detector response. A detailed detector description, hardware conditions and configurations, the configuration of the beams and the magnets are necessary for correct translation from the signals registered by sub-detectors into properties of the physical particle. These detector condition parameters are archived in the DCS condition database, which is linked to the ATHENA framework. The amount of data recorded by the experiments at the LHC are about 30 petabytes per year in total. It would be impossible to provide one central computing facility with sufficient computing power and disk storage to all members and collaborating institutes. The World-wide LHC Computing Grid [34] connects more than 170 computing centres in 40 countries to provide the resources needed for storing and analysing the LHC data. The Grid computing is a hierarchical system that consists of four levels, the so-called “Tiers”:

- Tier-0 located at CERN: it keeps the first copy of the raw data and performs the first pass reconstruction;
- Tier-1 runs in 13 centres with sufficient storage capacity to perform the reprocessing of the data and to provide the storage of raw, reconstructed, and simulated data;
- Tier-2 is formed by around 160 regional computing facilities at universities and scientific institutes around the world. They provide storage for data as well as the computing power for specific physics analysis and simulation tasks.
- Tier-3 is composed of local sites that focus on end-user analysis.

Chapter 3

The Detector Control System

3.1 The ATLAS Detector Control System

In order to operate the detector, two systems are required: the Detector Control System and the Trigger and Data Acquisition System. The ATLAS DCS [35; 36; 37] ensures coherent operation of the experiment and provides a homogeneous interface to all sub-components and to the technical infrastructure of the experiment. It must switch the detector between any requested operational states, continuously monitor, archive and analyse the operation parameters, signal suspicious behaviour. The DCS also forms an important part of the safety systems. Together with the interlocks and the Detector Safety System (DSS) [38], it protects the detector equipment over the experiment lifetime.

While the DCS does not have to respond in a bunch crossing time scale (here 25 ns) as the DAQ, it has to operate in a timely fashion and, what is most important, it must be functional at any time. The DCS is required to function not only during data taking, but also during the technical stops to ensure the detector's health and safety. The failure of the DCS could be disastrous for the detector equipment.

The control system is expected to serve the experiment for decades - from the phase of its installation up to the end of its lifetime. Thus an appropriate strategy for the system techniques and development is needed. Early on, during the development of the control systems, a group of representatives from the four big LHC experiments formed a common task force, the Joint Controls Project (JCOP) [39], which aims at finding common solutions to reduce the overall manpower cost required to build and run the experiment control systems and to ensure the uniformity and expertise for the whole experiment lifetime. After the evaluation of available products (commercial or open source), the JCOP decided to use an industrial product Prozessvisualisierungs und Steuerungs System (PVSS)[1], which later during LTS1 evolved into the SIMATIC WinCC Open Architecture (WinCC OA) supervisory control software toolkit [40] owned by SIEMENS AG. The WinCC OA is a Supervisory Control And Data Acquisition (SCADA) framework. It was chosen for its scalability and flexibility in architecture. These characteristics are particularly important for the high energy physics experiment control systems which differ from the industrial ones. Typically, they have many channels and use a variety of custom and industrial hardware and software solutions for the special needs of the detector equipment. The industrial systems are typically less complicated and more homogeneous. It should be noted that the WinCC OA is not a control system by itself, but a SCADA tool to build control systems.

3.1.1 Common hardware and software solutions

3.1.1.1 WinCC OA architecture

The WinCC OA is a system for visualizing and operating processes, production flows, machines and plants in all lines of business [40]. It has a highly distributed architecture, composed of several processes, called *Managers*, and is organised into layers, as shown in Figure 3.1. The Managers communicate via a WinCC OA specific, platform independent protocol over TCP/IP. The bottom layer is a driver layer. It provides the connection between the WinCC OA and hardware or software devices by means of Driver Managers (D). The WinCC OA framework provides drivers for most commonly used communication protocols. The heart of the system is the Event Manager (EV), which belongs to the communication and memory layer. This manager has many tasks, e.g. it receives and evaluates mes-

---

[1] Prozess-Visualisierungs-und Steuerungs-System delivered by ETM GmbH, Eisenstadt, Austria.

sages from different managers, distributes them further among other managers, administers user authorisation. The Database Manager (DM) administrates the run time database where all the data reflecting the status of the controlled processes are stored. It also archives recent values of alarms and it manages system parametrisation. The WinCC OA provides a database on the local drive where the project is running, and also supports a link to Oracle database via the DM. In the processing layer two types of managers porting a user's code into the WinCC OA are available: Control Managers (CTRL) and Application User Interface (API). The Control Manager executes interpreted user scripts (programs). It has a multi-threading capability. The scripts can be triggered on data change and/or on time events. The task of the API manager is to incorporate a user compiled code into the WinCC OA system, so that it can access the data in the project database. Finally, the User Interface (UI) Layer provides graphical tools for developers, process visualisation, and WinCC OA configuration.

Thanks to its modularity, the WinCC OA allows the control system to be built in various configurations: single systems on a single machine, a scattered system where a single system runs on multiple machines, a single redundant system and a distributed system.

3.1.1.2 JCOP framework

To provide a common tool to reduce the manpower needed for the development and maintenance of various LHC experimental control systems, a set of solutions has been developed at CERN as the JCOP framework [39]. This framework provides many ready-to-use components for controlling and monitoring standard devices in the experiments. The framework also extends the functionality of the underlying WinCC OA tools, such as the configuration database tool and framework installation tool. The framework is available as an additional package to be installed on top of the WinCC OA - its components can be also added or removed individually.

Within the JCOP, a number of technologies have been evaluated for their usability in the experiment control systems. Primarily, commercial solutions have been assessed. Among them were the field buses, commercial Programmable

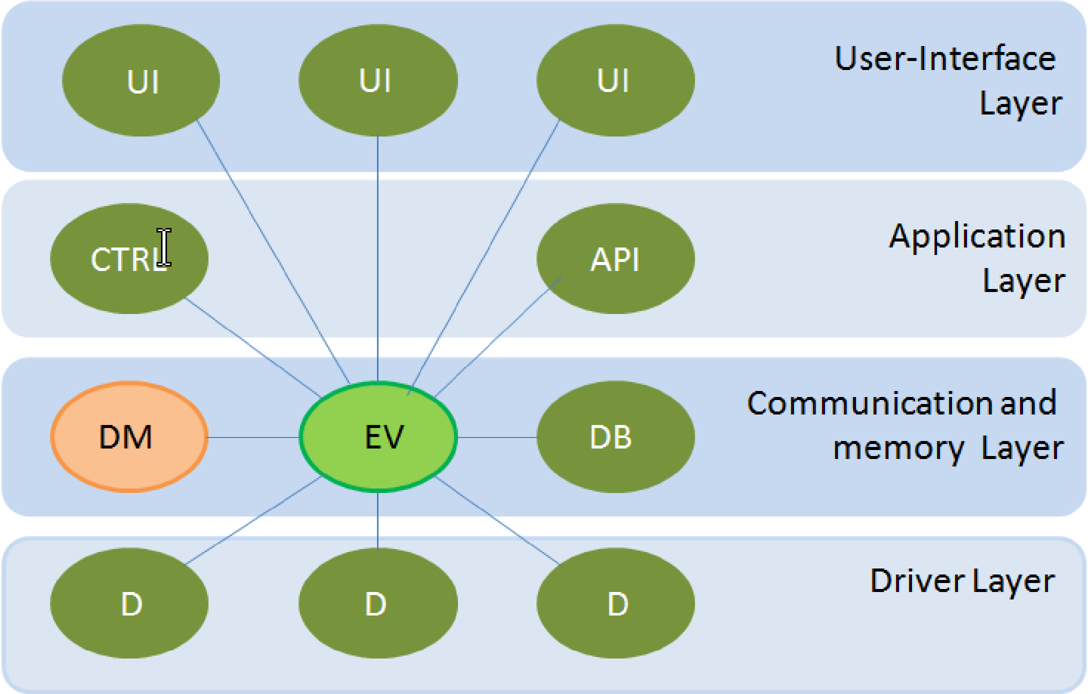

Figure 3.1: Schematic view of the WinCC OA system architecture.

Logic Controllers (PLC), or solutions for high and low voltage power supplies. Moreover, technological developments made in particular experiments have been incorporated in the JCOP framework and made available to the community. For example, the ELMB, initially developed for ATLAS, is now extensively used in all the LHC experiments.

3.1.1.3 Front-end systems

The Front-end systems are the responsibility of the subdetector groups. However, standardization is also required when it comes to interfacing hardware to the SCADA software. It is strongly recommended to use industrial standards and common DCS building blocks wherever possible. The main common DCS standards used in ID DCS are listed below.

CAN field bus. The Controller Area Network (CAN) [41] is used for communication with the majority of the DCS hardware. It is a serial bus that is insensitive to magnetic fields. It offers good industrial support, high flexibility, error detection and some recovery capabilities. The CAN protocol has been developed for the automotive industry and is very reliable and robust.

OPC. The Object Linking and Embedding for Process Control Unified Architecture (OPC UA) [42] developed by the OPC Foundation [42] is an industrial communication protocol used for nearly entire communication between the hardware components and the SCADA layer of the ATLAS DCS. It is a cross-platform successor of the original OPC UA communication model based on MS Windows proprietary technology. The OPC UA toolkits are OS agnostic[1] and are offered in many programming languages (C++, Java, .NET, Python and others).

ELMB. The ELMB [43] has been developed by the collaboration of the CERN ATLAS DCS, NIKHEF[2] and CERN PH-ESE[3] to provide a multi-function device with analogue inputs/outputs, digital inputs/outputs, Serial Peripheral Interface (SPI) connectivity and custom functionality. The ELMB is radiation-hard (qualified up to ~40 Gy [44]) and tolerant to magnetic field, thus it can be used in the experimental cavern. The ELMB consists of three galvanically isolated parts:

- CAN communication with the CAN transceiver chip (PCA82C251 by Philips) for processing communication on the CAN bus;
- digital part with Atmel ATmega 128 processor, the Infineon SAE 81C91 CAN controller, and digital I/O capabilities form the core of the board. The ATmega 128 processor runs a dedicated firmware which handles all ELMB functionalities and communication with the DCS computer. The firmware can be upgraded remotely over the CAN bus. Four digital ports, each with eight individual channels, are provided as the digital input/output entries.

---

[1] The “OS agnostic” term refers to the software that runs under any operating system or to development tools that support any operating system

[2] NIKHEF is the Dutch National Institute for Subatomic Physics

[3] CERN PH-ESE - CERN PH Electronics Systems for Experiments is an engeenering section which specialises in elecronics for High Energy Physics experiments at CERN.

- analogue part provides a 16 bit Analogue-to-Digital Converter (ADC) with four physical differential inputs, multiplexed to 64 channels;

The ELMB is extensively used in ATLAS (more than 5000 pieces) and in other LHC experiments (more than 10 000).

The ELMB board can be also used in a non-standard fashion, by modification of the firmware running on its ATmega 128 processor. The custom application ELMB firmware has been developed for the ATLAS Inner Detector in a few cases described in Chapter 5.

CAN-PSU. Three parts of the ELMB board require separate power. The input voltage for the digital and analogue parts can vary from 3.5 V to 12 V, while the CAN part takes from 8 V to 12 V. The voltages are then adjusted on-board to the required values. The CAN Power Supply Unit (PSU), developed by the CERN group, is used to provide power to ELMBs remotely via the CAN bus. The power supply parameters can be controlled and monitored from the level of dedicated framework components integrated with the WinCC OA. The PSU is a rack mounted unit that can provide up to 16 CAN buses with the required voltage. Each bus is supplied by two power sources: for the CAN bus power (12 V/25 W) and for the analogue and digital ELMB parts (12 V/35 W).

3.1.1.4 Finite State Machine

The ATLAS DCS infrastructure is very complex. It is represented in the DCS software by more than 12 million parameters corresponding to many different services, such as cooling, power, temperatures, detector modules etc. Ultimately, the ATLAS detector is supervised by just a few people during its operation. The DCS has to provide an easy and efficient way for the operator to spot anything that goes wrong in any part of the experiment just at a single glance. Thus, a higher level architecture is needed to address the issues of complexity and heterogeneity during the detector operations.

To allow high level operations, the detector control is mapped into an abstract tree structure or a hierarchy of functional components. These components behave as Finite State Machines (FSMs). To facilitate the implementation of the FSM models, a software tool-kit called the FSM [45], employing the State Machine Interface (SMI++) [46] framework, has been developed within JCOP.

In SMI++, the experimental set-up is described as a series of objects behaving as the FSMs. The hardware devices or software tasks are represented by the so-called associated objects. The associated objects interact with the concrete items they represent via the so-called proxy process. The higher levels of the control system are usually represented by the abstract objects that also behave as FSMs. They include the control logic and can send commands to other objects. The objects related functionally or operationally are organised in SMI++ in a hierarchical control structure - the so-called domain. The final control system is built as a hierarchy of many SMI++ domains. A schematic illustration of the hierarchy of controls is shown in 7.2. The main attribute of an SMI++ object is its state. In each state the object can accept commands that trigger actions. An abstract object, while executing an action, can send commands to other objects, interrogate the states of other objects and eventually change its own state. It can also spontaneously respond to state changes of other objects. The associated objects only pass on the received commands to the proxy processes and reflect their states [46].

The JCOP FSM framework component has adopted the hierarchical, tree-like SMI++ concept to represent the detector structures. The hierarchy is composed of two types of nodes: Device Units (DU) and Control Units (CU). The Device Units implemented as proxies correspond to the SMI++ concept of associated objects. The CU are implemented as SMI++ domains to provide hierarchical control and abstract behaviour modelling. They represent sub-systems, contain the control logic and can control the sub-tree below them. They can also send commands to other objects (CU or DU).

The most important features of the SMI++ and FSM framework which are of higher importance for large scale experiment control systems are:

- partitioning mechanism - each child of a CU can be dynamically included or excluded from the hierarchy. It allows for tests of part of the experiment control system in a stand-alone mode,
- distribution - the control hierarchy can be distributed over several comput-

ers and can run on mixed operating system platforms,

- automation - the functionality for complete automation and automated error-recovery are provided. The recovery mechanism starts at the bottom of the hierarchy, i.e. each object reacts in an asynchronous, event-driven fashion to changes of the states of its children. Thus, the recovery is done in parallel for all sub-systems.

Each object in the FSM hierarchy is described by the so-called state. The state summarises the operation conditions of a FSM object in a single parameter. The states are propagated upwards the controls hierarchy according to a predefined, system-specific logic. The commands are propagated downwards to the objects at lower levels in the hierarchy with some basic conditional logic.

The ATLAS DCS has introduced a few extensions on top of the JCOP FSM framework component. In the ATLAS DCS, the operational behaviour of a FSM node is defined by two independent objects: state and status. The state tells the operator about the operational mode of the system, while the status is linked to a possible error condition in the system. Extended description of state and status objects is given in 7.2.

To assure the homogeneous implementation and easy integration of the subsystem, some development rules and standards have been imposed. These rules define the project organisation, backup, code version controlling, naming conventions, alarm rules etc. For the FSM, compulsory states for the Control Units at the top node in a sub-detector are required to be the same for all the systems: READY and NOT READY. The standard status levels are: OK, WARNING, ERROR and FATAL. Other user-defined states can be used at lower levels in hierarchy to fulfil the specific sub-detector requirements, but the status levels cannot be changed. For the user, the FSM interface standardised colour codes are fixed for particular states and statuses of the detector, e.g. red is typically associated with an error condition, and green always denotes proper operation conditions.

3.1.2 The data storage and data exchange

There are two data categories in the DCS: input parameters (i.e. configuration parameters for both software and hardware elements of the detector installation) and output parameters (i.e. the measurements delivered by the experiment hardware). The input parameters are stored in the configuration database and the measurements are archived and stored in the condition database.

The input parameters are used to configure the considered sub-detector working points. Depending on the LHC run mode, beam condition or data-taking run, different sets of operational parameters are required. The predefined configuration sets are loaded from the database into the relevant DCS control system at the boot-up well in advance of the actual data taking, so that high data transfers are not required. However, the access to the configuration database must be guaranteed at all times, in the event that the update of the configuration sub-set is needed and for the consistency checks.

The DCS output data contain parameters measured by the detector hardware and parameters derived from direct measurements. Typically, they form a triplet structure: value, time and definition. The selected output parameters are stored in the condition database with individually tuned update frequencies and data smoothing. The total stored data volume is relatively high, e.g. it is over 1300 GB/year in case of the ATLAS DCS conditions.

A subset of condition parameters, crucial for the interpretation of the detector performance and physics data, is transferred to a dedicated database which can be accessed through the ATHENA framework and used in physics analysis.

3.1.3 Human aspects of control systems

In large experimental systems all the people involved (users, developers, experts) are considered the elements of the system. Their actions or a lack of action can influence the experiment. The same person can act as an operator in one situation and as an expert or developer in another. Thus the procedures and processes must be in place to help the people involved to achieve their objectives. On the other hand, to understand the system behaviour human actions must be tracked, archived and included into analysis. The DCS system must be also immune to undesirable human actions.

A simplified Role Based Access Control (RBAC) [47] system is used in ATLAS to manage the access to hardware and software resources for about 3000 users. The access control system regulates when and which operations can be executed on data and resources, preventing possible intentional or unintentional harmful actions.

3.1.4 Overall ATLAS Detector Control System design

The ATLAS DCS [35] is a distributed system running on more than 130 server machines. It has a hierarchical structure where the sub-detectors are feeding information to the top node. This node is used as the main control point during the ATLAS detector operations in the control room. The ATLAS DCS architecture is divided into layers, presented in Figure 3.2. At the bottom layer there is a hardware Front-End (FE) equipment, which consists of electronic devices and their associated services, e.g. power supplies, cooling circuits and various sensors. The Back-End (BE) is developed with the WinCC OA framework and is organised into three levels. The hardware control is performed by the Local Control Station (LCS) running a dedicated control software. At the LCS level the subsystems are free to implement the control software customised to their local needs. The LCS computers belonging to one sub-detector are supervised by a single Sub-detector Control Station (SCS), allowing the sub-detector stand-alone operations. The Global Control Station (GCS) is at the top of the DCS hierarchy. It includes references to all sub-detector top-nodes and runs the service applications and operator interface. To allow the detector parts to be run in parallel, the model of partitioning is introduced into the DCS. It matches one-to-one the TTC. The DCS is synchronised with DAQ via the DAQ-DCS-Communication (DDC) package, communicating via the Distributed Information Management System (DIM)[1] to ensure the platform independence. The DDC provides functionality for the command, message and data transfer. A command transfer is possible only from DAQ to the DCS to trigger transition to a requested operational state.

---

[1] DIM is a communication system for distributed / mixed environments. It provides a network transparent inter-process communication layer [48].

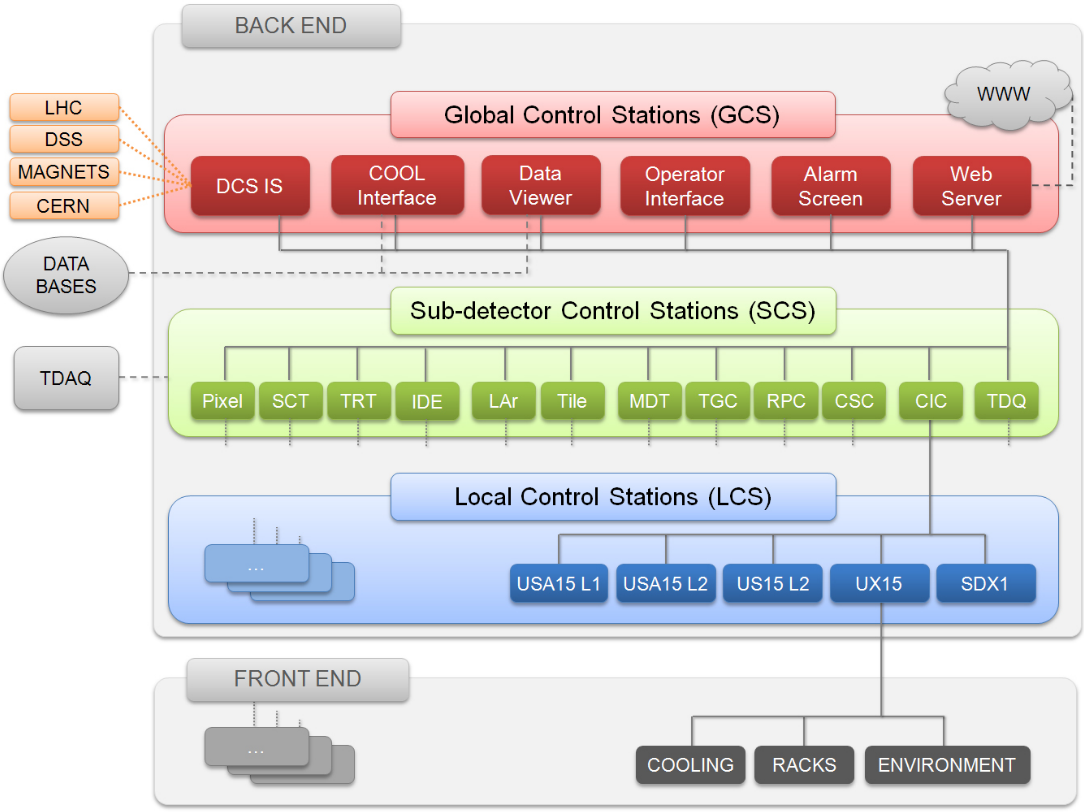

Figure 3.2: Schematic view of the ATLAS DCS architecture [36].

The messages can be passed from the DCS to DAQ to report the DCS state changes, especially if the DCS state deviates from the operational condition. The data exchange can be bidirectional. The DCS provides DAQ with information on powering and monitored parameters, which may be important for the run control and data quality. DAQ provides the DCS sub-detector with specific information, such as the measured luminosity and detector occupancies.

Experimental software facilities, such as DCS or DAQ, run on the technical ATLAS network, which is a private internet firewalled from the general network for safety.

The ATLAS GCS runs several services which facilitate the detector operation:

- Operator Interface - the experiment is controlled by a dedicated DCS workstation in the ATLAS control room. The station provides several displays which host major user interfaces: the FSM (see 3.1.1.4) screen and the alarm screen for alarm recognition and acknowledgement. More interfaces (e.g. the data visualization tools, process log viewer, operator logbook) are available on demand. The remote access to the DCS user interfaces outside of the ATLAS technical network is possible via a Windows Terminal Server. Such a remote access is granted only for registered experts having required access control privileges.

- The Information Server - ATLAS DCS needs to exchange certain data with facilities running outside the ATLAS technical network, e.g. with the LHC control, magnets or Detector Safety System. Such data are fed to a dedicated sever, and the data exchange is handled via Data Interchange Protocol (DIP) [49], which is a protocol designed for highly reliable event-base data exchange between very loosely coupled heterogeneous systems.
- COOL interface - it allows access to a relational database where the DCS data crucial for understanding the detector response and performance are stored. These data are later used in off-line physics analysis.
- Data visualisation - the DCS parameters may be archived in a database for further diagnostics or for monitoring the evolution of the system over time. Data visualization tools were put in place to provide fast and easy access to the archived data. One of the most practical tools is a trending tool. On-line displays of the trends for individual DCS parameters can be easily generated by the operator in the ATLAS control room. For more sophisticated visualization plots such as histograms, profiles, or scatter plots the off-line tools have been developed.
- Alarm Screen - displays the list of alarms currently active in the whole ATLAS DCS. It informs the operator about problematic detector elements and helps to undertake corrective measures.
- Web Server - publishes a static picture of the ATLAS status on a dedicated web site. All sub-detector information and corresponding panels up to the level of the sub-detector partitions are gathered from the persistent user interface instances every minute. The information is accessible world-wide using a common web-browser.

Chapter 4

The Inner Detector Common Services

4.1 Introduction

Functionally, the Inner Detector constitutes a single integral system used for the measurement of the charged particles trajectories and particle identification. However, in its structure the ID is a very complex system, with three different sub-detectors built using different technologies, as described in Chapter 2. Each subsystem, the Pixel Detector, the SCT and the TRT, is largely autonomous and has its own control systems to ensure its reliable operation. Nevertheless, they are all installed together inside the ATLAS barrel calorimeter cryostat and share several common items of the infrastructure and services. They can influence each other, and a substantial amount of data and control exchange is necessary for a safe and successful combined operation. Several hardware services have been designed and commissioned to address the needs of combined operations of the Inner Detector components. They can be roughly divided into two groups: the first group aims at monitoring and maintaining optimal environment parameters (see 4.2), and the second at beam condition and radiation monitoring (see 4.3) inside the ID volume.

4.2 Inner Detector environment

4.2.1 Inner Detector Thermal Management and Environmental Gas Management

The Inner Detector obeys the policy of thermal neutrality equally outside and inside its volume. This means that the sub-detector components are not allowed to impose a significant heat load on each other, and the ID does not affect the operations of the neighbouring ATLAS detector components.

A heat load of around 120 kW generated in the ID volume of 30 m^3 is balanced by appropriate cooling power [2]. The ID volume is divided into different regions where different subsystems of the tracker operate: the TRT, which operates at room temperature of $\sim$ 20°C and in the atmosphere of CO_2, and the SCT and Pixel detectors operating at lower temperatures (around -7°C and -20°C respectively) in the dry nitrogen atmosphere.

Special barriers (thermal screens or enclosures) have been constructed to separate the volumes with different temperatures and environmental gases and to maintain different operating conditions of the detectors [2]. Outside of the sub-detectors, the whole ID volume is filled with dry CO_2. At the end of the cryostat the ID volume is sealed by the ID end-plate.

4.2.1.1 Thermal interfaces inside the Inner Detector

Operational temperature differences among the different sub-systems of the Inner Detector can potentially lead to a thermal interference between those systems unless thermal isolation techniques are used. The biggest issue is between the outer edge of the SCT (at -7°C) and the inner edge of the TRT (at 20°C). The TRT straws are mechanically delicate, the temperature gradient along the detector straw could potentially cause its deformation. This is mostly relevant for the end-cap region where the straws are arranged radially [50].

In addition, the SCT modules should be kept cold to minimise the radiation damage effects during the shut-down and maintenance periods as well as during normal operation. This implies both continuous cooling of the SCT thermal enclosures, and heating on the outside to avoid condensation when the detector elements are exposed to the cavern air with an atmospheric level of humidity. All the detectors have to be able to operate independently of the others or together as a whole. A scheme of thermal barriers or screens between the various parts of the SCT, Pixels and TRT detectors is shown in Figure 4.1. The thermal screens between the SCT and TRT have to maintain a temperature difference of more than 25°C.

A typical passive thermal isolation takes up a lot of space. From the particle physics experiment's point of view an additional material inside the tracking detector measured in radiation length[1] (X_0) must be as thin as possible to minimise the contribution of the multiple scattering to the momentum resolution. In each service design emphasis is put on maximising the volume available for active detectors and minimising the radiation lengths. Instead of using a simple layer of insulation to thermally separate the TRT and SCT, an active system is used. This active system maintains the surfaces at the same level as the environment with which they have contact. With this technique, there is a heat transfer across the insulation but only from one surface to the other, leaving the temperatures of the local environments unaffected.

4.2.1.2 Thermal screens between the SCT outer radius and the TRT inner radius

The thermal screens between the outer radius of the SCT and the inner radius of the TRT are structurally parts of the SCT. The barrel outer thermal enclosure is composed of a double carbon fibre skin containing dry nitrogen (i.e. open to the SCT detector volume). The two skins are separated by localised strips of around 4.5 mm thick Airex® foam, running longitudinally along the barrel. This results in a stiff structure with a high degree of stability towards differential thermal expansion. The outer surface is covered with a total of 40 heater pads with a total power output of 1.6 kW. The end-cap outer thermal enclosure uses the Airex® foam panels with an average thickness of around 7 mm. Each outer enclosure is covered with a total of 28 heating pads with a total power output of 2.0 kW.

---

[1] The radiation length is a property of a material. It is defined as a mean distance over which a high-energy electron looses its energy by the factor $1/e$ by the Bremsstrahlung radiation, where e is Euler's number.

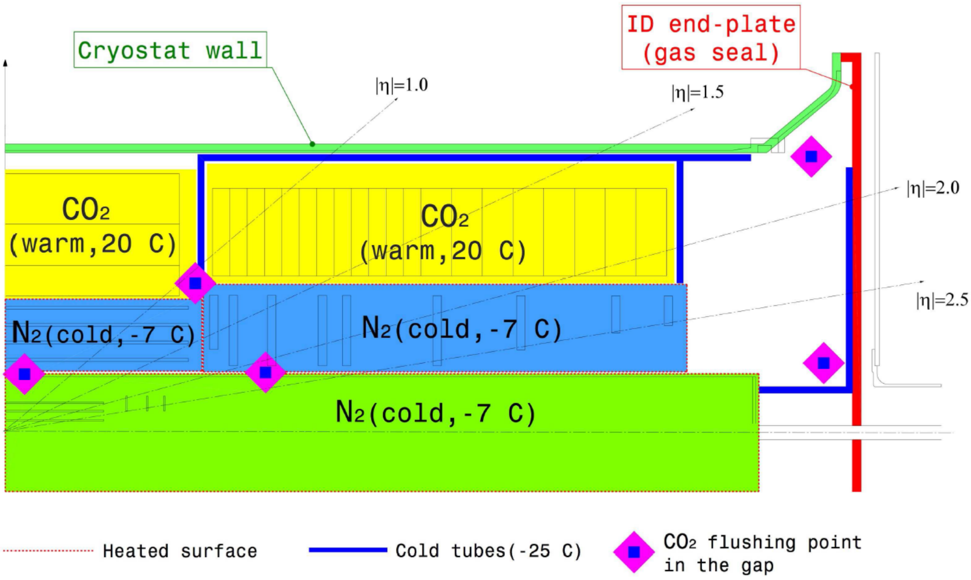

Figure 4.1: Schematic view of the environmental conditions inside the Inner Detector volume. Only a quarter od the ID volume is shown. The routing of the coolant to the Pixel Detector and SCT is also shown as well as the points where the CO_2 gas is flushed into the tracker volume. The TRT volume is marked in yellow, the SCT is blue and the Pixel Detector is green [2].

4.2.1.3 Thermal enclosure heating pads

Electric resistance heating pads are used in the ID in active thermal insulations to maintain a specified temperature at various thermal interfaces within the detector and to prevent water vapour condensation when a cold surface is exposed to a warm humid environment (for example in the event of opening the detector for service). Most of them are components in active thermal barriers which serve to maintain the temperature of the outer surface of the enclosure above the dew-point. The outer surface of the SCT barrel thermal barrier has no heaters, as there are heaters on the inner cylinder of the TRT. A fraction of the heater pads are also used on the service feed through at the outer radius of the ID end plate.

The heater pads are long-path thin (5 μm for TRT barrel pads, 8 μm for all the others) copper tracks between two Kapton (polyimide) sheets. They vary in size (0.04 to 0.64 m^2), shape (rectangular, curved, with holes etc.) and power output (from 12 to 120 watts). The pads are glued on the thermal enclosure shells. The size and segmentation of the heaters on various surfaces were defined in order to achieve a temperature distribution as uniform as possible and also to minimise the number and optimise the use of the cables required [51].

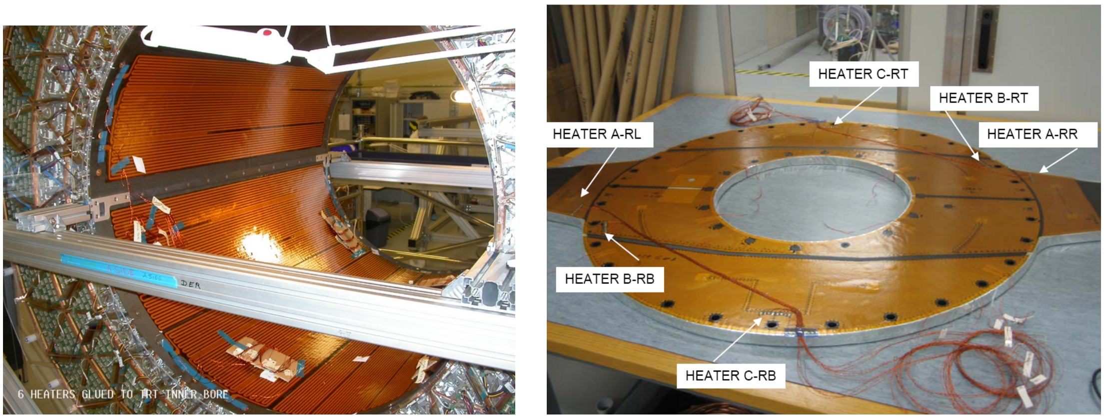

(a)

(b)

Figure 4.2: The thermal enclosure heaters glued inside the TRT cyliner (a) and on the end-cap enclosure (b). Several different shapes of heating pads are used to cover the end-cap enclosure.

A total of 290 heater pads are used in the Inner Detector. For redundancy, the heater pads in the areas critical for operation contain two parallel heating elements (channels) in one heating area and two thermistors for on-pad temperature monitoring. Each of them is sized for a rating 50% bigger than the nominal, thus in case of failure of one of the heating elements, the other can compensate by having up to 2/3 of the nominal power available. In other non-critical cases, single heater pads are connected in series to create one larger heating area.

The heater pad control system, described in Chapter 5.5, is used to control heating power delivered to the heater pads installed in the ATLAS Inner Detector.

4.2.1.4 The cooling system for the semiconductor detectors

The SCT and Pixel Detector modules, in particular their Front End chips, dissipate large amounts of heat inside the ID volume. It is estimated that the SCT and the Pixel Detector dissipate in total more than 25 kW [25] and 15 kW [23], respectively. The evaporative cooling system with C_3F_8 as a coolant [52] is used to remove the heat from the detectors modules and maintain the temperature of the silicon at -7°C or below.

The operating temperature of the silicon detectors has an influence on two important aspects related to radiation damage effects. The first one is the continuous production and accumulation of lattice defects due to displacement damage. The second group of radiation effects is related to the generation of trapping of a charge in the detector surface structures, resulting in higher electric fields and breakdown at lower voltage. The defects created in the sensor bulk act as deep energy levels in the energy gap and lead to an increase in the leakage current, trapping and change of the effective bulk doping concentration [6]. These effects have an influence on the silicon detector parameters, such as depletion voltage, bulk leakage current and a charge collection efficiency. The value of the depletion voltage for silicon detector of a given thickness directly depends on its effective doping, which (before irradiation) has two components - ionized shallow donor levels and charged deep acceptor levels. The displacement defects contribute to the removal of shallow donors and the creation of deep level acceptors. Acceptor-like deep levels predominate the shallow donors of the n-type material and the bulk material gets inverted from the n-type to the p-type. The displacement damage exhibits fast annealing that can be neglected at the LHC scales, and the long-term change of the effective doping, which depends on total fluence and temperature. In particular, after a type inversion an effect called the reverse annealing occurs, which results in further generation of acceptor-like defects independently of whether the detector is being irradiated or not. This reverse annealing effect depends strongly on temperature and can be limited by keeping the detectors at low temperature during irradiation (operations at the LHC) as well as during stops between data taking periods.

The second effect of a displacement damage is an increase of the bulk leakage current, which is proportional to the concentration of deep energy levels. For a higher leakage current the associated shot noise would dominate the signal-to-noise ratio of the front-end electronics. This current depends on the temperature according to Boltzman equation. The only way to hold it at an acceptable level below 2 μA per strip is to keep the module cold. Another effect to be taken into account is thermo-electrical positive feedback leading to the thermal instability of the detector modules, the so-called thermal runaway. In short, the heat generated in the sensor by the leakage current leads to an increase in the sensor temperature, which in turn results in a further increase in the leakage current in a positive feedback loop. If the cooling system removes the power dissipated by the sensors, this loop will reach a stable condition; if not, a critical thermal failure of the module can occur [53]. All these effects described here very briefly result in a very demanding requirement for monitoring and control of the detector cooling system.

In Figure 4.3 three main areas of the ID evaporative system are shown. The cooling plant with seven compressors, the condenser and the main system control are located in the USA15 service cavern of the ATLAS experiment. The cooling fluid is distributed via a system of pipes from the main plant to four distribution racks, located about 150 m away on the access platforms around the experiment in the main UX cavern. Finally, 204 individual cooling circuits, the so-called cooling loops, are connected to the distribution racks with one pressure regulator and one back-pressure regulator per circuit. Each cooling loop serves a small area of the Pixel or SCT detector.

The ATLAS ID evaporative cooling system is based on a physical phenomenon in which the evaporation of a liquid cools an object it has contact with. As a liquid turns to a vapour, the phase change absorbs the heat. The ID cooling system is a single-stage compressor cycle with warm transfer pipes. The phase diagram for C_3F_8 and the transformations of the system are shown in Figure 4.4.

The coolant condenses at 20°C and 17 bar and is then transferred in a liquid phase at room temperature from the condenser to the capillaries located immediately before the detector structures. Before entering the ID cooling structures, but inside the dry atmosphere in the ID thermal enclosure, the coolant is sub-cooled by means of the Heat Exchangers (HEX) between the inlet liquid (warm) and the return fluid (cold) of the same circuit.

The sub-cooling is implemented to increase the efficiency of the thermodynamic cycle by lowering the vapour quality at the inlet of the detector structures and hence allows for about 50% smaller mass flows. The smaller mass flow has a major impact on the size of the on-detector capillaries, the size and cost of the main plant, and on the overall system performance.

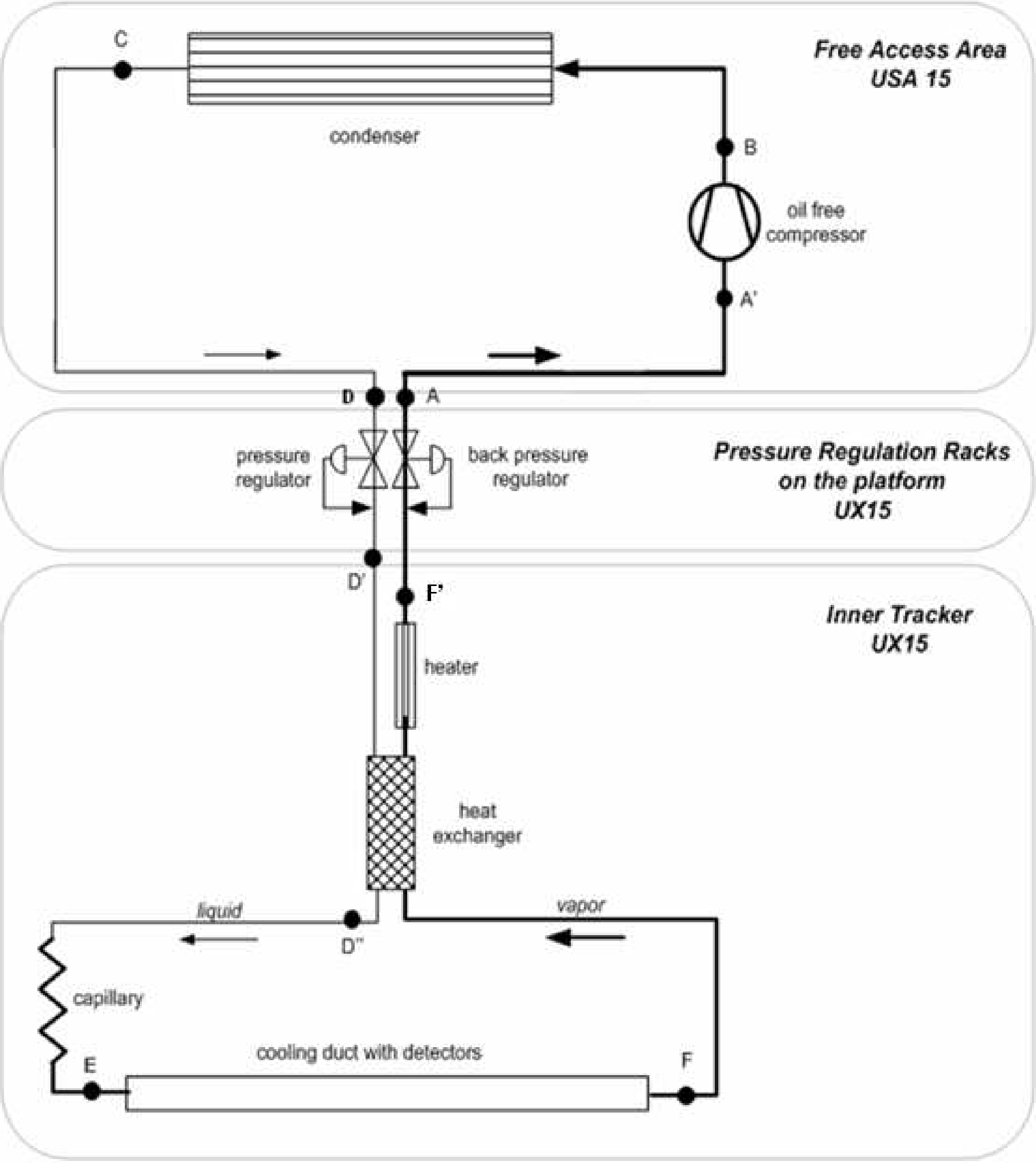

Figure 4.3: Schematic diagram of the ATLAS ID evaporative cooling system [52].

The fluid expands through the capillaries, its pressure is subsequently reduced and then remains in saturation (boiling) conditions along the cooling circuit on the detector structures. The target evaporation temperature in the on-detector cooling pipes is -25 °C, which corresponds to a saturation pressure of 1.6 bar. The temperature in the detector structures is determined by setting the saturation pressure of the fluid. This pressure is controlled by a back pressure regulator located at the end of the return lines in the distribution racks outside of ATLAS. The flow is defined by changing the pressure of the inlet liquid by means of the pressure regulator (PR) placed at the beginning of the inlet tubes.

The ID cooling system operates at a fixed flow to compensate load fluctuations due to varying power consumption in the front-end electronics. The excess of the return liquid is evaporated by the heater located inside the exhaust of each circuit, and the fluid is then heated to above the cavern dew point to allow the warm (uninsulated) return lines go back to the compressor and then to the condenser.

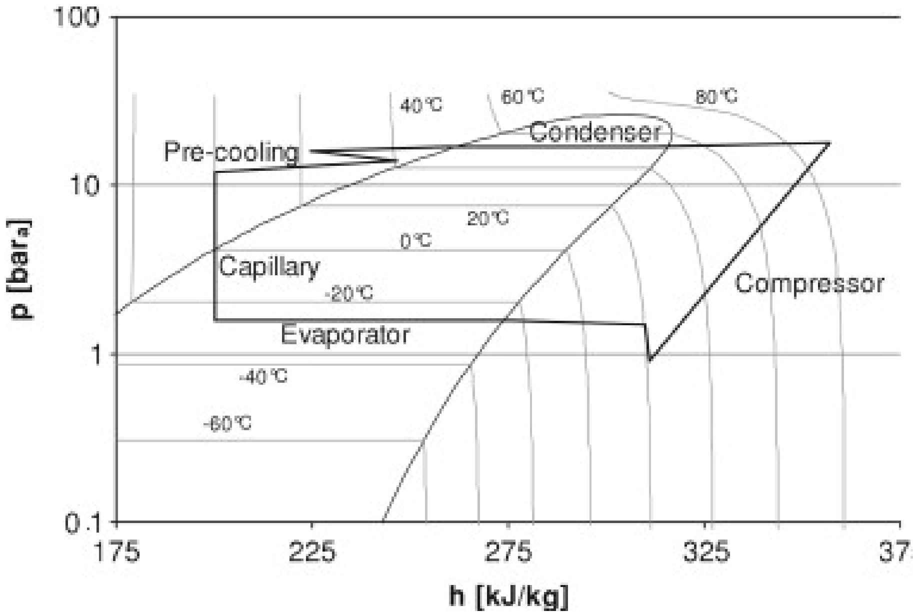

Figure 4.4: Phase diagram for C_3F_8 and thermodynamic cycle of the ATLAS Inner Detector evaporative cooling system [52].

It should be mentioned here that the compressor system has turned out to be the biggest maintenance issue in the cooling system. Thus it will be replaced by the gravity-driven thermosiphon natural circulation plant [54].

4.2.1.5 Environmental gas

There are several categories of the gas systems for the Inner Detector:

- TRT active gas inside the straw volumes (mixture of $Xe/CO_2/O_2$)
- TRT envelope gas (CO_2) circulating in the TRT modules between the straws, removing traces of Xe leaking from the straws and cooling the straws in the end-cap region;
- dry nitrogen (N_2) as an environmental gas circulating inside the SCT and the Pixel Detector thermal enclosures to provide a neutral atmosphere for the silicon detectors and to remove humidity;
- an environmental gas (CO_2) in the spaces between the SCT thermal enclosures and the TRT modules, and in the services regions.

The requirements for environmental gas management inside the Inner Detector volumes are very strict. One of the most important requirements is that the TRT and SCT environmental gases should not pollute each other.

The TRT straws operate with an active gas mixture of $Xe/CO_2/O_2$ and they are surrounded by an envelope gas of dry CO_2. The TRT modules and straws are not completely leak-tight and may exchange some gas with the global ID volume. Any amount of nitrogen or water vapour in the global ID volume might enter the TRT gas envelope and then the straws themselves, compromising the TRT performance. The maximum nitrogen concentration allowed in the TRT gas envelope and the global ID volume is 1%, while the water vapour content must be kept below 500-1000 ppm [55]. The global ID volume is therefore filled with dry CO_2 at a maximum overpressure of 0.5 mbar with respect to the ATLAS cavern. It flushes out the nitrogen and water vapour from the global ID volume.

On the other hand, a few possible problems have been anticipated when considering the operation of the silicon detectors in CO_2 atmosphere. As they run cold, there is a risk of water vapour condensation on cold surfaces. In an atmosphere containing CO_2, carbonic acid (H_2CO_3) can form and it may corrode the exposed aluminium elements of the detector [55]. The impurities of the CO_2 in N_2 atmosphere also affect the Frequency Scanning Interferometry system [56] used for the in situ SCT detector alignment. For this reason dry nitrogen was chosen as an environmental gas in the silicon detector envelopes.

To minimise the amount of the vapour present inside the whole ID volume, the volume is sealed off from the external atmosphere. However, it is not completely enclosed because of a gap between the barrel and end-cap calorimeters through which the services pass. Thus it is in contact with the cavern environment air having an average dew point of about 12°C, corresponding to a water vapour concentration of 13 800 ppm at atmospheric pressure. The operational temperature for the silicon detectors is approximately -7°C, but the coldest parts such as the cooling pipes can be as cold as -25°C, with an occasional excursion down to -30°C. At this temperature the water vapour concentration in the silicon detector gas envelopes must be kept below 600 ppm to prevent the condensation. The moisture inflow is counterbalanced by purging dry nitrogen into the SCT and Pixel Detector thermal enclosures.

The environment gas system to regulate the moisture level in the SCT and Pixel tracker is formed by four identical systems, two for the SCT end-caps, one for the SCT barrel, and one for the Pixel Detector.

The ID volume needs constant monitoring of its environmental gas parameters, in particular in the service regions and in the thermal enclosures. Sets of temperature and humidity sensors have been installed in the most sensitive areas. This allows the dew point temperatures to be calculated for a given area. The sensors for the ID environment monitoring are described in detail in 4.2.1.6

4.2.1.6 ID environment monitoring sensors

The ID volume and services environment must be constantly monitored. In particular, the knowledge of the humidity and the temperature on the cooling pipes scattered across the volume, is crucial for preventing and monitoring cooling incidents. There are about 1000 environmental sensors (measuring temperature, pressure and humidity) installed inside the ID volume. They are organised in three main groups serving different purposes [57]:

- Volume sensors - 18 integrated temperature and humidity sensors inside the ID volume. The humidity sensors are radiation hard Xeritron devices mounted in a carbon fibre package. The temperature sensors are Negative Temperature Coefficient (NTC) 10k thermistors and Semitek103 JT-025 sensors which are glued to the humidity sensor package. The volume sensors are situated in the proximity of the areas where the cold evaporative exhaust tubes are routed to provide information of the temperatures there.

- Cooling sensors - each cooling circuit (cooling loop) is equipped with four additional temperature sensors used for the calibration, control and safety. The sensors are mounted in diagnostic points - one sensor at the inlet tube between the capillary and heat exchanger, one sensor on the inlet to monitor the inlet liquid temperature and two redundant sensors connected to each outlet to monitor the coolant temperature in the exhaust tube. In total 408 cooling sensors are installed.

- Services sensors - 448 10k NTC sensors are located in cable trays on the cryostat flange, inside the cryostat barrel, at the Patch-Panel 2 (PP2), and at the Pixel Nose.

4.2.1.7 Ultrasonic system for gas monitoring

A custom ultrasonic instrumentation was developed for real-time monitoring of possible coolant leaks into the ID sub-detector volumes and to allow mass flow measurement in the evaporative cooling systems of the ID silicon trackers [58]. These instruments make use of a physical phenomenon according to which in a binary gas mixture at a given temperature and pressure the sound velocity depends only on the component molar concentrations. The mechanical envelope of the device is shown in Figure 4.5. It consists of a flanged stainless steel 853 mm long tube. The tube is wider in the side sections. Between the pair of diameter reduction cones a pinched tube (500 mm long and 44.3 mm in diameter) is mounted. A pair of 50 kHz capacitive ultrasonic transducers is centred and placed inside the wide ends of the tube, facing each other 600 mm apart.

The instrument with the co-axial geometry, shown in Figure 4.5, is optimised for binary concentration measurements in static gas or at low flow. Another geometry, shown in Figure 4.6, has an acoustic path crossing the gas flow at 45°. It is optimised for flowmetry at high C_3F_8 flow speeds of around 22 m/s, corresponding to mass flow rates of around 1.2 kg/s [58].

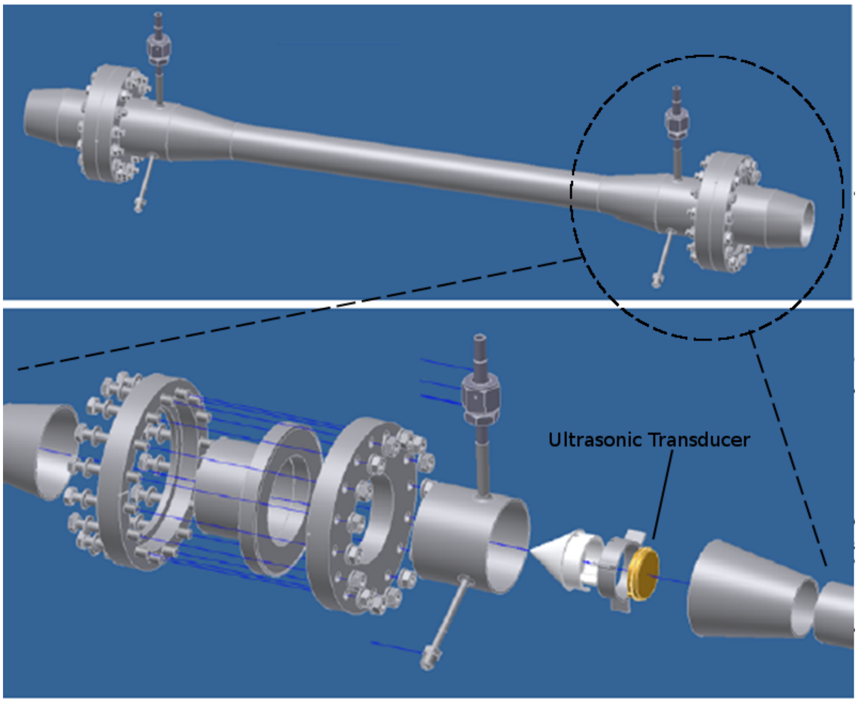

Figure 4.5: Representation of the sonar device mechanical envelope

The gas extraction and sampling system, composed of pipes, pumps and valves aspirates an environmental gas into the tube from the detector region being analysed. The gas is channelled through the instrument. The transducers serve as both receiving and transmitting devices. In this configuration the sound signal can be sent in two directions: in the same direction as the gas flow in the sonar tube and upstream the gas flow. The custom electronics based on an Analog Devices ADμC 847 microcontroller is used to measure the sound transit time. The temperature and pressure inside the tube are measured by means of six thermistors (precise up to ±0.2 °C) and a pressure transmitter with the measurement precision of ±15 mbar. The temperature and pressure readouts together with the measurement of the time between the transmitted and received sound pulses are sent simultaneously to the control system described in 5.6.

These data are further processed in the DCS computer where the gas flow rate is calculated and the gas composition is evaluated, see 5.6 for more detail.

Five sonar devices are currently installed in ATLAS. Three of them are dedicated to monitoring of the C_3F_8 coolant leaks into the Pixel, SCT and IBL

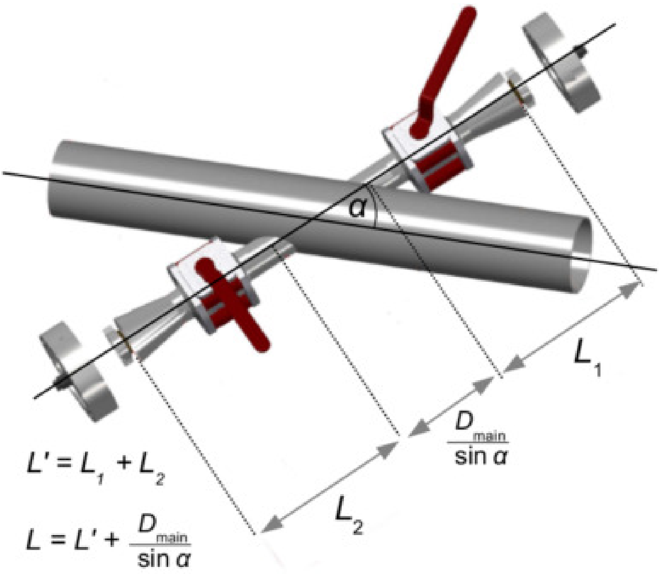

Figure 4.6: The angled path ultrasonic flowmeter installed in the C_3F_8 vapour return tube to the thermosiphon condenser. It consists of a pair of transducers separated by a distance L, and aligned on a sound path intersecting the main tube, of internal diameter $D_{main} \approx 135mm$, at an angle α=45°. The difference between the sound transit times in opposite directions is used to calculate the gas flow rate [59].

detectors envelope. Two other devices are dedicated for a new thermosiphon coolant recirculator, which in the near future will replace the compressor system in the ID cooling.

4.3 Beam condition and radiation monitoring inside the ID volume

The proton beams of nominal intensities and energy circulating in the LHC have a stored energy of 360 MJ each [60]. This is more than two orders of magnitude above the other particle colliders, such as Tevatron or HERA. An uncontrolled release of even a fraction of stored beam energy in the experimental areas can be detrimental to the equipment. The LHC have several active and passive protection systems implemented in order to ensure safe operations: the beam dumping system, beam interlocks, beam instrumentation and equipment monitoring, collimators and absorbers [61; 62]. The ATLAS experiment is considered to be the safest of all *pp* collision points on the LHC ring in terms of possible beam failure scenarios, as it is located far from the beam extraction and injection points. On each side of the ATLAS experiment, at $z = \pm 18$ m from the interaction point, the Target Absorber Secondaries (TAS) collimators are located. Their function is to protect the inner triplet of superconducting quadrupoles near the P1 interaction point from a flux of forward high energy charged and neutral particles produced in *pp* collisions. As the aperture of TAS is a limiting physical aperture in the ATLAS insertion point, it also protects the inner tracking elements of the detector from some beam failures.

Nevertheless, during the operation of the LHC some accidental beam losses may happen due to equipment failures, operational mistakes or magnet quenches. The faulty conditions developed locally near the ATLAS beam Insertion Region due to e.g. wrong magnet settings during the injection phase, could go undetected by the LHC protection system and cause local damage. A simulation of the beam orbits with wrong magnet settings near P1 has been performed [63]. Among others, the results show scenarios with the beam scraping the TAS collimator or the beam line. A very high instantaneous rate of secondary particles produced in TAS or by the beam pipe scrapping might cause the detector damage.

The losses can occur in a single beam turn, over multiple turns in a short time (< 1 s), or in a longer time scale. Single-turn losses are normally handled by the passive protection. Multiple turn losses may increase the radiation dose of the detector and affect the detector safety and performance.

Two systems have been commissioned in ATLAS to protect the tracking system against multi-turn beam loses: the BCM [64] and the BLM [64].

4.3.1 The Beam Condition Monitor

The aim of the ATLAS Beam Condition Monitor system is to monitor the beam conditions close to the interaction point. It also has the functionality to initiate a beam abort action in case of detecting dangerous beam instabilities that could potentially lead to apparatus damage. The BCM provides also the luminosity measurement as complementary information to LUminosity Cherenkov Integrating Detector (LUCID), the ATLAS main luminosity monitor.

4.3.1.1 The BCM detector stations

The BCM consists of two detector stations located symmetrically with respect to the interaction point at $z_{BCM} = \pm 1.84$ m. Each detector station consists of four modules, mounted on the ATLAS Pixel Detector support structure at 45°with respect to the beam direction, at $r \approx 55$ mm, which corresponds to pseudorapidity $\eta \approx 4.2$. The modules are located symmetrically around the beam line at $\phi = 0°$, 90°, 180°and 270°. The position of the BCM modules inside the ID is shown in Figure 4.7

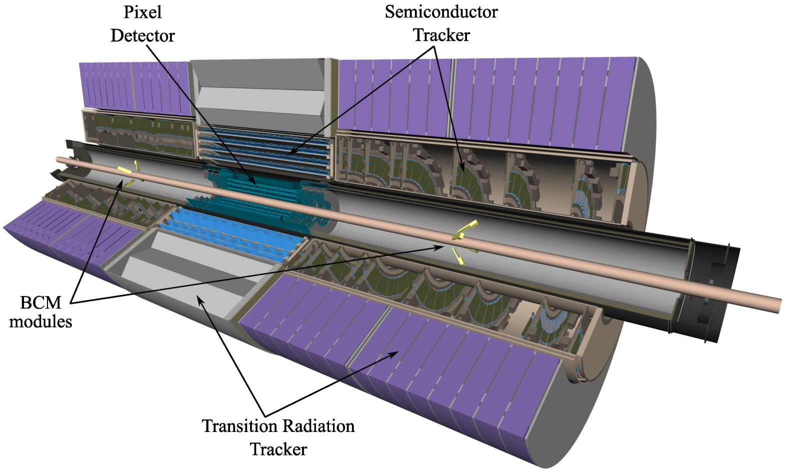

Figure 4.7: Position of the BCM detector modules inside the Inner Detector [64].

The location of the BCM detector stations has been chosen to be optimal for the discrimination between particles coming from a *pp* collision and those resulting from the beam losses. The particles originating from *pp* collisions occurring every bunch crossing give a coincident signal in both detector stations every 25 ns, whereas shower particles originating upstream at $|z| > |z_{BCM}|$ hit the nearest BCM station at a time $\delta t = 2z_{BCM}/c$ before the station on the other side of the interaction point. As a result, the shower particles induced by the beam losses give the signal in the nearest station 6.25 ns before the *pp* collisions at the interaction point (the so-called out-of-time hits), while the secondary particles from the genuine collisions reach the station 6.25 ns after the collision (the so-called in-time hits). This time difference makes it possible to distinguish between the signal and background events.

4.3.1.2 Detector sensors and modules

Each BCM module consists of two polycrystalline Chemical Vapour Deposition (pCVD) diamond pad sensors of 1 $\text{cm}^2 \times 1\ \text{cm}^2$ and 500 μm thick. The sensors are connected in parallel to increase the signal amplitude [65]. Two pad sensors are assembled back-to-back on a ceramic baseboard on which high voltage (± 1000 V) and signal lines are distributed. The middle surfaces of the two sensors are conductively glued together with small pieces of ceramic distance holders. They are connected to the signal line on the ceramic baseboard through multiple bonds. A schematic view of the sensor and ceramic assembly is shown in Figure 4.8.

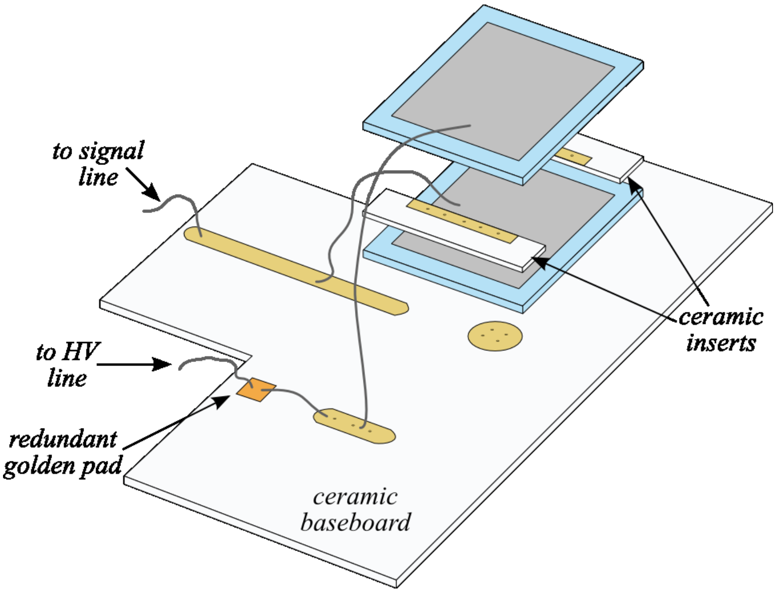

Figure 4.8: A diamond double sensor assembly with ceramic inserts and baseboard used in the final modules [64].

Diamond material has been chosen as the BCM sensor owing to its radiation hardness and fast signal response with signal rise time 1 ns, signal width ∼2 ns and baseline restoration in less than 10 ns. The big advantage is that a diamond sensor has a very low leakage current, which after irradiation does not exceed 1 nA/cm^2, and thus the sensors do not require cooling [66].

Ceramic plates with two diamond sensors are assembled into the front-end electronic box which also houses two front-end current amplifier stages, see Figure 4.9. The amplified analogue signals are routed out to the region where lower radiation levels are expected.

Figure 4.9: Layout of the two amplification stages in the module [64].

4.3.2 BCM readout chain

The BCM readout hardware and software are described in more detail in [67]. Here, only a summary is provided to set up the scene for the DCS aspects discussed further. A schematic view of the BCM readout chain is shown in Figure 4.10.

Analogue signals registered by the detector modules are transmitted via a 14 m long coaxial cables to the region outside the ATLAS calorimeter. The custom digitisation electronic boards are placed there. These electronics boards are based on an ultra-fast and low-power front-end amplifier/discriminatos, the so-called NINO chip [68], which features the radiation tolerant design fabricated using the 0.25 μm IBM technology. Each digitisation board serves one detector module and provides signal filtering, amplifying and discrimination with time-over-threshold measurement capability. The input signals are first filtered and split into two parts with the amplitude ratio of 1:10 in order to increase the NINO dynamic range [64]. The lower signal line is called a *high threshold channel*, while the

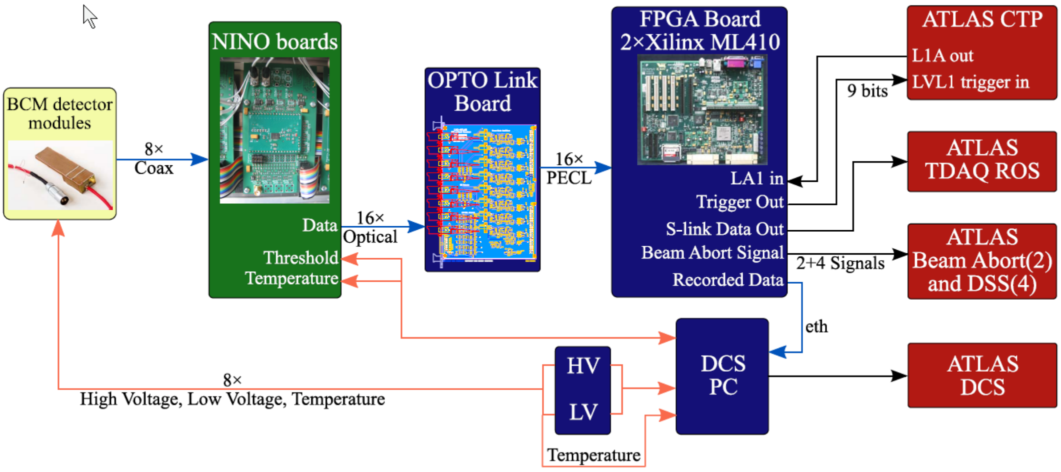

Figure 4.10: Overview of the BCM readout [64].

higher signal is called a *low threshold channel*. These two signals are digitised by the NINO chip, then converted into optical signals and transmitted through approximately 70 m optical fibers to the USA15 service room. Further, the signals are processed by two Data Processing Units based on Xilinx ML410 comprising Field-Programmable Gate Array (FPGA) [67]. The FPGA processes the signals in real-time [67]: it extracts the signal pulse width, which encodes the Time-Over-Threshold (TOT) from NINO, and the signal arrival time of each of the 8 modules. Next, the analysis done using the FPGA includes the determination of the in-time and out-off time hits as well as the summary of the rates for the detector modules and sides and coincidences for different combination of the modules. The processed detector readouts from the FPGA are fed into several ATLAS and LHC systems, e.g. the LHC Beam Abort system, ATLAS Detector Safety System, ATLAS Detector Control System, ATLAS Data Acquisition, ATLAS LVL1 trigger.

4.3.3 The Beam Loss Monitoring System

The ATLAS BLM is the second system constructed for protection against the beam losses and for beam surveillance in the region of the Inner Detector. It has a power of issuing a beam abort signal in the event that beam anomalies are detected. Six BLM modules are mounted on the ID end-pates on each side of the detector at a distance of $z_{BLM} = \pm 3.45$ m and radius of 6.5 cm. The detector modules are based on pCVD diamond sensors, 8 mm × 8 mm in size, and 500 μm thick. Each diamond is placed in a module box constructed from G10 plates providing electrical shielding and mechanical support. Contrary to the BCM, the BLM does not provide measurements on a collision-by-collision basis. The loss signals are integrated during 12 different time intervals, ranging from 40 μs (about half of the duration of one turn of the beam) to 84 s. In addition, the beam abort thresholds depend on the beam energy; they are defined in 32 energy intervals. Hence, each monitor has $12 \times 32 = 384$ beam abort thresholds associated.

4.3.4 The Radiation Monitoring System

The radiation field in the ATLAS Inner Detector created during the data taking consists of the neutral and charged particles, originating from primary *pp* interactions and from interactions of these particles with the detector material. The particles energy spectra range from thermal (in the case of neutrons) to TeV. The expected radiation doses in the innermost layers of the silicon detectors after collecting the integrated luminosity of 350 fb^{-1} exceed 100 kGy [69]. Predicted displacement damage in the silicon will be equivalent to exposure to a fluence of order of 10^{14} 1 MeV neutrons per cm^2 [70]. The measurements of the Total Ionising Dose (TID) and Non-ionising energy loss (NIEL) are vital for understanding the performance changes of the SCT and the Pixel detectors and their readout electronics during the operation, caused by the radiation damage. Moreover, the measured doses are needed to verify the fluence and dose prediction models that in turn make it possible to accurately estimate the evolution of the leakage current and depletion voltage in the silicon detectors.

Because of the facts presented above the system for monitoring radiation doses inside the Inner Detector has been set up [71; 72]. It is composed of 14 stations placed in various locations inside the ID volume and it provides on-line information of an ionization dose in Si0_2, NIEL in the silicon and damage to the DMILL [73; 74] transistors. Table 4.1 lists the locations and expected doses for the ID radiation monitor modules.

Table 4.1: Locations and expected doses after ten years of LHC operation at a designed luminosity for the RadMon modules in the ATLAS Inner Detector [75].

Location	r [cm]	z [cm]	ϕ [^{o}]	Φ_{eq} [10^{14} Neq/cm^2]	TID [10^4 Gy]
Pixel support tube	23	+89(-89)	90, 270 (0,180)	2.33	14
ID end-plate	54	+345 (-345)	15, 195 (105,285)	2.35	6.7
ID end-plate	80	+345 (-345)	15, 195 (105,285)	1.06	1.91
Cryostat wall	110	0	90,270	0.51	0.76

4.3.4.1 Radiation Monitor Sensor Board

The basic element of the radiation monitor system is the Radiation Monitor Sensor Board (RMSB), shown in Figure 4.11. It hosts several silicon radiation detectors using different measurement techniques to measure different types of radiation a wide range of doses:

- TID Measurement

  The Radiation Field Effect Transistors (RADFET) are used to measure a total ionising dose. The sensing technique exploits the fact that the electrical parameters of the transistor change with the absorbed dose. An electrical measurement of the threshold voltage shift gives a relative value of the dose in rad or Gy(Si) [76]. The thickness of the transistor oxide determines its sensitivity and dynamic range. Three types of RADFET with different oxide thickness are used on each RMSB to cover a wide dynamic range: 1.6 μm oxide thickness with a sensitivity range from mGy up to 10 Gy total dose [77], 0.25 μm oxide thickness for doses up to tens of kGy from the Radiation Experiments and Monitors (REM) [78], and 0.13 μm oxide thickness for measurements up to 105 kGy from REM.

- NIEL Measurements

  Silicon diodes are used to measure a non-ionising energy loss. The bulk damage in the silicon caused by irradiation manifests itself in changed electrical properties of the diodes. Two measurement methods are used: a change in the forward voltage on a p-i-n diode at a given forward current, and a leakage current increase in a reverse biased, fully depleted epitaxial pad diode. The bulk damage in a p-i-n diode causes minority carrier lifetime degradation and in a consequence an increase in the resistance. In the first method, the measured parameter is therefore the voltage change when driving a specific current through the diode. Two diodes are mounted on each radiation monitoring unit:

- p-i-n diode from CMRP, Wollongong, Australia, capable of measuring the fluence in range from 10^8 Neq/cm^2 to 2×10^{12} Neq/cm^2 [79].
- photo diode BPW34F from OSRAM [80], capable of measuring the fluence in range from 10^{12} Neq/cm^2 to 10^{15} Neq/cm^2.

In the second method, the monitoring of the leakage current in a diode in reverse bias mode is used to measure the NIEL. The leakage current increase after irradiation is directly proportional to the non-ionising energy loss. A silicon pad detector-diode with a guard ring structure (0.5 x 0.5 cm^2) from CiS [81] is used to measure an increase in the leakage current. Its active thickness of 0.25 μm allows depletion with less than 30 V for the whole lifetime of the experiment. Annealing studies have shown that it can also be used for fluences greater than 10^{15} Neq/cm^2.

- Thermal Neutron Fluence Measurement

  The n-p-n DMILL transistors are used in the on-detector readout electronics in the SCT and TRT systems. They are sensitive to irradiation with fast hadrons as well as thermal neutrons, which causes degradation of the common emitter current gain factor $\beta = I_c/I_b$ (collector current/base current). The degradation of β caused by irradiation with fast hadrons and thermal neutrons can be described by the formula [82]:

$$\frac{1}{\triangle\beta} = k_T \times \Phi_T + k_{eq} \times \Phi_{eq} \tag{4.1}$$

  where Φ_{eq} is the 1 MeV equivalent fluence and Φ_T is the fluence of thermal neutrons. The coefficients k_T and k_{eq} refer to the corresponding damage factors determined from transistor calibration measurements. The fast neutron fluence Φ_{eq} is measured with diodes, as mentioned above. In order to measure the fluences of thermal neutrons in the range a few times larger than 10^{12} n/cm^2, two n-p-n DMILL bipolar transistors are mounted on each RMSB.

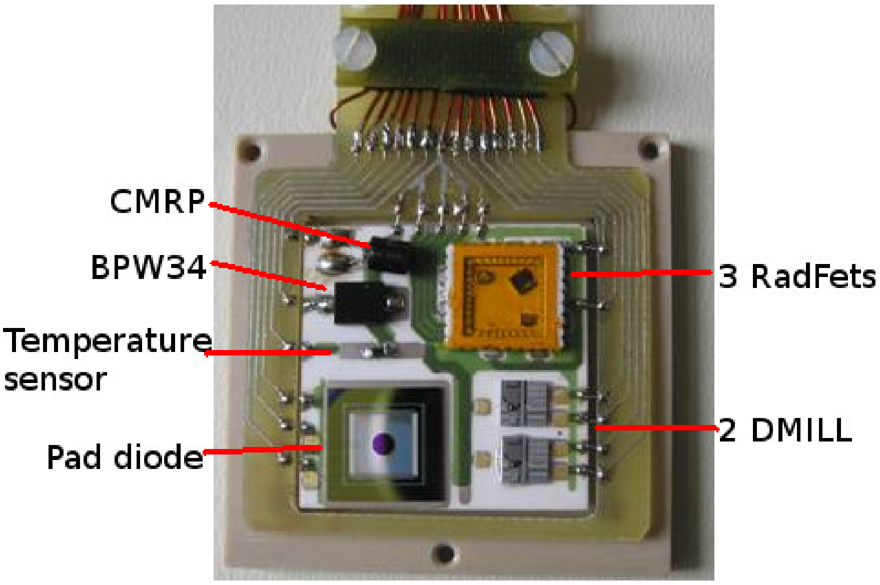

Figure 4.11: Top side of the ID Radiation Monitor Sensor Board. The hybrid contains RADFET package, CMRP diode, BPW34F diode, epitaxial Si diode, two DMILL test structures and a temperature sensor. Foto taken from [75].

The Inner Detector RMSB hosts three RADFET (three oxide thicknesses: 1.6, 0.25 and 0.13 μm), one CMRP diode, one BPW-34 diode, one epi-Si diode and two DMILL test structures. The temperature of the board is monitored with a 10 kOhm NTC sensor. There are 14 RMSB located in the Inner Detector: four hosted on the pixel support tube, eight on the ID end-plate at two different radii, and two on the cryostat wall. Their exact locations and expected doses after 10 years of operation at a designed luminosity are presented in Tab. 4.1

Chapter 5

The Inner Detector Control System

All the sub-detectors of the Inner Detector have their own control systems, which are under responsibility of dedicated sub-detector working groups. However, as described in Chapter 4, the SCT, the Pixel Detector and the TRT share services and control to address their common issues or (sometimes) conflicting needs. A dedicated control system, called the Inner Detector Environment DCS (IDE DCS), was built to address those issues. The IDE DCS comprises several projects, which in most cases are designed with the use of typical software and hardware solutions and strategies described in Chapter 3. For this reason, instead of giving technical details for each of the IDE DCS sub-projects, we focus on selected operational aspects or non-standard solutions.

5.1 The overall architecture of the Inner Detector DCS

The IDE DCS forms one branch of the ATLAS DCS and serves to control all the services described in Chapter 4. The IDE DCS is distributed among eight computers. A schematic overview of the IDE DCS is shown in Figure 5.1. One computer, the IDE SCS, operates at the highest levels of the IDE control hierarchy. The SCS plays the role of an interface to the ATLAS DCS. The remaining seven systems are designated as the LCS: four needed to operate environmental systems (cooling, environment conditions, sonar, thermal enclosure heater pads) and three more being responsible for operation of the beam condition and radiation monitoring (BCM, BLM, RADMON). Each LCS is directly interfaced to control the hardware by means of a CAN bus, Modbus or custom communication protocols. The connection between all the workstations of the DCS is over an ATLAS private network with a firewall to external internet to enhance cyber-security. Different portions of the hierarchy can be taken under control by different operators. For example each project may be operated as a distinct entity apart from the rest of the Inner Detector and ATLAS. This gives operational independence for commissioning, debugging, calibration etc.

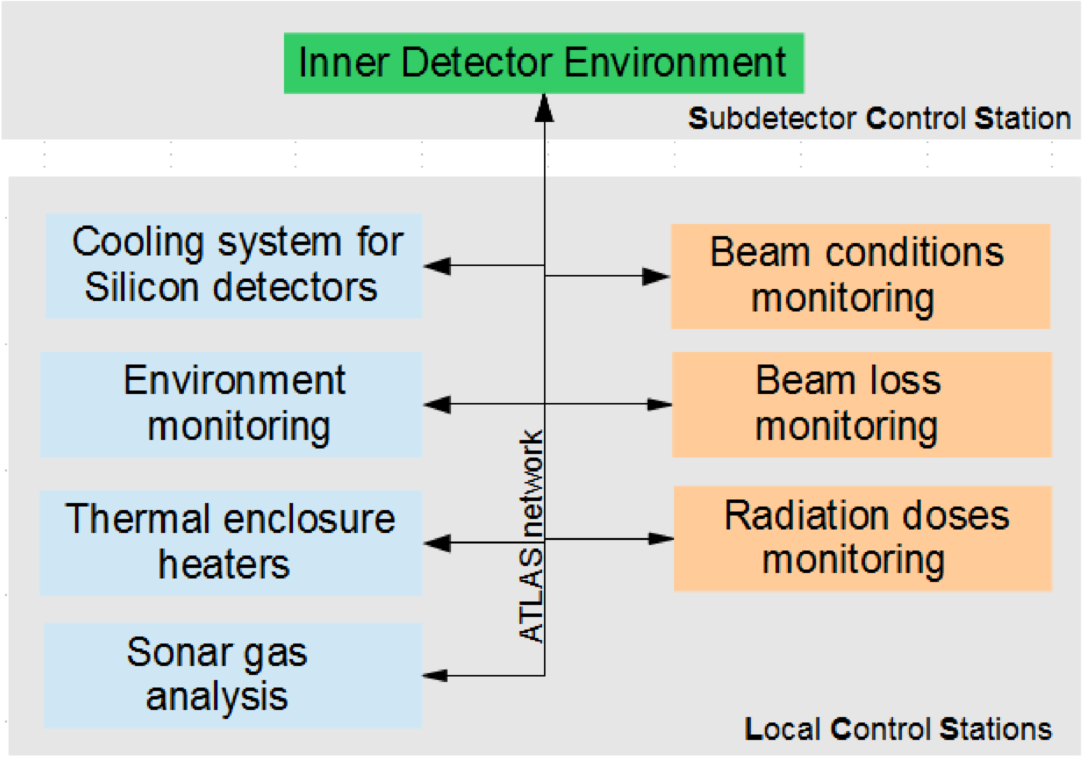

Figure 5.1: Schematic view of the Inner Detector Environment control system.

The hardware equipment of the IDE DCS is distributed over two areas: the underground electronic rooms USA15 (computers and FE electronics) and US15 (FE electronics) located on both sides of the ATLAS experiment cavern. The US15 is closer to the experimental cavern, thus during the LHC operation it is not accessible to the personnel. A small fraction of the IDE DCS equipment is also located in the ATLAS experiment cavern, UX15, thus it must be rad-tolerant and immune to the magnetic field.

5.2 The IDE Sub-detector Control Station

The primary function of the sub-detector control station is to run the main FSM tree for the IDE system, to enable the stand-alone operations and to serve as a link between the IDE subsystem and ATLAS DCS. The most crucial and sophisticated automatic safety actions which involve checks and actions crossing a single system boundary are implemented into the SCS.

5.3 Cooling DCS

The cooling for the silicon detectors described in 4.2.1.4 is supervised by a dedicated control system [83], shown in Figure 5.2. The Local Control Station plays a supervisory and monitoring role for a set of PLCs that perform actual control of the cooling plant and individual loops [84]. The PLC controls also the heater power by means of the Proportional-Integral-Derivative (PID) controller to maintain a temperature at the exhaust of the cooling pipe always around 20°C. The fundamental components of the cooling system i.e. compressors, PLCs, vacuum pumps, are powered by the Uninterruptible Power Supply (UPS). In case of power failure minimal operation and save recovery of the cooling plant is guaranteed. The PLCs can work autonomously with the control interface provided by a manual panel, or supervised by the DCS computer.

The *interface PLC* handles communication to the external DCS system and PLC plant and acts as a firewall protecting the control PLCs. It communicates with the DCS computer via Modbus over TCP/IP ATLAS technical network[1]. The *interface PLC* distributes commands from the DCS to worker PLCs and sends back readouts of the cooling plant parameters.

The cooling system is described in the DCS project by $\sim$ 100 thousand configuration and monitoring parameters in total. Expert users have access to all these

---

[1] The ATLAS technical network is a private experiment network, which for safety is firewalled from general network.

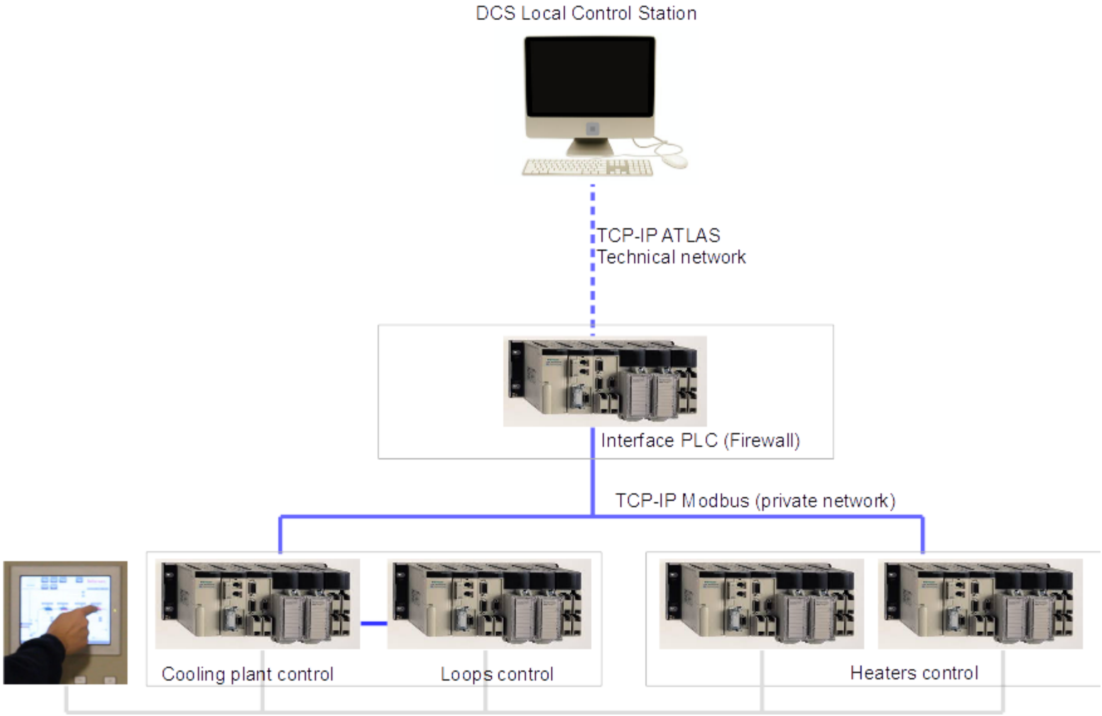

Figure 5.2: An architecture of the control system for the ID evaporative cooling system.

parameters by means of dedicated panels and tools. However, during normal operations a hierarchical control, the FSM representation shown in Figure 5.3, is used. In the FSM, the evaporative cooling system is divided into parts that correspond to the TTC partitions of the sub-detectors - Pixel, SCT barrel, SCT end-cap A, SCT end-cap C. Each of them is then split into four quadrants, numbered Q1 through Q4. Each quadrant contains a number of “loop” device units, one for each cooling circuit of the relevant TTC partition serviced through the corresponding quadrant.

Besides the FSM nodes related to the TTC partitions, there are four control units that represent infrastructure elements: general plant, power supplies for heaters, IDE gas system and distribution racks. All of them have again a substructure of device units that correspond to particular hardware elements.

There are 204 loop device units (88 in the Pixel Detector, 44 in the SCT Barrel, 36 in the SCT end-cap A, 36 the SCT end-cap C) representing each in-

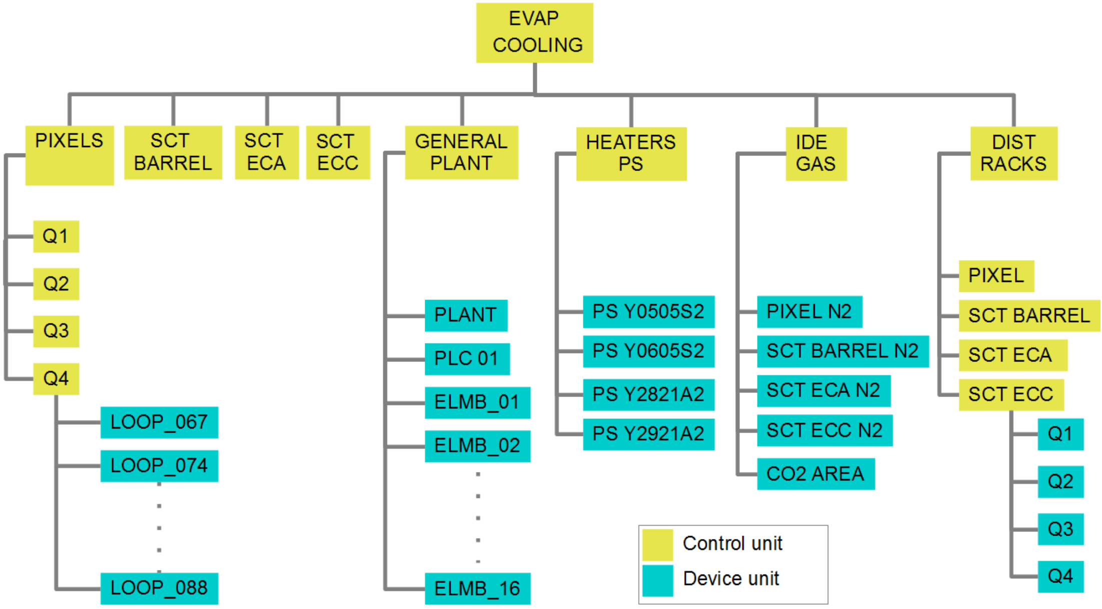

Figure 5.3: FSM control hierarchy for the ID evaporative cooling system.

dividual cooling circuit in the FSM tree. Each loop device unit is characterised by several monitoring and configuration parameters. In general, all loop DUs have the same functionality; however, there are small differences in the number of the temperature sensors. The DCS user interface for one SCT loop DU is shown in Figure 5.4. The temperature is measured in four different places of the on-detector cooling circuit (the temperature sensors marked as C1, C2, C31, C32, S1, S2), as shown in Figure 5.4. Two redundant sensors (S1, S2) placed on the exhaust of the tube on the detector structure are dedicated to a hard-wired interlock system, which protects the silicon detectors against overheating in case of cooling malfunctioning. These sensors measure the temperature next to the last silicon detector module on the cooling loop. If the mass flow of the coolant is insufficient to cool all the silicon modules on the cooling loop, the last module on the structure will sense this anomaly the earliest. The hard-wired interlock system maps appropriate temperature sensors to the power supply channels serving the silicon modules belonging to a given loop. If the temperature at the sensor position measured by a sensor exceeds a predefined threshold, the interlock system cuts off the corresponding power supply channels. Another hard-wired interlock mechanism is commissioned to protect the heater against overheating.

The temperature sensor attached to the heater surface deliver an interlock input signal.

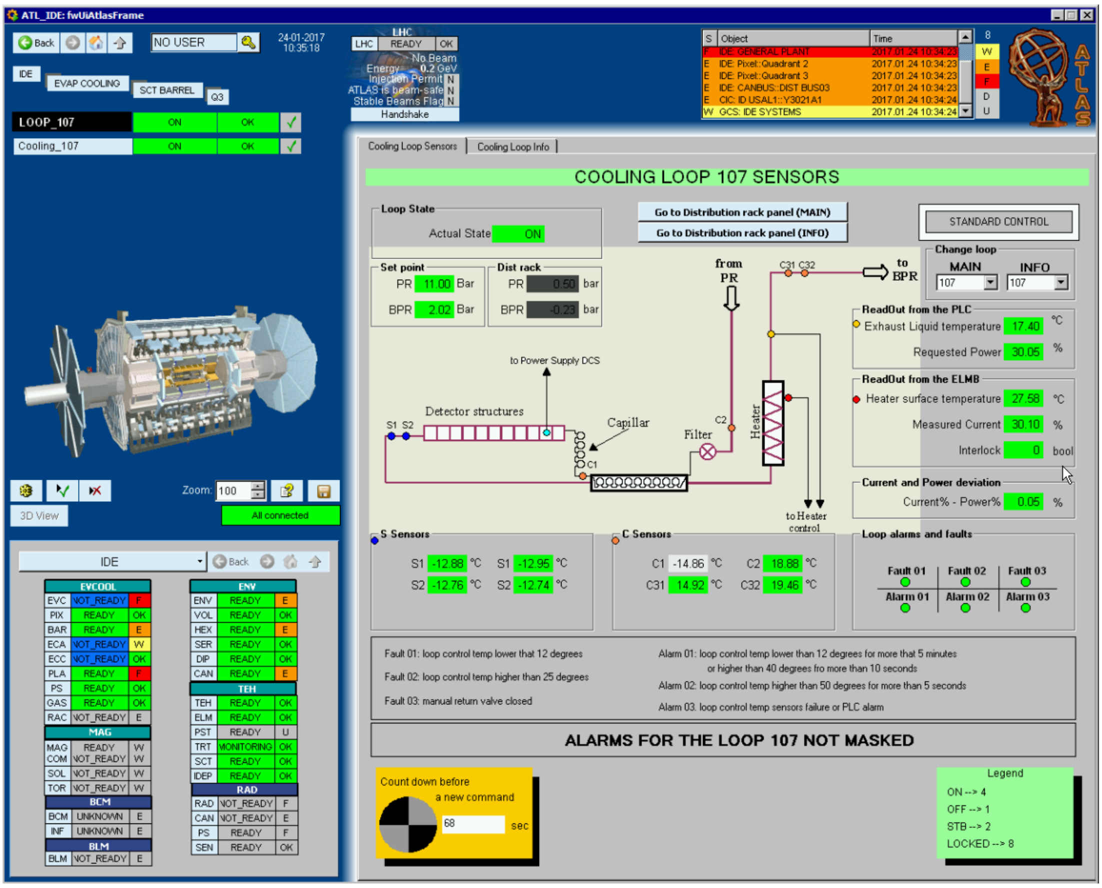

24-01-2017 10:35:18

LOOP_107	ON	OK	✓
Cooling_107	ON	OK	✓

LHC	READY	OK

No Beam
Energy 0.2 GeV
Injection Permit N
ATLAS is beam-safe N
Stable Beams Flag N

S	Object	Time
F	IDE: GENERAL PLANT	2017.01.24 10:34:23
E	IDE: Pixel::Quadrant 2	2017.01.24 10:34:23
E	IDE: Pixel::Quadrant 3	2017.01.24 10:34:23
E	IDE: CANBUS::DIST BUS03	2017.01.24 10:34:23
E	CIC: ID USAL1::Y3021A1	2017.01.24 10:34:24
W	GCS: IDE SYSTEMS	2017.01.24 10:34:24

8
W
E
F
D
U

Loop State
Actual State ON

Set point
PR 11.00 Bar
BPR 2.02 Bar

Dist rack
PR 0.50 bar
BPR -0.23 bar

Change loop
MAIN 107
INFO 107

ReadOut from the PLC
Exhaust Liquid temperature 17.40 °C
Requested Power 30.05 %

ReadOut from the ELMB
Heater surface temperature 27.58 °C
Measured Current 30.10 %
Interlock 0 bool

Current and Power deviation
Current% - Power% 0.05 %

S Sensors
S1 -12.88 °C S1 -12.95 °C
S2 -12.76 °C S2 -12.74 °C

C Sensors
C1 -14.86 °C C2 18.88 °C
C31 14.92 °C C32 19.46 °C

Loop alarms and faults

Fault 01	Fault 02	Fault 03
●	●	●
Alarm 01	Alarm 02	Alarm 03
●	●	●

Fault 01: loop control temp lower that 12 degrees
Fault 02: loop control temp higher than 25 degrees
Fault 03: manual return valve closed

Alarm 01: loop control temp lower than 12 degrees for more that 5 minutes or higher than 40 degrees fro more than 10 seconds
Alarm 02: loop control temp higher than 50 degrees for more than 5 seconds
Alarm 03. loop control temp sensors failure or PLC alarm

ALARMS FOR THE LOOP 107 NOT MASKED

Count down before a new command 68 sec

Legend
ON --> 4
OFF --> 1
STB --> 2
LOCKED --> 8

Zoom: 100

All connected

IDE

EVCOOL		
EVC	NOT_READY	F
PIX	READY	OK
BAR	READY	E
ECA	NOT_READY	W
ECC	NOT_READY	OK
PLA	READY	F
PS	READY	OK
GAS	READY	OK
RAC	NOT_READY	E
MAG		
MAG	READY	W
COM	NOT_READY	W
SOL	NOT_READY	W
TOR	NOT_READY	W
BCM		
BCM	UNKNOWN	E
INF	UNKNOWN	E
BLM		
BLM	NOT_READY	E

ENV		
ENV	READY	E
VOL	READY	OK
HEX	READY	E
SER	READY	OK
DIP	READY	OK
CAN	READY	E
TEH		
TEH	READY	OK
ELM	READY	OK
PST	READY	U
TRT	MONITORING	OK
SCT	READY	OK
IDEP	READY	OK
RAD		
RAD	NOT_READY	F
CAN	NOT_READY	E
PS	READY	F
SEN	READY	OK

Figure 5.4: The FSM user interface for loop device unit. The main panel display monitoring parameters and alarm information for one cooling loop. The color coding convention is used to create intuitive operator interface: green indicates good operation state of given object; yellow, orange and red indicate warning, error and fatal condition, respectively.

Operation modes. In the course of routine operation of the detector four predefined configurations, the so-called recipes, are used for moving cooling loops from one operation state to another. The recipes contain the alarm and warning levels for each operational state, information about inactive cooling loops and the settings of the pressure and back-pressure regulators. The configurations are stored in the Configurations Database and loaded when the FSM command to change the operation mode is issued. The following operation modes are defined:

- ON mode - the cooling mode with refrigerant circulating in the cooling loop(s). The transition to ON mode is triggered by the FSM command, which triggers appropriate commands to the PLC. In ON mode the inlet pressure and back pressure regulators are open and set to nominal pressure and back-pressure values, the heater power is switched on, the coolant in liquid state is injected into the circuit and the PLC controls the supplied heater power.

- STB mode - this is a transient state used to move the cooling loops to OFF state smoothly without thermal shocks. Upon the STB command from the DCS, the PLC closes the loop inlet valve and pressure regulator so that refrigerant is no longer delivered to a given circuit. The back pressure regulators remain open at the operation set point, letting the remaining coolant liquid evaporate from the circuit. In this way the temperature on the cooling loop does not fall below the operating temperature. The heater power is reduced gradually to zero with a decreasing flow. When the whole coolant is evaporated and there is no request for heater power, the loop is turned to OFF mode.

- OFF mode - on the reception of the command from the DCS, the PLC opens fully the back pressure regulator. The vapour remaining in the cooling circuit can return to the plant. At this stage only a small amount of the coolant vapour should be present in the loop in order to avoid thermal shocks.

- LOCKED mode is reserved for unused or faulty loops that should stay closed. The coolant distribution lines to the loop are closed and the heater power supply is off.

The commands implemented in the FSM allow a single cooling loop or a group of loops serving a given detector partition to be moved into a desired state.

Performance and plans. The IDE cooling system operates reliably; however, the commissioning of the ID cooling system was a challenging task because of a high level of the system complexity and scale. One of the most important issues was to establish optimal set points to avoid dangerous thermal shocks during the loop start-up and shut-down procedures. In Figure 5.5 the temperature evolution measured at the SCT end-cap cooling loop during state transition from ON to STANDBY and from STANDBY to ON is shown.

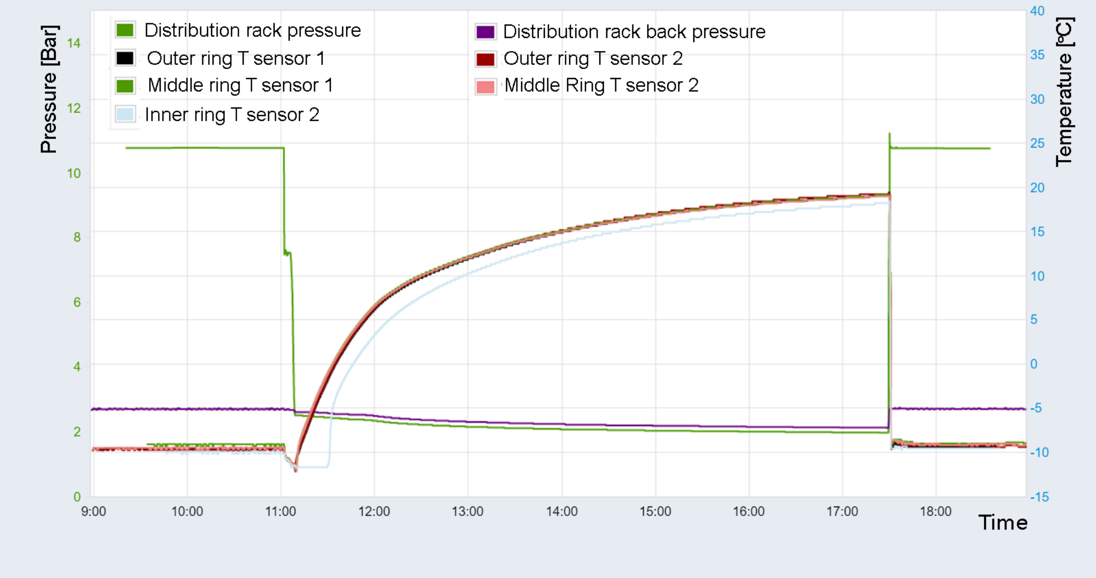

Figure 5.5: Temperature evolution measured in five positions at the SCT end-cap cooling loop144 during state transition from ON to STANDBY and from STANDBY to ON. The measurement was done on 8th of March 2017, when the cooling was switched OFF for hardware intervention. The distribution rack pressure and back pressure are also shown. After setting the distribution rack pressure to the value corresponding to STANDBY, the temperature drops only slightly (about 2°C) and then rises smoothly as the remaining coolant evaporates.

The reliability of the compressor system turns out to be the major issue in the present cooling system maintenance. Because of a high compression ratio and thus high compressor stress, the oil-free compressors suffer from fatigue cracks that can cause failures and leaks. The external part of the cooling system will be modified by replacing the compressors with a gravity-driven thermosiphon natural circulation plant [54].

5.4 Environmental DCS

The Environmental Control System (IDE ENV) [85] is designed to monitor the Inner Detector environmental sensors described in Chapter 4.2.1.6. The hardware readout chain consists of a series of cables connecting the sensors with the ELMBs located on the galleries in the ATLAS cavern. The readouts are further transferred over 100 m via a CAN bus to the experiment service rooms where the DCS computer is installed. The environmental project collects and displays the temperatures and humidities along with the values calculated from these sources, such as the dew point. The FSM representation of the environmental sensor is designed to be easily matched with the other DCS projects, especially the cooling project and the SCT or Pixel DCS. The first layer in the FSM hierarchy is divided according to functionality into five control units. Three units are for environmental sensor monitoring: ID VOLUME for the temperature and humidity information for the Inner Detector volume; HEX Heaters for the sensors associated to the cooling loops in the Pixel Detector and SCT; and SERVICES, which represents the temperature sensors in the cable trays. Two additional control units are designated to monitor the quality and state of communication protocols.

5.5 Thermal enclosure heaters DCS

The heaterpads used in the thermal barriers in the Inner Detector volume vary in terms of their electrical characteristics and power wire connections. At the time when the experiment was being installed, there was no commercial system available which could comply with a wide spread of the pad's electrical characteristics. For this reason a custom control system has been designed. The system has been installed in one rack in the US15 cavern and one rack in the USA15 cavern. The two racks are independent of each other; however, a few control signals can be passed between them, e.g. the reset of the interlocks and the ELMBs. Power supplies used to power different sections of the control system (48 volts and ±5 volts power supplies) are also held in racks. The power is delivered from the rack through hardware switching cards into the ATLAS detector heater pads. The whole heater pad control system consists of 33 switching cards housed in two electronic racks. In addition there is one controller card installed in each technical cavern. It distributes control and DSS signals to the switching cards. The heater pad control hardware draws the power from 48 volt power supplies and delivers it to the heater pads. The control system also monitors the temperature sensors on the pads which are used in feedback closed-loop temperature control. Control parameters and status information (temperatures, alarms, currents etc.) are sent to the DCS computer every 5 seconds. The hardware cards communicate with the DCS computer running a dedicated project via a CAN bus protocol. On a daily basis the hardware control system is fully autonomous, it regulates the temperature and can run without being supervised by the DCS project.

The switching card. The basic building element of the heater pad control hardware is a switching card. It contains 16 identical channels (also called switching elements) and power handling electronics. The switching card control and monitoring circuitry is based on the ELMB board and FPGA (FLEX10K10 series). The ELMB is running a custom firmware.

The heater power is switched on and off in a pulse-width modulation fashion. The amount of power going to the resistive heating elements is regulated by a temperature control algorithm, the PID controller, running on an on-board processor. The PID is a control loop feedback mechanism. The PID controller continuously calculates the difference between the set point and the measured on-heater temperature, and attempts to minimize this difference over time by adjusting the power supplied to the heating element $v(t)$. The new value $v(t)$ is calculated in each loop iteration according to the weighted sum formula:

$$v(t) = K_p e(t) + K_i \int_0^t e(\tau) d\tau + K_d \frac{de(t)}{dt} \tag{5.1}$$

where $\mathrm{K_p}$, $\mathrm{K_i}$ and $\mathrm{K_d}$ are non-negative coefficients for the proportional, integral and derivative terms respectively. The loop cycle duration is about two seconds and the minimal step for power on-off transition is 1 millisecond to limit the detector interference and the power dissipation to the acceptable level. The heater duty cycle changes between 0 and 100% depending on the temperature difference to compensate. The current, temperature and duty cycle of each heating element are monitored.

All switching cards are identical hardware-wise; however, for flexibility their software can be configured to serve different heater pads power wiring and temperature sensors schemas. Each switching element can be controlled autonomously or a group of two or four channels can follow one leading channel. The configuration for one switching card comprises a map of active/broken heater pads and a map of active/broken temperature sensors, leading channel configuration, temperature set point, interlock multiplexing and interlock mask, PID coefficients, alarm levels for monitored temperature and current. All these parameters are stored in an on-board non-volatile memory, and in this way the system is ready to work immediately after power cycling. These extended configuration features are implemented for system flexibility, as the requirements during the life of the ATLAS may evolve owing to the changes of the detector working conditions.

The Control Card. The main operational functions of the Control Card are supervisory level control and system monitoring, security of the system and safety of the connected detector hardware. The Control Card receives and distributes the DSS control signals to the appropriate number of switching cards. The granularity of the DSS corresponds to the functional parts of the detector: End-cap A, End-cap C, Pixel Support Tube (PST), End-plate and Barrel. It distributes the Master Enable and ELMB reset signals to each of the switching cards on command from the DCS. The Control Card provides also the functionality to reset the hardware interlock signals in the switching cards. The two parts of the control system located in the UA15 and USA15 service caverns are connected to each other via three control lines, so that the control card in USA15 can issue reset of ELMBs and hardware interlock signals to the system located in US15 and vice-versa.

Hardware and software interlocks. Several tiers of safety precautions are implemented in the Thermal Enclosure Heaters (TEH) DCS software and hardware. The first line are alarms implemented within the DCS project. If the heater pad temperature or current exceeds the level of warning or alarm, the op-

Table 5.1: Summary of TEH DCS hardware and software safety interlocks.

Type	Level	Typical limits	Automatic action
DCS	Warning	13°C<T>25°C	Inform operator
DCS	Alarm	13°C<T>25°C	Inform operator, send SMS to the on-call expert
Firmware	Warning	T>27°C	Switch OFF affected heating element(s), send status to DCS
Firmware	Error	T>30°C	Disable 48 V to affected pad(s); Send status to DCS
Hardware	Interlock	T>40°C	Interlock cut off 48 V to affected pad(s)

erator will be notified by means of alarm screen and FSM displays. The second level of safety is implemented in the switching card processor firmware. In case of over-temperature or an over-current event, the firmware automatically turns off the power to the affected channel (or group of channels if they work in the FOLLOW mode). The ultimate safety is provided by a hardware interlock based on comparators installed in the temperature and current lines. The summary of temperature safety interlocks in the TEH system is given in Table 5.1.

The control hierarchy and operations. The thermal enclosure heaters DCS runs on a single computer located in the USA15 service room. It provides functionality to configure and monitor associated hardware elements. Two main groups of the software tools are provided. The expert tools for system configuration and control comprise dedicated libraries, scripts and panels. They are available to authorised experts under access control regime and provide such functions as loading configurations to switching cards, reset of the switching card processor, direct read and write access to on board FPGA registers, power supply control etc. An example of the expert control panel for a switching card is presented in Figure 5.6.

The expert actions are used rarely, only during the start-up after technical stops or power cuts or in case of failure. On a daily basis the FSM system representation and user interface are used by the operator. A subset of the FSM

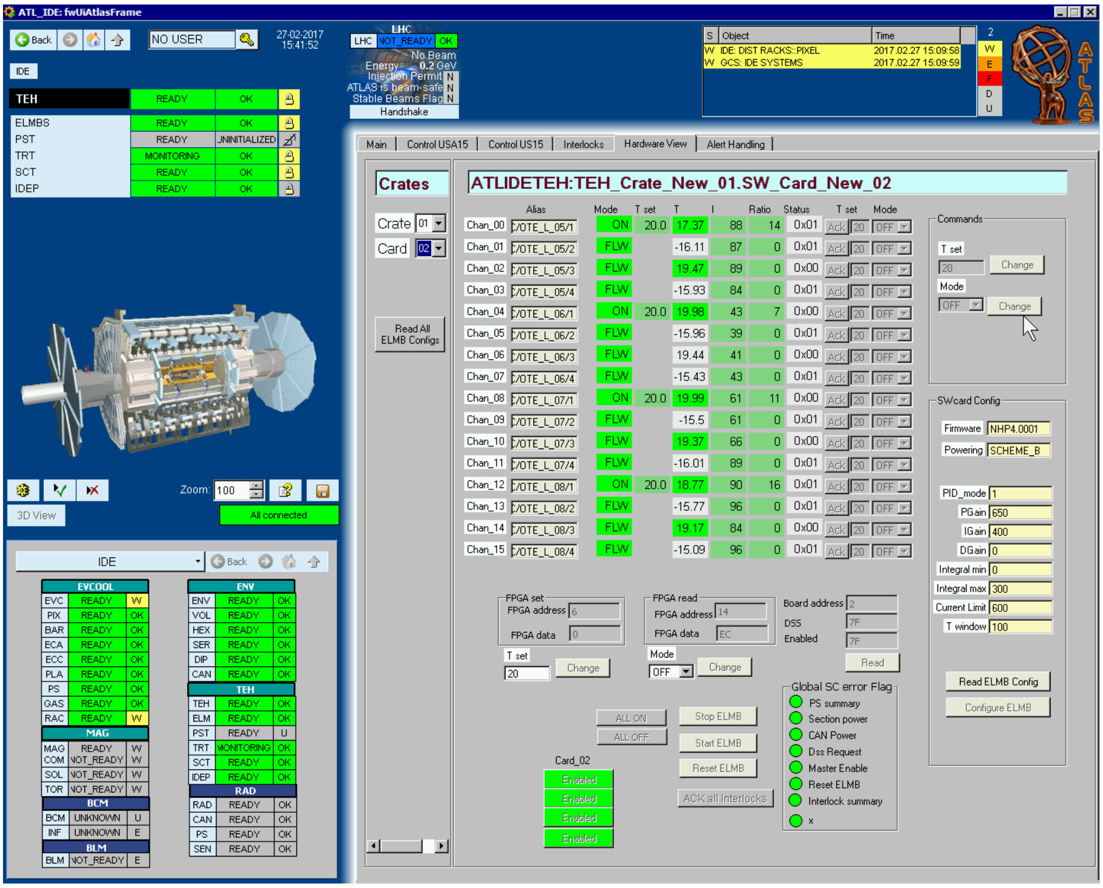

NO USER

27-02-2017 15:41:52

LHC: LHC NOT_READY OK
No Beam
Energy 0.2 GeV
Injection Permit N
ATLAS is beam-safe N
Stable Beams Flag N
Handshake

S	Object	Time
W	IDE: DIST RACKS::PIXEL	2017.02.27 15:09:58
W	GCS: IDE SYSTEMS	2017.02.27 15:09:59

2: W E F D U

TEH	READY	OK
ELMBS	READY	OK
PST	READY	UNINITIALIZED
TRT	MONITORING	OK
SCT	READY	OK
IDEP	READY	OK

Crate 01
Card 02

ATLIDETEH:TEH_Crate_New_01.SW_Card_New_02

	Alias	Mode	T set	T	I	Ratio	Status		T set	Mode
Chan_00	:/OTE_L_05/1	ON	20.0	17.37	88	14	0x01	Ack	20	OFF
Chan_01	:/OTE_L_05/2	FLW		-16.11	87	0	0x01	Ack	20	OFF
Chan_02	:/OTE_L_05/3	FLW		19.47	89	0	0x00	Ack	20	OFF
Chan_03	:/OTE_L_05/4	FLW		-15.93	84	0	0x01	Ack	20	OFF
Chan_04	:/OTE_L_06/1	ON	20.0	19.98	43	7	0x00	Ack	20	OFF
Chan_05	:/OTE_L_06/2	FLW		-15.96	39	0	0x01	Ack	20	OFF
Chan_06	:/OTE_L_06/3	FLW		19.44	41	0	0x00	Ack	20	OFF
Chan_07	:/OTE_L_06/4	FLW		-15.43	43	0	0x01	Ack	20	OFF
Chan_08	:/OTE_L_07/1	ON	20.0	19.99	61	11	0x00	Ack	20	OFF
Chan_09	:/OTE_L_07/2	FLW		-15.5	61	0	0x01	Ack	20	OFF
Chan_10	:/OTE_L_07/3	FLW		19.37	66	0	0x00	Ack	20	OFF
Chan_11	:/OTE_L_07/4	FLW		-16.01	89	0	0x01	Ack	20	OFF
Chan_12	:/OTE_L_08/1	ON	20.0	18.77	90	16	0x01	Ack	20	OFF
Chan_13	:/OTE_L_08/2	FLW		-15.77	96	0	0x01	Ack	20	OFF
Chan_14	:/OTE_L_08/3	FLW		19.17	84	0	0x00	Ack	20	OFF
Chan_15	:/OTE_L_08/4	FLW		-15.09	96	0	0x01	Ack	20	OFF

Commands: T set 20; Mode OFF

SWcard Config:
Firmware NHP4.0001
Powering SCHEME_B
PID_mode 1
PGain 650
IGain 400
DGain 0
Integral min 0
Integral max 300
Current Limit 600
T window 100

FPGA set: FPGA address 6; FPGA data 0
FPGA read: FPGA address 14; FPGA data EC
Board address 2
DSS 7F
Enabled 7F
T set 20
Mode OFF

Card_02: Enabled, Enabled, Enabled, Enabled

Global SC error Flag:
● PS summary
● Section power
● CAN Power
● Dss Request
● Master Enable
● Reset ELMB
● Interlock summary
● x

Zoom: 100

IDE

EVCOOL		
EVC	READY	W
PIX	READY	OK
BAR	READY	OK
ECA	READY	OK
ECC	READY	OK
PLA	READY	OK
PS	READY	OK
GAS	READY	OK
RAC	READY	W
MAG		
MAG COM	READY NOT_READY	W W
SOL	NOT_READY	W
TOR	NOT_READY	W
BCM		
BCM	UNKNOWN	U
INF	UNKNOWN	E
BLM		
BLM	NOT_READY	E

ENV		
ENV	READY	OK
VOL	READY	OK
HEX	READY	OK
SER	READY	OK
DIP	READY	OK
CAN	READY	OK
TEH		
TEH	READY	OK
ELM	READY	OK
PST	READY	U
TRT	MONITORING	OK
SCT	READY	OK
IDEP	READY	OK
RAD		
RAD	READY	OK
CAN	READY	OK
PS	READY	OK
SEN	READY	OK

Figure 5.6: The expert interface for switching card control and configuration in TEH DCS.

tree for the thermal enclosure heater pad system is shown in Figure 5.7. The TEH top node branches lower down into four Control Units corresponding to the sub-detector areas: PST, SCT, TRT, Inner Detector Endplate (IDEP); and one unit representing readout infrastructure (ELMBS). Each sub-detector is further split into geographical areas, e.g. the SCT breaks into two end caps, and further into elements representing different localisation of the heater pads. The bottom level of the tree is composed of the Devices Units representing single heater pads. While it is possible to send a command directly to a single pad control element using the channel device unit, broadcast commands can be sent to the switching cards through the sub-detector control units. A summary of the heater pad device unit is shown in Table 5.2

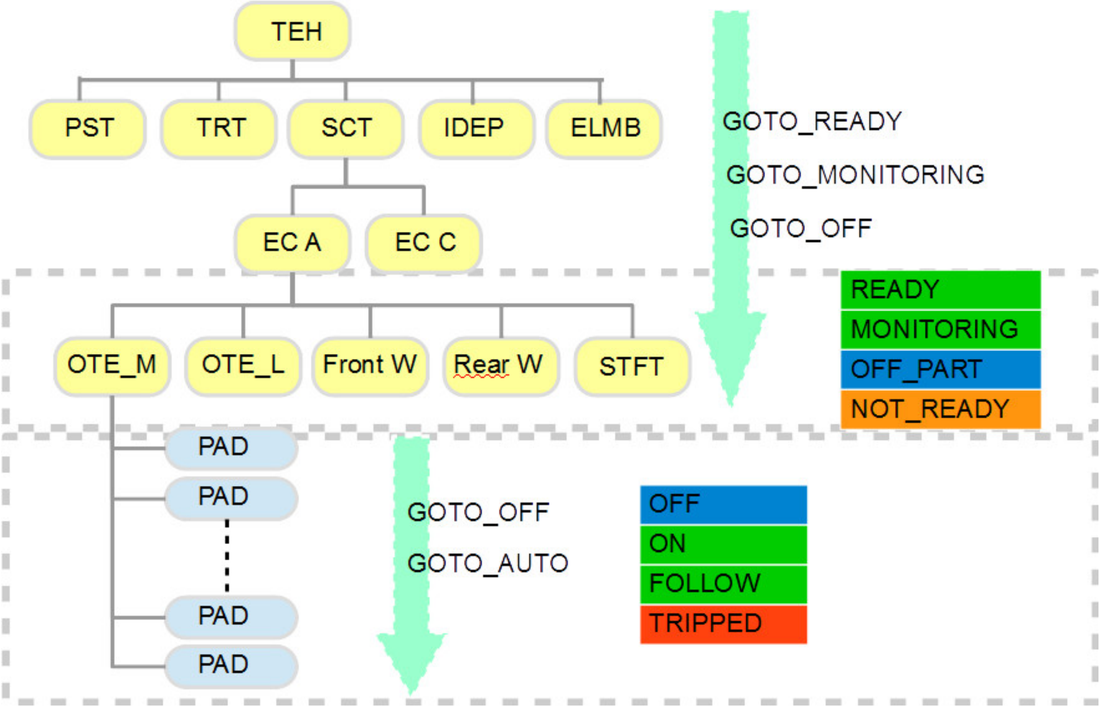

Figure 5.7: The subset of the TEH FSM tree with the state transitions at the level of partition control units and pad device units.

5.6 Sonar DCS

The ultrasonic instruments described in 4.2.1.7 are controlled and monitored by a dedicated DCS subsystem. It communicates with custom sonar electronics via Modbus protocol to control valves and pumps and to read back the measurements of temperature, pressure and transient time of sound pulses. The DCS provides also control over the measurement and calibration sequences that can be carried out manually by means of expert commands or in an automatised fashion via FSM functions and scripts. The DCS project provides also process visualisation tools via user panels, archiving of the sound transient times, velocities, flow rate, mixture composition, temperature and pressure into the ATLAS condition database.

The read-back parameters are processed in the DCS. The differences between the transit times in opposite directions are used to compute the gas flow rate, while the average of the transit times is used together with the known distance

Table 5.2: Operational states of the heater pad Device Unit.

State	Description
ON	Channel is enabled and 48 V output is enabled, the temperature regulation algorithm is running
FOLLOW	Reserved for heater pads connected parallely in groups of four or two. The control of the whole group is performed by one leading channel.
OFF	Channel not regulating, 48 V output closed.
TRIPPED	Channel in OFF state due to software or hardware trip.

between the transducers to calculate the sound velocity [59].

Gas composition analysis. Two types of gas composition measurements are carried out:

- The envelope gas contamination with C_3F_8 is measured to spy for possible coolant gas leaks inside the SCT, Pixel Detector and IBL volumes.
- Detection of ingressed non-condensible vapour (air, N_2) in a sub-atmospheric pressure surface condenser in the thermosiphon system.

The measurements exploit a physical phenomenon in which the sound velocity in a binary gas mixture at known temperature and pressure is a unique function of the molar concentration of two components with differing molecular weight [86]. The sound velocity in sonar instruments with moving gas, is continuously determined from bidirectional transient times of the sound pulses according to the formula:

$$\nu_s = \frac{2L(t_{up} + t_{down})}{4t_{up}t_{down}} \tag{5.2}$$

where L is the acoustic path length, ν_s is the sound velocity and t_{up}, t_{down} are sound transient times in two directions.

At the same time the temperatures and pressure measurements inside the instrument are provided. The sound velocity data are then compared with the velocity-composition look-up table. The reference data in the table are gathered from theoretical derivations made with the package called the NIST Reference Fluid Thermodynamic and Transport Properties Database (REFPROP)[1] [87]. The sound velocity in the look-up table is calculated in temperature and pressure steps of 0.5°C and 20 mbar. An on-line algorithm implemented in the DCS project performs bilinear interpolation between the values in the table that are closest to the measured temperature and pressure to calculate the molar composition of the N_2/C_3F_8 mixture. The precision of the gas composition measurement depends on the difference between the molecular weights of the two gas components and on the precision of the sound velocity measurement, and it was determined to be ±0.002% [58].

Gas composition analysis is performed on a regular basis in the SCT, Pixel Detector and IBL N_2 volumes, especially during cooling restart after a technical stop to check for coolant gas leaks. The concentration of C_3F_8 in the N_2 around the Pixel Detector measured during cooling restart in January 2016 is shown in Figure 5.8.

After a simultaneous start of all 88 Pixel Detector cooling loops, a steep rise in the C_3F_8 concentration was observed. Then the concentration increased slowly to a value of about 0.14% [59].

5.7 Radiation monitor control

The control system for radiation monitors in the Inner Detector volume is composed of the standard ATLAS DCS hardware building blocks, as shown in the diagram in Figure 5.9

The radiation monitor readout uses seven ELMB boards, each serving two radiation monitor sensor boards. The ELMBs are powered by 12 V CAN PSU modules. Modified 16 channel 12-bit ELMB Digital-to-Analog Converter (ELMB-DAC) boards [88] are used as the current source to power radiation monitoring modules. They provide the maximum output current of 20 mA per channel and the maximum output voltage up to 48 V. The power supply units and the

---

[1] REFPROP is a program based on the most accurate thermodynamic and transport properties models to calculate the state points of a fluid or mixture, provided by NIST - National Institute of Standards and Technology.

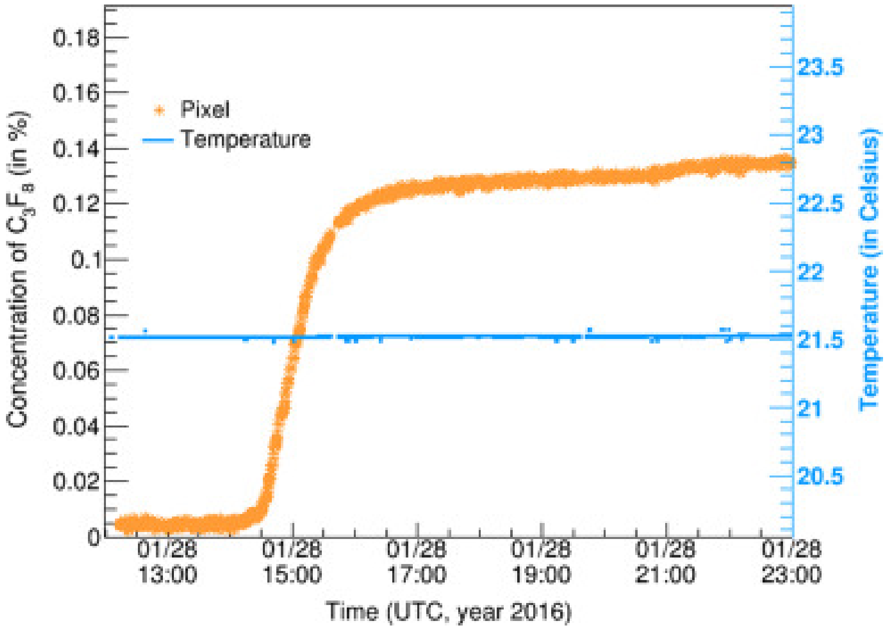

Figure 5.8: C_3F_8 concentration in the N_2-flushed enclosure of the Pixel Detector during cooling restart on January 28, 2016 [59].

computer which runs the DCS software are located in the USA15 service room, while the ELMBs and ELMB-DAC boards are located in the patch panel area in the first layer of muon chambers.

Both the configuration and control of the radiation monitor system are implemented in the DCS project. The sensor readout is triggered on a DCS request, within a configurable time interval, typically every two hours. Raw readout values are processed on-line in the DCS: the measured voltages and leakage currents are translated into fluences and doses employing parametrisations based on calibrated irradiation data and taking into account temperature and magnetic field dependent corrections [71]. The raw values are archived in the database to be used for a detailed offline analysis. These measurements are crucial to validate the simulations describing the radiation environment inside the ID volume. The simulations in turn play a fundamental role in understanding the radiation damage effect in the silicon detectors. Figure 5.10 shows measurements of TID and NIEL from the radiation monitor sensors placed at the Pixel Support Tube, ID end-plate and cryostat wall. The measurements for each localisation are average values for the sensors placed at the same radius and z, but at different azimuthal

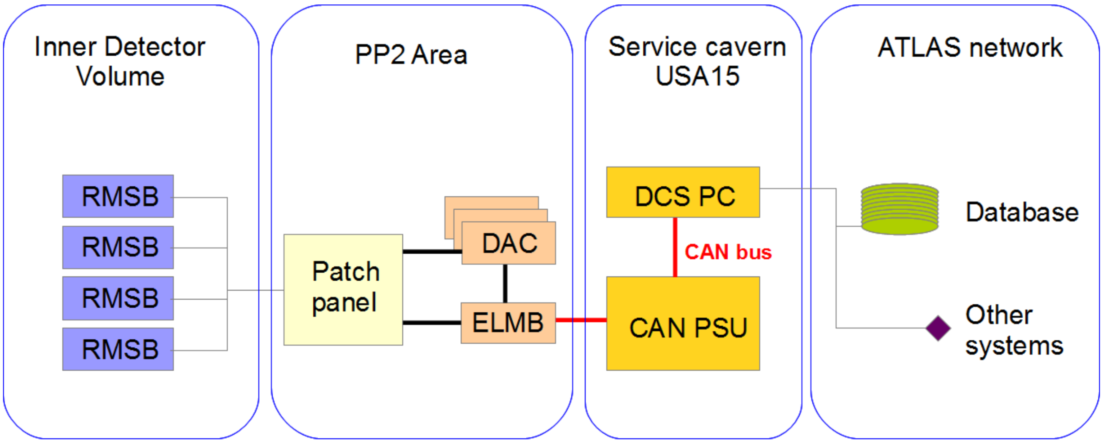

Figure 5.9: Simplified schematic view of the readout chain for radiation monitoring system. The ELMB-DAC is used as a current source. The readout is done by ELMB ADC.

angles.

5.8 The Beam Condition Monitor control system

The hardware layer of the BCM DCS system comprises standard building blocks: bipolar high voltage power supplies ISEG EHQ-8210 units [90] delivering +1000 V or -1000 V, depending on the type of a diamond sensor, and modified to provide the current monitoring resolution of 1 nA. The front-end electronics and amplifiers are powered by custom made low voltage power supplies used in the ATLAS SCT [91]. The configuration of the readout electronics thresholds and on-module temperature monitoring is handled by the ELMB-DAC and ADC functionality. The DCS software project runs on a dedicated machine and has a typical architecture with the implemented FSM hierarchy.

The most interesting part of the BCM DCS system is a module designed to control, configure and monitor the BCM readout driver boards. The read-out driver communicates with the outside world by means of the User Datagram Protocol (UDP) [92] over the internet. The core functionality of the WinCC OA was extended by developing a C++ library compiled into the framework. This extension handles exchange of UDP data packets between the WinCC OA project

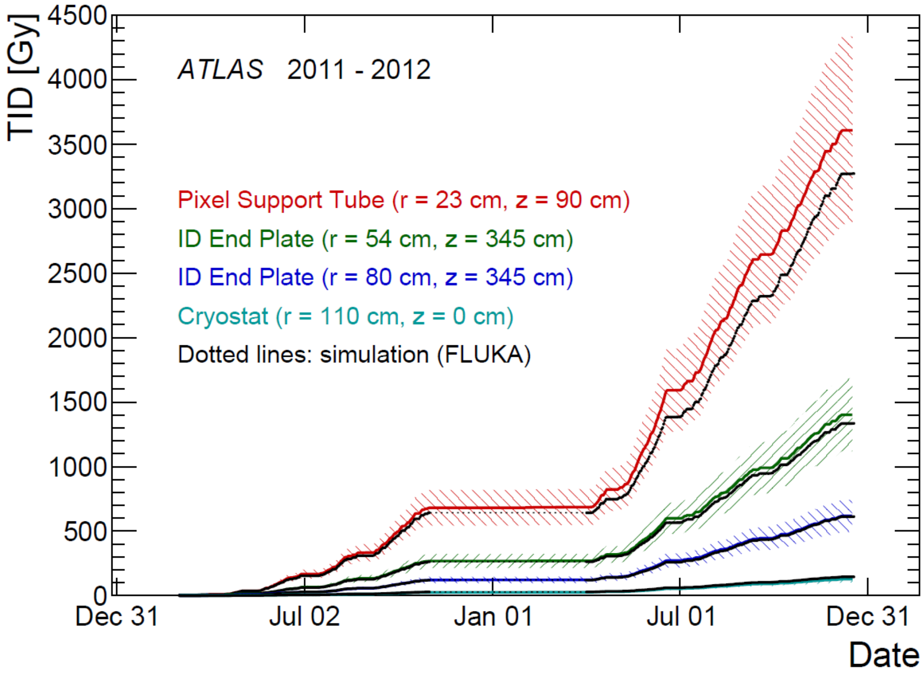

(a)

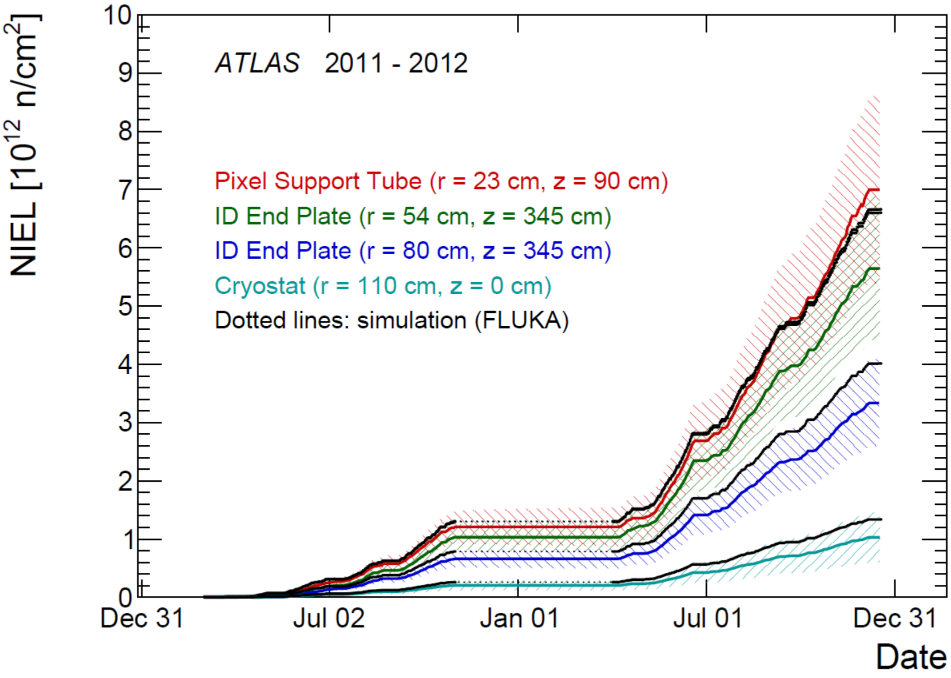

(b)

Figure 5.10: Total ionising dose (left) and non-ionising energy loss (right) in four localisations inside ID volume. The coloured bands represent measurement uncertanity. The simulation predictions for each localisation are shown with black dotted lines [89].

and the readout driver. The DCS receives data packages on a regular basis, with frequency of about 1 Hz.

Read-out driver monitoring parameters. The DCS project receives an extensive set of monitoring parameters that fully describe the read-out driver status and configuration as well as signals registered by the BCM detector modules. A large part of DCS is dedicated to DAQ related parameters, e.g. configuration data for the RocketIO transceiver, ReadOut Driver (ROD) status signals, LVL1 trigger counts, signals delay settings (inhibit delay, trigger delay, latency delay) and the FSM state indicating the current mode of the ROD.

The second large group of the monitoring parameters are processed signals from the BCM detector modules:

- The reconstructed hit counts for all eight detector channels.
- Coincidence counters:
  - **A-C coincidences** a counter which requires coincidence in-time hits in the modules on both sides of the BCM detector;
  - **background A** - counts the bunch crossings for which at least one of the modules on side A registers out-of-time hits, while the module(s) on side C register(s) an in-time hit;
  - **background C** counter is analogical to the background-A counter.

The third group of monitoring parameters is related to the beam safety mechanisms. The beam abort flags are reported, including the beam-abort occurrences counter and configuration for algorithms generating the beam abort signal. The current status of injection permit and beam permit signals along with the mask status and value is also provided.

Read-out driver configuration from the DCS level. Several commands can be sent from the DCS software to the read-out driver. The fine and coarse delay settings determined during the time-calibration procedure are configured via the DCS. The DCS controls also configurations for disabling the DSS, beam-abort functionality and a reset of the ROD firmware.

Finally, at the FSM level the functions for rebooting and reprogramming of the read-out driver firmware are provided. To achieve that, the DCS software triggers a callback within a process running on the BCM DCS computer. This process then runs a Xilinx Impact tool that reloads the firmware to the ROD via the USB cable.

5.8.1 IDE BCM DCS configuration for the Beam Interlock System

The IDE BCM is included into the LHC Beam Interlock System (BIS) [93]. The BIS role is to collect the input *user permit* signals from the client systems (e.g. experiment BCMs, machine beam loss or beam position monitors etc.) and to deliver the beam dump request to the LHC Beam Dumping System if any of the client system reports not ready state. The BIS maintains a light signal, named the Beam Permit, in two redundant optical fiber loops around the LHC when all conditions are met. When any of the user permit is removed, the Beam Permit signal is interrupted [94]. In each insertion region two beam interlock controllers are installed. They provide the programmable logic for the decision for beam/extraction permit and record state changes. Input signals to the programmable logic unit may be masked. The injection of proton bunches from the Super Proton Synchrotron (SPS) is allowed only if all the systems report being ready for the beam via BIS. If the Beam Permit signal is removed while the beams are circulating, the beam dump system is fired and the injections from the SPS is blocked.

The BCM beam permit signal is generated in the readout drivers based on the processed data from the detector modules. The pulses from the detectors are counted within each bunch-crossing interval and the algorithm for the calculation of the beam permit flag is applied.

There is a handful of algorithms implemented in order to provide robust calculation for different beam operating conditions and to avoid false aborts [67]:

- The *basic algorithm* requires that at least 3 out of 4 low threshold readout channels and at least 3 out of 4 high threshold readout channels registered a hit within the same bunch crossing interval. This algorithm was used during the early LHC runs, but it is not suitable for high luminosity operations, when the probability to meet 3 out of 4 requirements, even with a good beam condition, increases.

- *X out of Y* algorithm extends the decision-making time window. It demands at least X bunch-crossing to satisfy the basic algorithm in any interval of Y consecutive bunch-crossing.
- *A forgetting factor algorithm* is a recursive method which gives less weight to the older occurrences of bunch intervals satisfying the basic algorithm condition over the recent ones.

The BCM generates five beam abort signals. One signal corresponds to the basic algorithm and two signals per each of the two extended algorithms (one signal for monitoring only and one to be used in the beam abort logic).

The configuration parameters for all signals are independently set and monitored from the DCS. The logic for generating a beam abort signal is also configurable. It can take into account the output of only one of the algorithms mentioned above, or a logic combination (AND, OR) of all three. The beam abort signal output can be also totally disabled.

5.8.2 BCM Safe for beam flag

The combined information about the BCM detector state, including data from the DCS hardware and ROD monitoring, is used in the DCS to calculate the so-called *safe for beam flag*. This flag is then used by the ATLAS detector during the LHC hand-shaking procedure described in Section 5.9. The safe for beam flag indicates whether the BCM is fully functional, powered and configured, ready to abort the beam if necessary. Several parameters are taken into account to calculate the BCM flag. The basic requirements are that the hardware beam permit flag is OK, the FSM DCS state of the whole BCM detector is READY, which means it is fully operational for data-taking, and that both readout drivers are in the correct state and the monitored detector noise level (average hit rate) is below a configurable threshold. The details of the BCM safe for beam flag and its ingredients are shown in the DCS panel (see Figure 5.11). Notice that the flag can be also masked or unmasked from this panel.

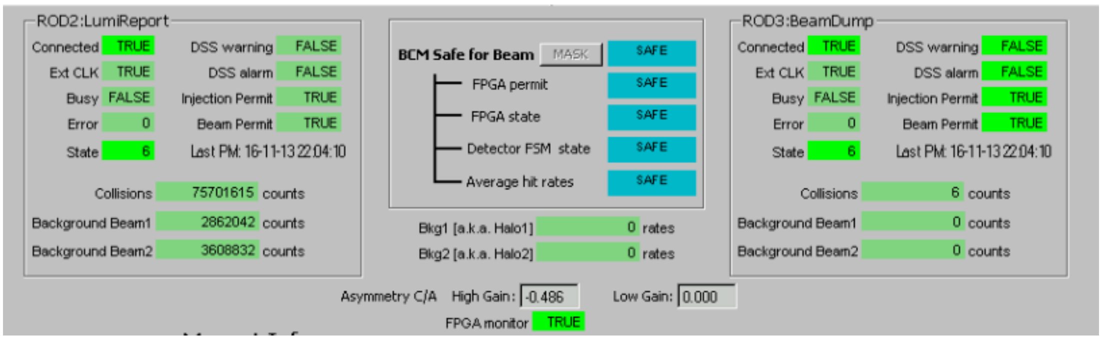

ROD2:LumiReport
Connected TRUE
Ext CLK TRUE
Busy FALSE
Error 0
State 6
DSS warning FALSE
DSS alarm FALSE
Injection Permit TRUE
Beam Permit TRUE
Last PM: 16-11-13 22:04:10
Collisions 75701615 counts
Background Beam1 2862042 counts
Background Beam2 3608832 counts

BCM Safe for Beam SAFE
FPGA permit SAFE
FPGA state SAFE
Detector FSM state SAFE
Average hit rates SAFE
Bkg1 [a.k.a. Halo1] 0 rates
Bkg2 [a.k.a. Halo2] 0 rates

ROD3:BeamDump
Connected TRUE
Ext CLK TRUE
Busy FALSE
Error 0
State 6
DSS warning FALSE
DSS alarm FALSE
Injection Permit TRUE
Beam Permit TRUE
Last PM: 16-11-13 22:04:10
Collisions 6 counts
Background Beam1 0 counts
Background Beam2 0 counts

Asymmetry C/A High Gain: -0.486 Low Gain: 0.000
FPGA monitor TRUE

Figure 5.11: The DCS user interface for the BCM safe for beam flag representation and its' ingredients.

5.9 LHC-ATLAS handshaking

Before the beam can be injected into the LHC ring, the so-called handshaking procedure [95] between the LHC control center (CCC) and the experiments must take place. This procedure consists of the exchange of predefined messages and comments which give a more detailed description of the LHC operation mode. The DIP protocol is used for this dialogue between the LHC control system and the control systems of the experiments. The LHC warns the experiments of the planned beam injection and waits for the answer from the experiments confirming that they are ready and in a safe mode for injection. The experiment can *permit* the LHC to inject the beam only if all the relevant sub-systems give the injection permit and safe for beam flag. While the injection permits are hardware signals, the safe for beam flags are generated by the DCS systems based on the equipment state.

The IDE includes three sub-detectors relevant to the handshake that give input to the overall ATLAS safe for beam flag: SCT, Pixel Detector and BCM. The silicon trackers have sensitive equipment, located at a minimum distance of 25.7 mm from the beams. Although the beam cannot be directed into the SCT, very intense flux of secondary particles from the interaction of part of the beam with the collimators can still damage the detector. This is particularly important during the injection and ramp. For this reason both the SCT and Pixel Detector go into the so-called STANDBY state in preparation for the beam injection. The STANDBY has a slightly different sense for both detectors. For the SCT it means that the modules are powered and configured, but with lowered sensor bias voltage (50 V instead of 150 V) just below full depletion. The Pixel Detector STANDBY corresponds to the modules being powered and configured, but not depleted, and with pre-amplifiers disabled [1].

5.9.1 IDE DCS beam-induced background monitoring script and warm-start

During the LHC operation, protons are continuously lost from the beam due to the various processes, e.g. collisions, beam cleaning, beam-gas scattering etc. Most of these backgrounds are mitigated by the cleaning collimator system; however, in some cases the beam-induced background can be a concern for the detector's operation and physics analysis. The background close to the beam-line may pass the aperture for the beam and make a large charge deposition in the inner-most layers of the detector, thus increasing the detector occupancy. The increased detector occupancy can in turn affect the dead-time of front-end electronics and degrade data-taking efficiency. The summary and characteristics of beam-induced backgrounds observed in the ATLAS are described in [96].

The Inner Detector DCS implements the software module for monitoring the beam induced background inside the IDE volume. This software runs on the IDE DCS SCS and combines the information available from several sources. The key input parameters are:

- the SCT detector occupancies (separate for barrel, end-cap A and end-cap C) recorded in the SCT Read-Out-System,
- the BCM background rates from both detector stations,
- the BLM rates,

---

[1] This is to avoid the front-end damage in anticipated events with highly localized charge densities created due to unstable beam conditions.

- the positions of the collimator system in the ATLAS insertion region,
- the residual beam vacuum pressure[1] measured at a distance of 22 m from the proton-proton interaction point.

The SCT occupancy, BCM and BLM rates are direct indicators of the beam-induce background presence inside the ID volume. The analysis of the 2011 data has shown that the beam-induced background seen in ATLAS at small radius is correlated with the pressure measured at 22 m [97]. For this reason, the beam vacuum pressure is included into the algorithm.

If the beam-induced background is low enough, the beam monitoring script publishes a flag for the silicon detectors to signalise that it is safe to perform the so-called warm-start procedure. As described in Section 5.9, the silicon detectors are set to STANDBY state during the beam injection and machine development. Only after the LHC finishes the beam commissioning and declares Stable Beams can the SCT and the Pixel Detector be switched on to nominal settings. The SCT warm-start procedure is fully automatised, a DCS thread is running to monitor the handshake with the LHC, the Stable Beam flag and IDE beam monitor flag. If all the flags are OK, the DCS propagates the command to go to nominal operational state (READY) to all the detector modules. It takes less than 50 seconds to bring the whole SCT detector to the READY state. The automatism of beam condition checks and the warm-start procedure significantly shortens the time needed to bring the detector to a data-taking state, as before it required shifter checks and actions. This improves the data taking efficiency and minimises data losses.

---

[1] The residual pressure of the beam pipe vacuum is monitored by the dedicated instruments (several vacuum gauges of Penning and ionisation gauges), placed at distances of: 22 m, 58 m, 150 m and 250 m from the interaction point in the ATLAS experiment.

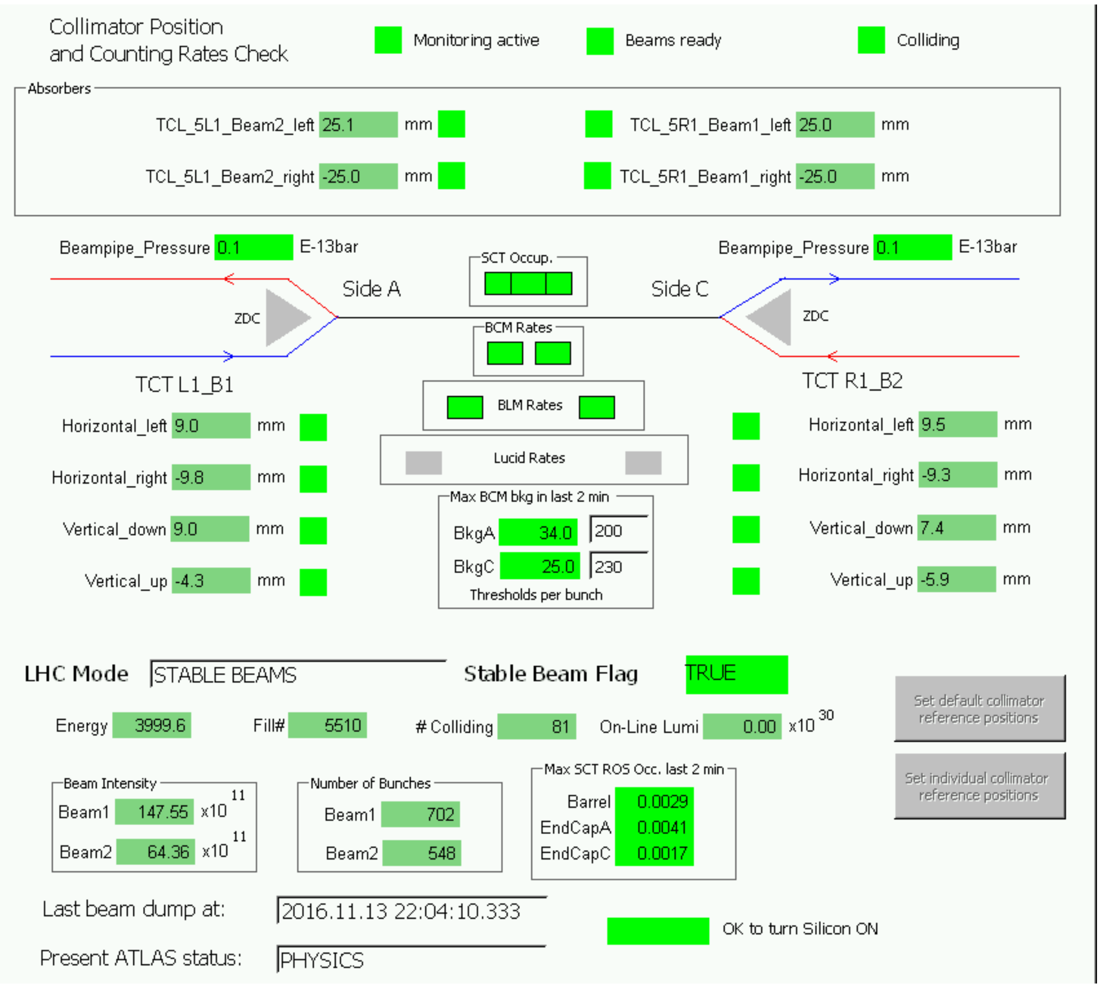

Monitoring active 🟩
Beams ready 🟩
Colliding 🟩

Absorbers
TCL_5L1_Beam2_left 25.1 mm 🟩
TCL_5L1_Beam2_right -25.0 mm 🟩
TCL_5R1_Beam1_left 25.0 mm 🟩
TCL_5R1_Beam1_right -25.0 mm 🟩

Beampipe_Pressure 0.1 E-13bar
Beampipe_Pressure 0.1 E-13bar

TCT L1_B1
Horizontal_left 9.0 mm 🟩
Horizontal_right -9.8 mm 🟩
Vertical_down 9.0 mm 🟩
Vertical_up -4.3 mm 🟩

TCT R1_B2
Horizontal_left 9.5 mm 🟩
Horizontal_right -9.3 mm 🟩
Vertical_down 7.4 mm 🟩
Vertical_up -5.9 mm 🟩

Max BCM bkg in last 2 min
BkgA 34.0 200
BkgC 25.0 230
Thresholds per bunch

LHC Mode STABLE BEAMS
Stable Beam Flag TRUE
Energy 3999.6
Fill# 5510
Colliding 81
On-Line Lumi 0.00 x10^{30}

Beam Intensity
Beam1 147.55 x10^{11}
Beam2 64.36 x10^{11}

Number of Bunches
Beam1 702
Beam2 548

Max SCT ROS Occ. last 2 min
Barrel 0.0029
EndCapA 0.0041
EndCapC 0.0017

Last beam dump at: 2016.11.13 22:04:10.333
Present ATLAS status: PHYSICS
OK to turn Silicon ON 🟩

Figure 5.12: The main panel interface for IDE DCS beam background monitoring.

Chapter 6

The Inner Detector maintenance, operations and performance

As described in Chapters 2 - 3, the ATLAS Inner Detector is a complex instrument composed of three independent sub-detectors and many common services. Ultimately all these elements must work in a perfectly synchronised way to provide the best possible measurements of charged particle trajectories for physics searches. In this chapter some of the operational aspects are described and the combined performance of the Inner Detector in *pp* collisions at the LHC is briefly discussed.

6.1 The LHC and ATLAS data taking

The LHC and ATLAS data taking so far comprises two periods, the so-called Run-1 and Run-2. The LHC Run-1 data taking started in 2010. During the initial phase of the LHC machine commissioning and establishing confidence in the collider protection system, the performance limits were exploited in 2011 and 2012 with centre-of-mass energy of 7 and 8 TeV. After more than two years of running the LHC delivered around 30 fb^{-1} of data, which enabled ATLAS and CMS to discover the Higgs boson [98]. In 2013 the LHC entered the LTS1 dedicated to conducting upgrades necessary for increasing the beam energy and luminosity. The LHC operations restarted in 2015 with $\sqrt{s} = 13$ TeV (Run-2) .

Table 6.1: The ATLAS data taking characteristics for all periods of Run-1 and Run-2 [99; 100].

Run	$\sqrt{s}$	Peak instantaneous luminosity [$cm^{-2}s^{-1}$]	LHC delivered [fb^{-1}]	Recorded [fb^{-1}]	Good for physics [fb^{-1}]
Run-1					
	7 TeV	4.0×10^{33}	5.46	5.08	4.57
	8 TeV	8.0×10^{33}	22.8	21.3	20.3
Run-2					
2015	13 TeV	5.0×10^{33}	4.2	3.9	3.2
2016	13 TeV	13.8×10^{33}	38.5	35.6	33.3(+0.6)[1]

The ATLAS data taking performance in pp collisions is summarised in Table 6.1. The Table lists: the centre-of-mass energy ($\sqrt{s}$), the peak instantaneous luminosity, the total luminosity delivered by the LHC, the total luminosity recorded by ATLAS and the amount of data suitable for physics analysis. The delivered luminosity accounts for the luminosity delivered from the start of stable beams until the LHC requests ATLAS to put the detector in a safe standby mode to allow a beam dump or beam studies. The recorded luminosity reflects the DAQ inefficiency as well as the inefficiency of the so-called warm start: when the stable beam flag is raised, the tracking detectors undergo a ramp of high-voltage and turn on the pre-amplifiers in the case of the Pixel Detector. The *good for physics* physics criteria require all the reconstructed physics objects to be of good data quality [99].

The Inner Detector data taking efficiency was high in all runs. Figure 6.1 shows the luminosity weighted relative fraction of good quality data delivery by the various components of the ATLAS detector/trigger subsystems during the LHC fills with stable beams in pp collisions at $\sqrt{s}$=13 TeV, and after switching the tracking detectors on. The runs with 25 ns bunch spacing taken between 28th April and 26th October 2016, corresponding to a recorded integrated luminosity

---

[1] The toroid magnet was not switched on during some runs corresponding to ~0.7 fb^{-1} of the total luminosity recorded in 2016. Out of these data 0.6 fb^{-1} was marked as good quality data and can be used for some analysis.

of 35.9 fb^{-1}, are shown [101].

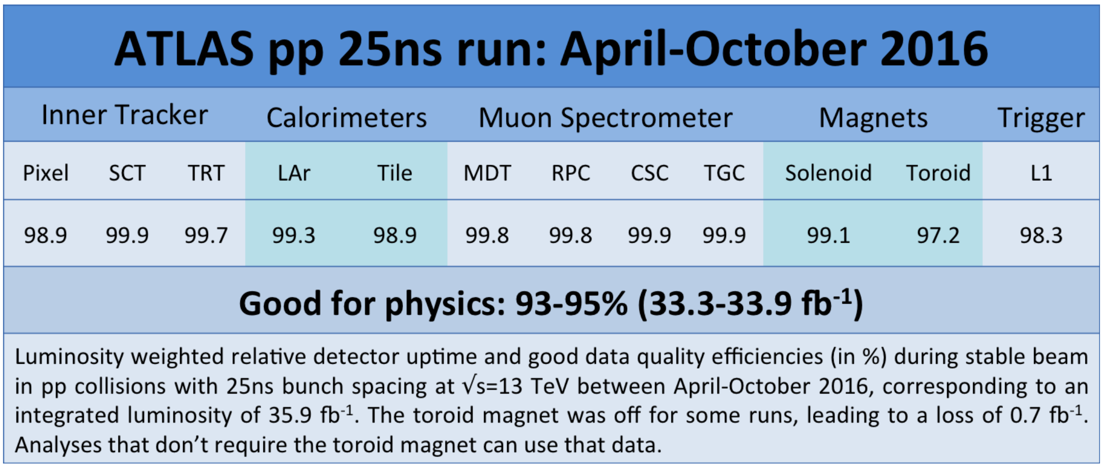

ATLAS pp 25ns run: April-October 2016

Inner Tracker			Calorimeters		Muon Spectrometer				Magnets		Trigger
Pixel	SCT	TRT	LAr	Tile	MDT	RPC	CSC	TGC	Solenoid	Toroid	L1
98.9	99.9	99.7	99.3	98.9	99.8	99.8	99.9	99.9	99.1	97.2	98.3

Good for physics: 93-95% (33.3-33.9 fb^{-1})

Luminosity weighted relative detector uptime and good data quality efficiencies (in %) during stable beam in pp collisions with 25ns bunch spacing at √s=13 TeV between April-October 2016, corresponding to an integrated luminosity of 35.9 fb^{-1}. The toroid magnet was off for some runs, leading to a loss of 0.7 fb^{-1}. Analyses that don't require the toroid magnet can use that data.

Figure 6.1: The data taking efficiency summary for various ATLAS detector components [101]

6.1.1 Data quality monitoring

Not all *pp* collision events recorded by ATLAS are suitable for physics analysis. Only the data meeting certain quality requirements are considered as good for the analysis. The data quality assessment is an important part of the data taking process and is performed both online [102] and offline [103]. In ATLAS, a dedicated Data Quality Monitoring Framework (DQMF) was developed for automated on-line and off-line checks of the recorded experimental data[104] quality. The DQMF indicates whether or not the considered data set[1] is flagged suitable for use in physics analysis. To make this decision, the DQMF runs algorithms analysing the parameters from the subdetectors (e.g. hit efficiency, noise occupancy, readout errors, fraction of modules excluded from readout configuration) and the tracking performance distribution for reconstructed events. An important input for data quality assessment are also data supplied by the Detector Control System. Selected sub-detector DCS information is copied every 15 min-

---

[1] The ATLAS data taking is composed of long periods of stable beams called the *Run*. Each *run* is divided into short time intervals of about 1 minute called luminosity blocks or *lumiblocks*. *A lumiblock* is the smallest unit of time (typically 1 min.) in the ATLAS data-taking where all the data-taking configurations are constant.

utes to the ATLAS condition database COOL [105]. The DCS data from COOL folders is then used as inputs to the DCS status calculator, a tool which combines this data and provides a status flag for each sub-detector to be used by the DQMF and in offline analysis. The DCS conditions data stored in COOL are used by offline reconstruction software in different ways. For example, the SCT module bias voltage values and temperatures are taken into account by cluster-formation and reconstruction algorithms. The data from modules which are not at their nominal bias voltage value are excluded from the reconstruction at the cluster-formation stage. This condition removes modules which suffer from an occasional high-voltage trip, resulting in high noise occupancy, for the duration of that trip [89].

The on-line Data Quality Monitoring (DQM) checks during data taking are performed constantly by a dedicated shifter. This person oversees the histograms sensitive to tracking performance created by DQM tools from data sampled in real time directly from the trigger. Thanks to such histograms, a trained shifter can at a glance spot a potentially problematic detector region. The DCS conditions also have an impact on the tracking performance and thus some DCS related failures shown up in the DQM performance plots. For example, the distribution of dead SCT modules per track in $\eta - \phi$ plane is shown in Figure 6.2. The red spot in the top left corner in Figure 6.2 corresponds to the group of non-operational modules in the SCT end-cap due to the faulty cooling loop. Of course, it is rather unlikely that the data quality shifter will be the first person to report a DCS problem. However, this illustrates the dependencies between DCS and data quality monitoring.

6.2 The luminosity challenges

One of the main features of the operations in 2011 and 2012 was the use of high bunch intensity with 50 ns bunch spacing. It gave good instantaneous luminosity performance but at the cost of high pile-up [107].

With increasing luminosity, the number of simultaneous proton-proton interactions per bunch crossing, the so called pile-up, gets bigger. The mean number of pp interactions (μ) per beam crossing in Run-1 reached 40, while the design

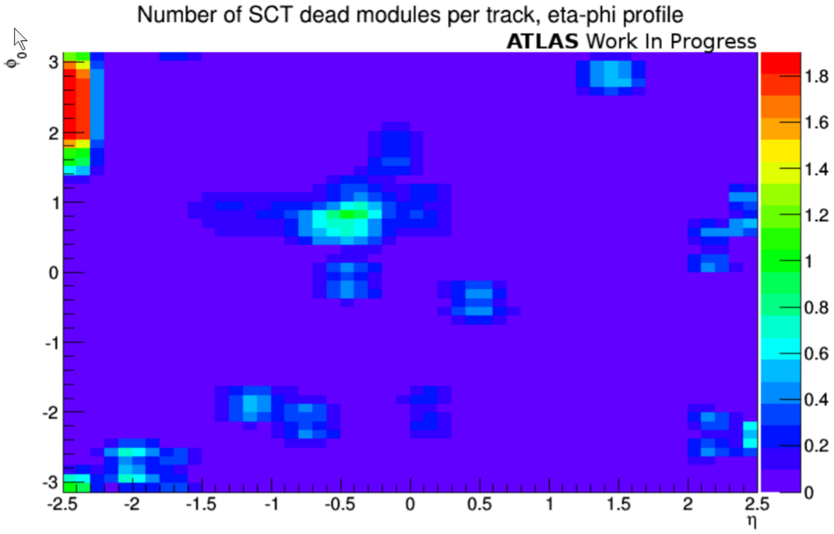

Figure 6.2: The average number of dead SCT modules traversed by reconstructed tracks [106].

specification for the Inner Detector is μ=23 [6]. The pile-up increased even more during Run-2 in 2016 with increasing luminosity. The distributions of the mean number of interactions per bunch crossing for Run-1 and Run-2 are shown in Figure 6.3. The amount of data delivered to ATLAS during stable beams is shown, and the integrated luminosity and the mean μ value are given in Figure 6.3. The mean number of interactions per crossing corresponds to the mean of the Poisson distribution of the number of interactions per crossing calculated for each bunch. The number of interactions per crossing is calculated from the instantaneous per bunch luminosity as $\mu = L_{bunch} \times \sigma_{inel}/f_r$ where L_{bunch} is the instantaneous luminosity per bunch, σ_{inel} is the inelastic cross section which was taken to be 80 mb for 13 TeV collisions, and f_r is the LHC revolution frequency [99]. An example of a very dense pile-up event with 25 reconstructed vertices recorded in 2016 is shown in Figure 6.4. The Higgs boson candidate event is reconstructed in the two muons plus the two electrons final state. In the left display the red lines show the reconstructed paths of two muons including the hits in the muon spectrometer, the green lines show the paths of two electrons together with the energy deposit in the electromagnetic calorimeter, and the yellow tracks are the remaining charged particles from the Higgs boson candidate vertex. The grey tracks correspond to

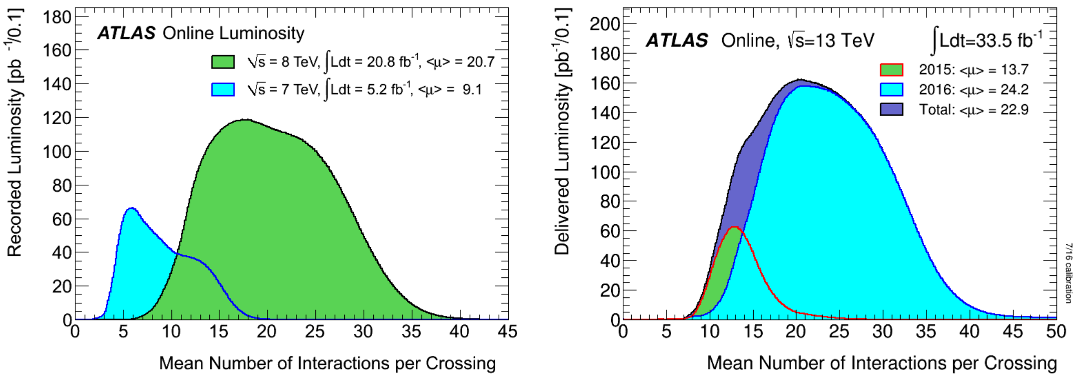

(a)

(b)

Figure 6.3: Luminosity-weighted distribution of the mean number of interactions per crossing for: (a) full 2011 and 2012 *pp* runs; (b) combined 13 TeV data from 2015 and 2016 [99; 100].

the charged particles from 25 pileup vertices with transverse momentum above 0.5 GeV and the coloured squares in the lower display correspond to the position of the reconstructed vertices [108]. The existence of the pile-up puts even harsher requirements on the tracking system than it was anticipated during the design and construction phase.

6.3 Upgrades and consolidation work during the technical stop

A high pile-up has a big impact on tracking detectors, as they are particularly sensitive to an increase in charged particle multiplicity. As the luminosity increases, the number of interesting events per second grows, thus the rate of the Level-1 trigger is higher. A larger number of collisions result in a higher detector occupancy, and a higher data volume needs to be read out upon reception of the Level-1 trigger decision. Finally, the data taking can be disturbed by an increasing number of readout chip errors caused by Single Event Upsets (SEU), where a charged particle passes through the on-detector electronics and changes a value stored in the memory cell [109].

The Inner Detector subsystems took advantage of the long LHC technical

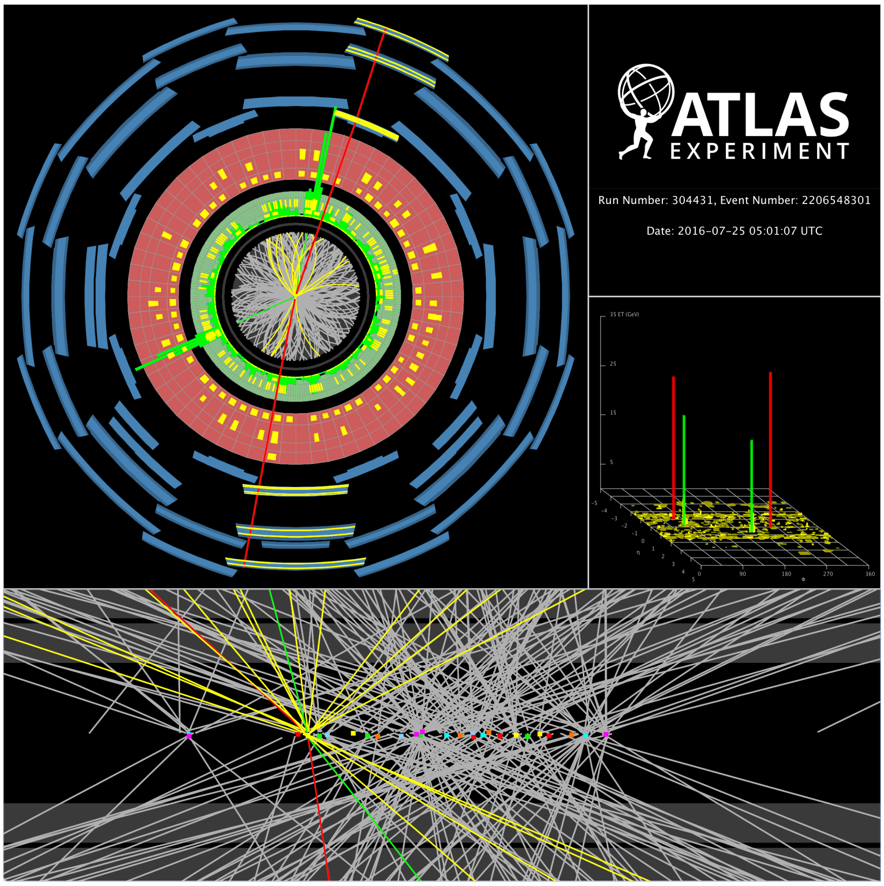

Figure 6.4: A display of a Higgs boson candidate event from proton-proton collisions recorded by ATLAS with the LHC stable beams at a collision energy of 13 TeV. The Higgs boson candidate is reconstructed in a beam crossing with 25 additionally reconstructed primary vertices from the minimum bias interactions [108].

stop to adjust for increasing luminosity and pile-up conditions and to perform consolidation works. Between March 2013 and March 2015, the major consolidation and improvements were performed in all ID subsystems. Most notably, a new pixel layer was installed closest to the beam-pipe, the readout system for the silicon detectors was expanded to allow the expected higher data rates to be transferred, and the Detector Control System was migrated to a new operation system platform.

6.3.1 The Pixel Detector and the Insertable B-Layer

At the end of Run-1 88 out of 1744 (5%) Pixel Detector modules were excluded from operations, which was due to various failures, mostly the failures of the electrical-to-optical converter boards and broken high voltage lines. In Figure 6.5a the number of pixel module failures at the end of Run-1 classified by the type of the failure is shown. The Pixel Detector was extracted from the experimental cavern and moved to the surface laboratory where all accessible module failures were repaired and electrical services were refurbished. The percentage of the disabled modules before and after reparation is shown in Figure 6.5b.

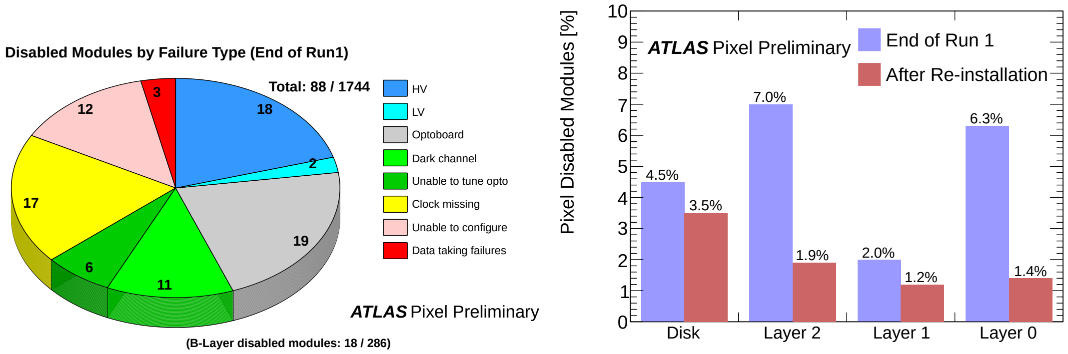

(a)

(b)

Figure 6.5: Number of disabled modules of the Pixel Detector at the end of Run-1 classified by the type of the failure (left). Percentage of disabled modules at the end of Run-1 and after the re-insertion of the Pixel Detector into the ATLAS Experiment for disk and three layers (right) [110].

The optical data transmission electronics were moved to a location outside the ID cryostat for easier access - for reparations during short technical stops.

The extraction of the detector gave the opportunity to install new optical links with an increased data bandwidth capability for Run-2. The bandwidth for the Pixel Layer-1 was increased to 160 MBit/s, and for the Layer-2 to 80 MBit/s to withstand data transmission rates expected with the increased LHC instantaneous luminosity up to $3 \times 10^{34}\text{cm}^{-2}\text{s}^{-1}$ [111].

The performance of the innermost layer of the Pixel Detector is critical for fulfilling the physics analysis requirements for tracking and vertexing. At the same time this layer suffers from radiation damage effects and inefficiencies at high luminosities because of its proximity to the interaction point. To improve the precision of vertexing and tracking and to maintain a robust tracking despite effects arising from luminosity and radiation, the fourth layer of pixel detectors, the IBL [112], was installed between the existing Pixel Detector and a new smaller radius beam-pipe. The IBL is designed to withstand a fluence up to 5×10^{15} 1 MeV $\mathrm{n_{eq}}$ expected at the end of the LHC Phase-I operations. Figure 6.6 shows the IBL installation in the ATLAS experiment.

The tracking performance of the ID is significantly improved thanks to additional high resolution measurement at a closer distance from the beam line provided by the IBL (see 6.5.1).

6.3.2 The Semiconductor Tracker

Various consolidation and upgrade activities were carried out in the SCT during LTS1 to provide high quality data for physics analysis in Run-2. The most important improvements were done in the data acquisition system, which was expanded to cope with the expected higher detector occupancies and high Level-1 trigger rates up to 100 kHz. The readout links were designed to accommodate up to 2% detector occupancy at the Level-1 trigger rate of 100 kHz without imposing any dead-time. There are two limiting bottlenecks within the SCT DAQ, if the trigger rate or occupancy significantly increases beyond these limits. These are the bandwidth of the data links which transmit the data from the front-end chips at 40Mbps, and the bandwidth of the data fibres (S-links) which transmits data fragments containing readouts for up to 48 modules at 1.28 Gbps. The data volumes in these links were studied in pp collision data at $\sqrt{s}$=8 TeV to identify any potential problems and it was concluded that the DAQ hardware must be extended during LTS1 to cope with higher trigger rates and pile-up levels anticipated in Run-2 [89]. The data transfer in S-links had to be expanded to satisfy Run-2 requirements. Extra 38 Read-Out-Drivers were installed to remove a critical DAQ bottleneck and the number of the optical links for data transfer increased accordingly. The incoming front-end data links were redistributed across more RODs, thus reducing the number of modules processed by each ROD from

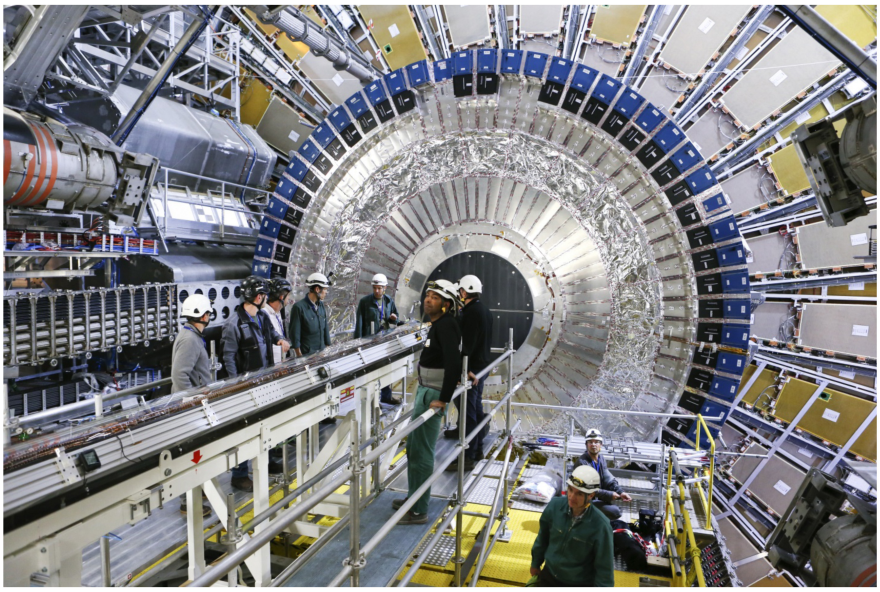

(a)

(b)

Figure 6.6: Installation of the IBL into the ATLAS detector: (a) insertion tooling with IBL package stands in front of the sealed Inner Detector End-Plate (photo by Claudia Marcelloni); (b) an engineer performs a final envelope check just before the IBL sensors and electronics, enter into the inner support tube (photo by Heinz Pernegger) [113].

up to 48 to up to 36 [114]. The maximum sustainable trigger rate as a function of pile-up for both front-end links and S-links with the newly expanded DAQ is shown in Figure 6.7.

Figure 6.8 shows the number of front-end links and S-links that exceed 90% of the available bandwidth as a function of pile-up assuming a 100kHz Level-1 trigger rate. The values are calculated from the measured event sizes in pp collisions at $\sqrt{s}$=13 TeV. The plots indicate that the bandwidth limits are exceeded on an increasing number of links from a pile-up of 55 upwards [114].

Hardware expansion together with the ROD firmware upgrade for data compression improvements makes it possible to read out the SCT at luminosities up to $3 \times 10^{34}\mathrm{cm}^{-2}\mathrm{s}^{-1}$ at 25 ns bunch spacing.

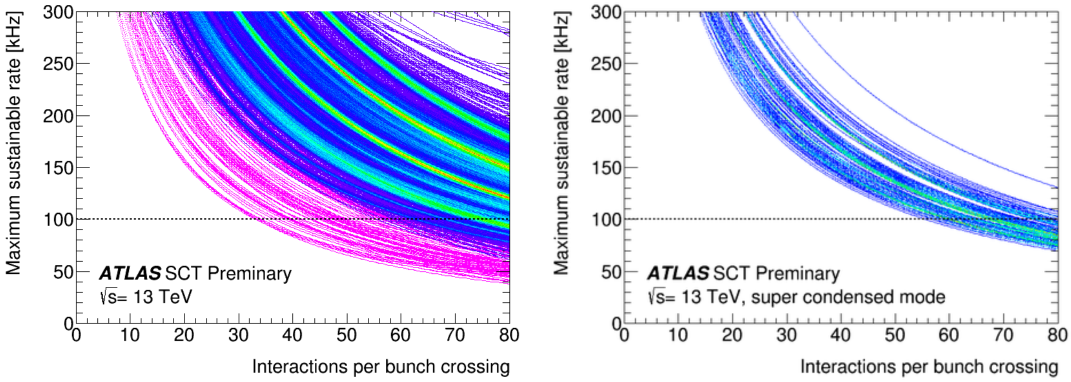

(a) (b)

Figure 6.7: The maximum sustainable Level-1 trigger rate in kHz as a function of pile-up for each of the 8176 SCT front-end links (left plot) and each of the 128 SCT S-links from the ROD to ATLAS DAQ (right plot). The front-end links in magenta indicate those links that use redundancy which transmit data for up to 12 chips instead of the nominal 6 chips [115].

6.3.3 Inner Detector DCS upgrades

The most significant upgrades in the ID DCS were imposed by the fast evolution of computer architecture, operating systems and software technologies over the last

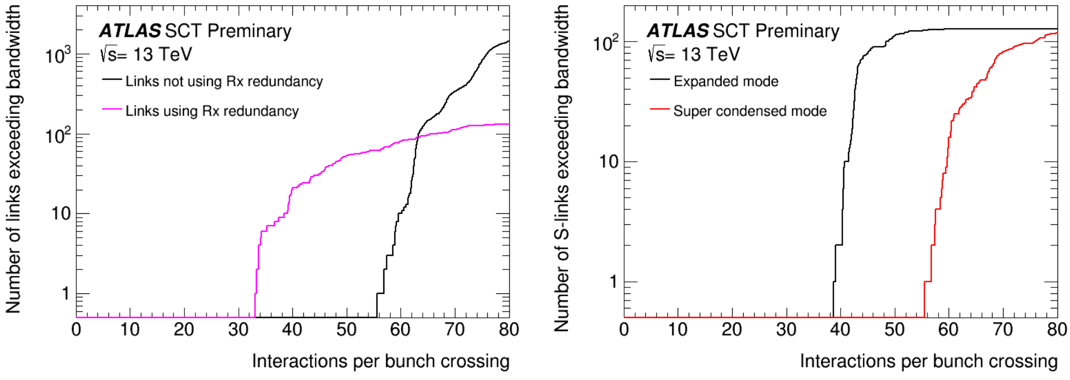

(a) (b)

Figure 6.8: The number of SCT data links which exceed bandwidth limitations at 100 kHz trigger rate as a function of pile-up for the front-end links (left plot) and S-links (right plot). The front-end links in magenta indicate links that use redundancy which transmits data for up to 12 chips instead of the nominal 6 chips [115].

several years. The operating systems were upgraded to Scientific Linux CERN 6[1] and Windows Server 2008 R2. The software toolkit WinCC OA was moved to a new release 3.11 SP1 and the JCOP framework as well as custom IDE DCS implementation had to be adopted in connection with version dependency issues.

Owing to its platform restrictions and expiring long-term support, OPC DA was replaced by the succeeding OPC Unified Architecture (UA) standard. OPC UA offers powerful object-oriented information modelling capabilities, platform independence, secure communication and allows server embedding into custom electronics [116].

In the hardware domain, the USB-CAN module 16 from SYS TEC Electronic GmbH [117] replaced the old PCI CAN bus interfaces. This change was imposed by the operating system change. Nevertheless, it made it possible to re-organise the CAN bus connection in a more balanced and efficient way.

A completely new hardware control system (see 5.5) for thermal enclosure heater pads was installed and commissioned during LTS1. The system addresses safety issues identified in the previous system.

---

[1] Scientific Linux CERN 6 is a Linux distribution built within the framework of Scientific Linux to integrate into the CERN computing environment.

Table 6.2: The Inner Detector Run-2 status in October 2015. The SCT operational fraction was rised to 98.9% after including temporarily disabled modules [118].

Subdetector	Nb. of channels	Approx. operational fraction
Pixel	80 M	98 %
IBL	12 M	99.5 %
SCT	6.3 M	98.6 %
TRT	350 k	97.3 %

6.4 Inner Detector recommissioning for Run-2

Because of the removal of the Pixel Detector for refurbishment and installation of the IBL, the ID environment systems including cooling were not ready for operation during LTS1. The SCT was kept in a dry environment at room temperature, so the periodical calibration could not be done. The recommissioning of the ID environment systems started after the re-installation of the Pixel Detector in 2014. All cooling loops were checked for leaks and the mapping of the sensors and function of the cooling system was verified step-by-step.

Before the restart of data taking, all the ID sub-detectors were recommissioned and all performance metrics were found to be comparable to Run-1. The total fraction of operational modules in the various systems of the Inner Detector at the beginning of Run-2 is presented in Table 6.2.

6.4.1 Radiation Damage

The radiation environment in the ATLAS detector comprises a full spectrum of particles, as reviewed in [2]. The harmful effects of radiation on the silicon detectors affect both the sensors and the readout electronics. The effects include rising of the leakage currents, the charge accumulation in the silicon oxide layers, decreasing the signal-to-noise ratio, change of depletion voltages, and radiation-induced activation of the components. The readout electronic chips also suffer from single-event upsets.

The SCT was designed to withstand the fluences and radiation doses corresponding to the integrated luminosity of 700 fb^{-1} [89]. After six years of operation only a fraction of the designed integrated luminosity has been delivered to the ATLAS experiment. Nevertheless, some effects of the radiation damage on the detectors are already visible and were analysed. In particular, the detector sensor leakage-current measurements were performed for all SCT modules and the results were used to verify the Monte Carlo fluence predictions [119].

The increase in the detector leakage current is proportional to 1 MeV neutron-equivalent fluence[1] and is sensitive to the temperature and annealing effects [89]. The leakage current prediction models make certain assumptions of the annealing behaviour which depends on the sensor temperature. For this reason, the history of the sensor temperature must be carefully tracked including warm-up periods, even if they are short. The sensor temperature during the periods without cooling was assumed to be the same as the environmental gas temperature monitored by the environmental DCS project. The leakage current has been monitored with a precision of 20 nA per module using the high voltage power supplies [120]. The measured currents, I_{HV}, are normalized to those corresponding to the temperature of 0°C, I_{norm}, according to the temperature scaling formula for the silicon bulk generation current [121]:

$$(\frac{I_{norm}}{I_{HV}}) = (\frac{T_{norm}}{T_{meas}})^2 exp[-\frac{E_{gen}}{2k_B}(\frac{1}{T_{norm}} - \frac{1}{T_{meas}})] \tag{6.1}$$

where T_{meas} is the sensor measured temperature, T_{norm} is the sensor normalisation temperature, E_{gen}=1.21 eV is the energy of the silicon band gap, k_B is the Boltzmann constant.

Figure 6.9 shows the average normalised leakage current of each barrel layer compared with the predictions of the Hamburg/Dortmund model [122; 123]. The coloured bands indicate 1σ uncertainties on the model predictions. The increase in the leakage current is proportional to the integrated luminosity. The small drops in the current are connected to the effect of beneficial annealing during the periods when the cooling was not active, e.g. technical stops. The beneficial annealing effect is illustrated in Figure 6.10, showing leakage currents in the barrel

---

[1] 1 MeV neutron-equivalent fluence is defined as the number of particles causing damage equivalent to that of 1 MeV neutrons traversing 1 cm^2 of the sensor's surface.

SCT modules before and after the long technical stop LTS1.

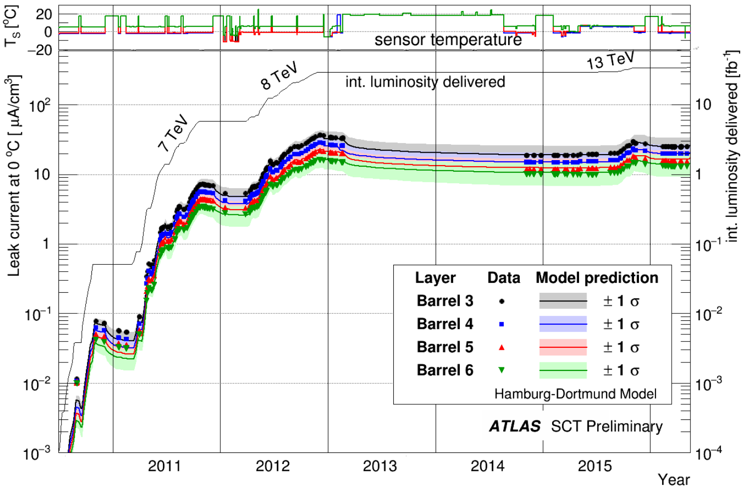

Figure 6.9: Comparison between data (points) and Hamburg/Dortmund model predictions (lines with uncertainties shown by the coloured bands) of the leakage current per unit volume at 0°C of the four barrel layers. The integrated luminosity and beam energy are also shown. Sensor temperatures are shown indicating periods of normal operation as well as the extended periods with no beam in the LHC when the SCT was off [115].

6.5 The combined tracking performance

A very good performance demonstrated by the separate ID sub-systems ensures the accurate measurements of charged particle trajectories for ATLAS physics analysis. Precise track reconstruction forms the basis for measurements of primary and secondary interaction vertices, identification of flavour jets[1], tau leptons and is indispensable for analysis of many new physics phenomena or for precision measurements of the Standard Model parameters. The combined Inner Detector tracking performance after upgrades done during the LTS1 was tested with pp collision data on the LHC collected during Run-2 at the centre-of-mass energy of $\sqrt{s}$=13 TeV. Selected benchmarks are briefly discussed below.

---

[1] A jet is a narrow cone of hadrons and other particles produced in the process of hadronization of a quark or a gluon.

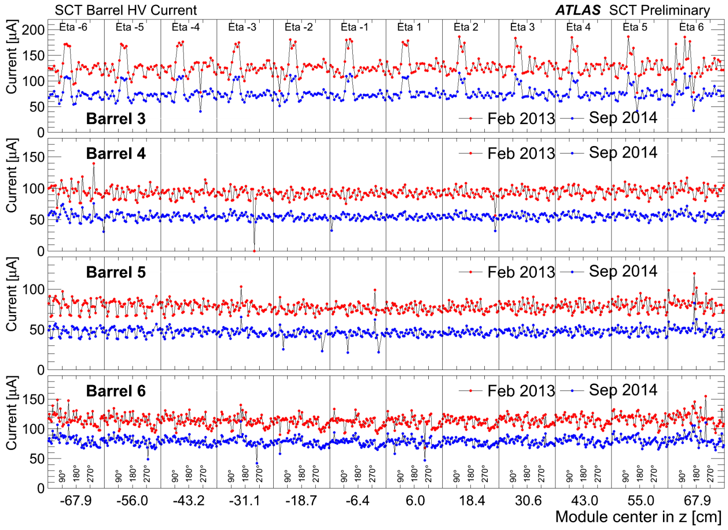

Figure 6.10: High voltage current for each barrel module for each of the SCT barrel layers comparing currents in February 2013 (red - at the end of Run-1) with September 2014 (blue - after cooling and powering the SCT again after 15 months with the SCT unpowered and at room temperature due to the Long Shutdown 1 period). The figure indicates the drop in the leakage currents due to 15 months of annealing at room temperature [115].

6.5.1 Impact parameter resolution

Trajectories of the charged particles with transverse momentum $p_T > 0.5GeV$[1] and $|\eta| < 2.5$ are reconstructed and measured by the Inner Detector in the solenoid magnetic field. In a nut shell, the track reconstruction is made in two stages: finding track candidates by the pattern recognition algorithms and estimating the parameters that describe the particle properties. Charged particles traversing the Inner Detector generate hits[2]. A dedicated software package using advanced pattern recognition methods selects hits generated by a single charged particle [124]. This subset of hits is further processed by the track fitting algorithm to estimate the trajectory parameters. Charged particle trajectory in the

---

[1] The ATLAS ID is capable of reconstructing trajectories of particles with transverse momenta down to $p_T \sim 0.1GeV$. However, the pattern recognition combinatorial background increases and as a consequence the required computing time and event size also grows.

[2] A hit in the Pixel Detector and SCT it is a small cluster of pixels or strips that registered signal above the certain threshold, created by a charged particle or noise. A hit in the TRT is a raw timing information turned into calibrated drift circles.

magnetic field is described by five parameters of a helix. The track parametrisation used in ATLAS is the perigee representation [125] with the following parameters:

$$p = (d_0, z_0, \phi_0, \theta_0, \frac{q}{p}) \tag{6.2}$$

where:

- d_0 - the transverse impact parameter measured with respect to the origin (see Figure 6.11, signed by the angular momentum of a track with respect to the z-axis,
- z_0 - the longitudinal impact parameter - the z-coordinate of the track at the point of the closest approach to the z-axis,
- ϕ_0 - the azimuthal angle of the track at the perigee,
- θ_0 - the polar angle of the track,
- the charge to the momentum ratio $(\frac{q}{p})$.

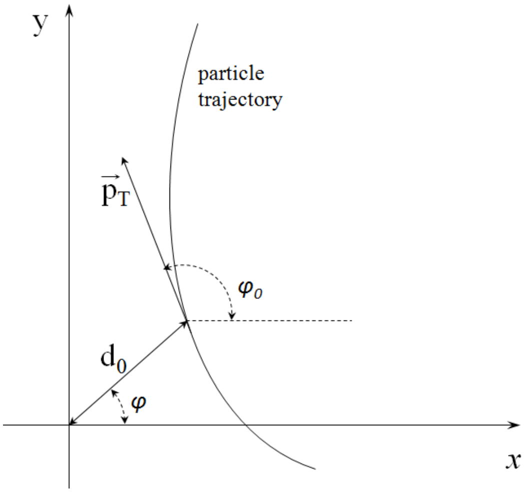

Figure 6.11: Illustration of the particle trajectory perigee representation.

A precise measurement of the track impact parameter is essential for physics analysis which requires secondary vertex reconstruction e.g. processes involving

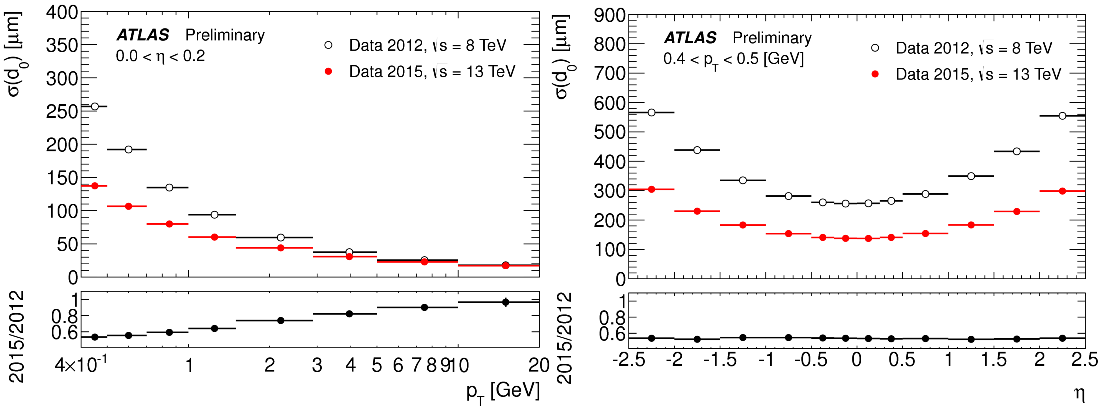

(a) (b)

Figure 6.12: Unfolded transverse impact parameter resolution measured from data in 2015 at $\sqrt{s}$ = 13 TeV with the Inner Detector including the IBL, as a function of p_T (a) and η (b) compared to that measured from data in 2012 at $\sqrt{s}$=8 TeV [126].

decays of B mesons or long-lived particles, heavy-flavour tagging or lifetime measurements. They are also important for associating a track to the correct primary vertex in a high luminosity environment. Therefore the track impact parameter resolution is a good benchmark for tracking performance. It is routinely measured in data. Figure 6.12 and 6.13 show the comparison of the Run-1 and Run-2 impact parameters resolutions. The influence of the IBL on the impact parameter resolution is clearly visible.

6.5.2 The vertex reconstruction

Reconstruction of the primary interaction vertex as well as the reconstruction of the secondary interaction vertices are crucial for physics analysis. The vertex reconstruction strategies and performance are described in detail in [127; 128; 129; 130]. A brief overview is given below.

The basis of the reconstruction of the interaction vertex is the measurement of a charged particle track in the ID. The tracks that fulfil quality requirements are selected for the primary vertex finding algorithm and used to select the vertex seed position. The tracks and seed are then used in the adaptive vertex fitting algorithm [131] to fit the best vertex position. The vertex fitting algorithm uses

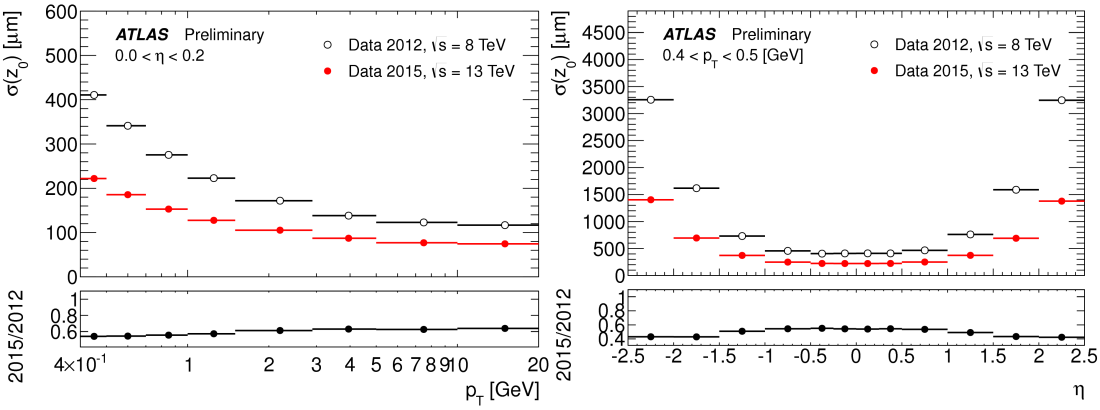

(a) (b)

Figure 6.13: Unfolded longitudinal impact parameter resolution measured from data in 2015 at $\sqrt{s}$ = 13 TeV with the Inner Detector including the IBL, as a function of p_T (a) and η (b) compared to that measured from data in 2012 at $\sqrt{s}$=8 TeV [126].

a method formulated as an iterative re-weighted Kalman filter [132]. At the end of the procedure the tracks that are incompatible with the determined vertex position are used to seed a new vertex (pile-up). Vertices are required to have at least two associated tracks. The procedure is repeated until no more vertices can be found in the remaining set of tracks. The beam spot position and width can be used as an additional input to the primary vertex fit to constrain the transverse position resolution of vertices reconstructed from a small number of tracks.

The performance of the vertex reconstruction has been evaluated by a data driven split-vertex method on data collected with random trigger at $\sqrt{s}$=13 TeV [133]. In split-vertex technique, the tracks associated with the reconstructed primary vertex are split into two sets and the vertex fitting procedure is applied again, separately to both sets. The intrinsic resolution of the primary vertex is then derived from the spatial separation between the two resulting vertices. The resolution of the vertex position in the transverse and longitudinal directions is shown in Figure 6.14 as a function of the number of tracks associated to the vertex. The resolutions in the transverse coordinate converge to a value of 20 μm. The longitudinal resolution reaches 30 μm.

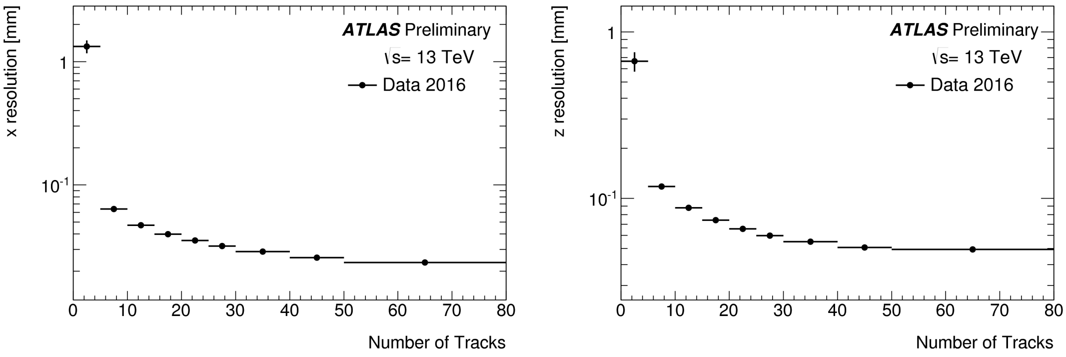

(a)

(b)

Figure 6.14: The vertex position resolution in transverse (left) and longitudinal (right) direction as a function of the number of tracks per vertex [134].

6.5.3 Material studies

As a consequence of the Pixel Detector refurbishment, the IBL and the new beam pipe installation, the material composition and the structure of the Inner Detector have changed with respect to Run-1. A precise knowledge of the material distribution inside the tracking detectors is crucial for correct detector simulations and for establishing the track reconstruction performance in Run-2 data. The material within the innermost barrel regions of the Inner Detector was studied using different techniques, e.g. using reconstructed hadronic interactions vertices in samples of minimum bias events collected at $\sqrt{s}$=13 TeV in 2015 [135].

The hadrons created in the pp collision interact inelastically with the detector material and multiple secondary charged particles are created. The hadronic vertices analysis helps to establish a precise description of the material structure in the Inner Detector [135].

Figure 6.15 shows the radial distribution of the hadronic secondary interaction candidates reconstructed in the data and simulations. The structures of the tubes of the beam pipe at $r \approx 24$ mm, the Inner Positioning Tube (IPT) at $r \approx 29$ mm, and the Inner Support Tube (IST) at $r \approx 42.5$ mm are clearly visible and consistent between the data and the simulation. The structure between the IPT and IST at $30 < r < 40$ mm is the IBL stave. The default geometry model was found to be missing the surface mount elements, e.g. the capacitors located on the front-end chip at $r \approx 32$ mm. The corresponding amount of material was added to the updated geometry model. This correction significantly improves the agreement, as demonstrated in Figure 6.15 [135].

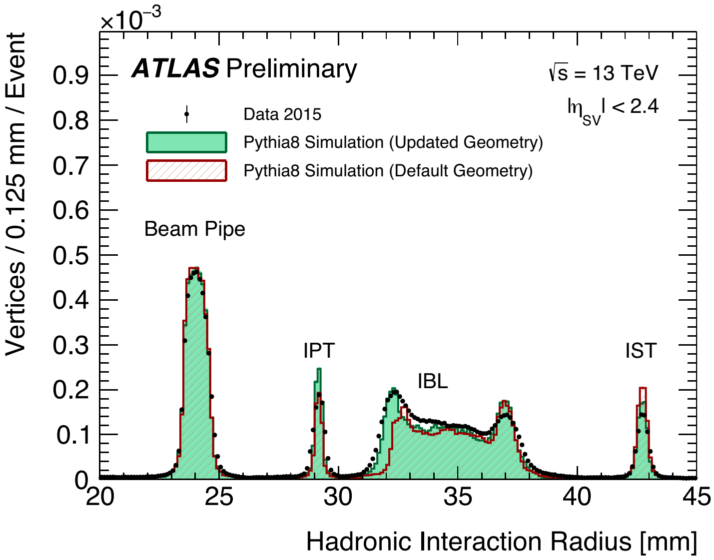

Figure 6.15: Comparison of the radial distribution of hadronic interaction candidates between data and simulation for $20 < r < 45$ mm. The secondary vertices are required to have the pseudorapidity $|\eta_{SV}|$ <2.4 [135].

Chapter 7

Summary and outlook

7.1 The Inner Detector Control System, operations and performance

In large high energy physics experiments, the controls are no longer standalone systems used for the so-called slow control. They are an integral part of the experimental apparatus, connecting physics and technology and having a substantial influence on the detector performance and the quality of the recorded data. The industrial solutions for a process control cannot be directly ported to the control of high energy physics experiments, as typically they are more complex and heterogeneous than industrial systems. An in-depth knowledge of the experiment hardware behaviour and its technologies is compulsory in order to design an adequate control system. This monograph has presented the challenges and solutions applied during the development of the complex control system for the ATLAS Inner Detector and its influence on the detector operation, data taking and performance.

The control system is expected to serve the experiment for several decades - from the commissioning through operations at the Large Hadron Collider. Moreover, it should be anticipated that the DCS will evolve with time to adapt to changing experiment operation conditions due to e.g. increasing luminosity at the LHC. To facilitate and standardise the detector systems development and maintenance a common task force (the Joint Control Project) was established by representatives from all LHC experiments. The standardised hardware and software building blocks have been evaluated and assessed and eventually selected to be used for the DCS development. The WinCC OA framework has been chosen as a tool for the development of the DCS software layer. The JCOP framework components have been implemented on top of the WinCC OA to address common software tasks for all LHC experiments, e.g. to interface communication protocols (CAN bus, Modbus, TCP/IP, OPC UA), to implement alarm handling and to interface external database storage. The ELMB board has been developed by the ATLAS collaboration as a universal input/output device. The standard hardware and software tools make a solid frame for the sub-detectors DCS development, but still a significant amount of expertise and dedicated solutions is needed to address the particular needs of a given detector.

The Inner Detector is a large complex system dedicated to measure the trajectories of charged particles and vertices of interactions. It is composed of three independent sub-detectors built using different technologies. The innermost and the most precise are the silicon semiconductor devices: the Pixel Detector and the Semiconductor Tracker. The outer is a gaseous straw detector - the Transition Radiation Tracker. All these subsystems are installed in a common volume inside the ATLAS calorimeter cryostat.

Although the three components of the ID serve the same purpose of measuring the tracks of charged particles, the requirements concerning their operations are different and in some cases even contradictory. The silicon devices must be kept in a cold and dry N_2 environment in order to suppress radiation damage effects and to avoid water condensation on cold parts of the detector electronics. The TRT, on the other hand, requires room temperature and CO_2 atmosphere to achieve the best tracking performance. In order to ensure proper management of thermal conditions, a group of services has been installed in the ID volume shared by the Pixel Detector, the SCT and the TRT. These services for environment management have a vital role for the detector operation, performance and safety. The evaporative cooling system with C_3F_8 as a coolant is used to remove a total of about 40 kW dissipated by the SCT and Pixel Detector modules and to keep the temperature of the silicon at -7°C or below. The thermal screens combining both active and passive insulation among various elements of the ID have been installed, including the thermal enclosure between the SCT and TRT covering the temperature difference of more than 25°C. A total of 290 electric resistance heating pads are used in active thermal insulations to maintain a specific temperature at various thermal interfaces within the ID. The temperature and humidity in the strategic positions inside the ID volume, e.g. at important points of the cooling circuits, are constantly monitored by about 1000 sensors. Ultrasonic instruments have been developed and introduced to detect the coolant leaks into the ID volume by means of the gas composition monitoring.

The second group of services installed inside the ID volume are systems related to beam condition and radiation monitoring inside the ID volume. During the operations of the LHC, some accidental beam losses may happen due to the equipment failures, magnet quenches or operation mistakes. A faulty condition developed locally near the ATLAS beam insertion region could go undetected by the LHC protection system and could cause local but potentially severe damage in the innermost layer of the Inner Detector. Two systems have been commissioned to protect the Pixel Detector and the SCT against accidental multi-turn beam losses: the Beam Condition Monitor and the Beam Loss Monitor. The BCM consists of two detector stations placed symmetrically on two sides of the interaction point. Each station contains diamond detector modules located at an optimal distance from the interaction point to distinguish between events originating from the collisions and those originating from the beam losses. The Beam Loss Monitor is the second system constructed using the diamond detector technology for protection against the beam losses and for the beam surveillance in the Inner Detector region. Both, the BCM and BLM provide inputs to the LHC Beam Interlock System and safety flags for the ATLAS Control System. The radiation doses inside the ID volume are monitored on-line by the Radiation Monitoring system. This system comprises 14 Radiation Monitor Sensor Boards equipped with several devices to measure the TID, NIEL and thermal neutral fluence in 14 different localisation in the ID.

The complex Detector Control System for the ATLAS Inner Detector has been developed and commissioned to ensure reliable, safe and efficient common operations of the three ID sub-detectors and their services. The IDE DCS is a distributed system consisting of eight projects, each running on a separate server.

The control of the environmental parameters critical for suppressing radiation damage effects and ensuring the best performance of the ID is provided by a set of four complementary DCS projects associated to the corresponding services: the cooling, the environment monitoring, the heater pad control and sonar gas analyser. The cooling control system is distributed over a supervisory server and a set of PLCs that control each of 204 individual on-detector cooling circuits. The predefined operation model and the implementation of the FSM provide a comprehensive operator interface and overview of the cooling system state and allows switching between the defined states in an automatic way. The thermal enclosure heater pads are controlled by a custom designed control hardware and dedicated supervisory DCS software DCS. The temperature control on the thermal enclosures is fully automated in a customised ELMB firmware with the PID algorithm running on the switching board. The hardware and software protection has been implemented to ensure the system safety in case of faults. The Sonar DCS project supervises five ultrasonic instruments installed in the ID. It communicates with custom electronics via the Modbus protocol and provides the system control, monitoring and archiving of the parameters needed for gas composition analysis (temperature, pressure, transient time of sound pulses in the sonar instrument). The analysis of the gas composition is performed in real-time in the DCS project to search for contamination of N_2 with C_3F_8, which could occur in case of the coolant leaks inside the SCT or Pixel Detector volumes.

The control system for the Radiation Monitor System provides tools for radiation monitoring inside the detector volume. The delivered data are used for validation of the radiation damage models and, as a consequence, help the physicists to understand the detector response. The beam conditions and beam induced backgrounds inside the ID volume are cross-checked by the DCS software in course of the LHC beam set-up in order to provide input information for safety procedures for the considered sub-detectors. The IDE DCS also provides input signals to the LHC safety systems.

The ID DCS has been reliably serving the experiment since the first proton beams at the LHC in 2010, providing the tools for detector experts as well as for operators. Thanks to the automation of the operational and safety procedures in the DCS, the whole ID can be operated by a single non-expert shifter.

The hardware and software improvements carried out during the LTS1, in particular the installation of the additional layer of the pixel silicon detectors - the IBL - at the radius of 33.25 mm from the beam line, enables precise track and vertex reconstruction in a high pile-up environment. Hardware expansion of the read-out system in the SCT and the Pixel Detector made it possible to increase the data bandwidth and to read out the detector up to instantaneous luminosity of $3 \times 10^{34}\text{cm}^{-2}\text{s}^{-1}$ at 25 ns bunch spacing. During the LTS1 the IDE DCS ensured safety and appropriate environmental conditions for the detectors. As a consequence, the performance metrics of the sub-detectors after the restart for Run-2 were comparable to those in Run-1. In particular, the radiation damage effects monitored in the SCT detector agreed with model predictions, giving the confidence in our good understanding of the detector. A continuous effort of the sub-system teams, both in hardware and software domains, resulted in the excellent ID performance during data taking. The fraction of good quality data delivered by the components of the ID in Run-2 was 98.9%, 99.0% and 99.7% for the Pixel Detector, the SCT and the TRT respectively. The total luminosity recorded in Run-1 and Run-2 by the end of 2016 exceeded 60 fb^{-1}. The combined tracking performance of the ID measured in Run-2 in proton-proton collisions at a centre-of-mass energy of 13 TeV was measured and it confirmed the improvement in the track impact parameter resolution connected to the IBL. The measured resolution of the vertex position in the transverse and longitudinal directions converge to 20 μm and 30 μm, respectively. The ID material distribution was studied using the reconstructed hadronic interaction vertices and photon conversions. The discrepancy between the IBL material description used in the software and the real hardware was found and removed.

In the final words of the summary, it should be mentioned that the detector control, operation and performance aspects typically go behind the scenes. Nevertheless, they have a pivotal role in the ATLAS experiment physics studies.

7.2 Upgrade plans for the ATLAS inner tracking system

The scientific programme of the LHC (see Table 2.1) contains a series of upgrades aiming at collecting an integrated luminosity of 3000 fb^{-1} using *pp* collisions. The extensive improvements to the accelerator planned for the long shutdown 3 (LS3) will increase its performance and bring the accelerator to the high-luminosity phase - the so-called High Luminosity LHC (HL-LHC). The HL-LHC will provide an instantaneous luminosity of $\sim 7.5 \times 10^{34} cm^{-2} s^{-1}$ and an average number of inelastic *pp* interactions per beam-crossing of about 200.

Taking into account the anticipated increase in the luminosity along with the associated data rate and accumulated radiation damage, the current Inner Detector will reach its performance limits by the time of the LS3. The ATLAS collaboration has decided to replace the Inner Detector with a new all-silicon tracker, ITk, to maintain the tracking performance in this high-occupancy environment and to cope with the integrated radiation dose increased by approximately a factor of ten [136]. The new ITk will consist of two sub-detectors with total acceptance covering $\eta \pm 4$. The new Pixel system will cover twice the radius and four times the length of the current Pixel Detector; a highly segmented ITk Strip Detector will cover a full radius of the solenoid inner bore. At the time of writing this document the final layout of the ITk is still under detailed studies, considerations and decisions. However, it is clear that the ITk will highly exceed the number of channels in the current ID: from $\sim$ 80 million to 600 million in the case of the Pixel system and from $\sim$ 6 million to $\sim$ 70 million in the case of the strip detector. The large system scale together with a harsh radiation environment will raise the main challenges for the future control system for the ITk.

Acknowledgements

The work described in this monograph is the result of several years of the Inner Detector collaboration's efforts, and I am very proud to be part of it. I would like to thank the former and present Inner Detector management and project leaders: dr. Pippa Wells, dr. Steven McMachon and dr. David Robinson, for inviting me to the group and giving me the opportunity to work on interesting and challenging tasks. I would like to thank all the people involved in the Inner Detector Control System I had pleasure to work with over the years as a developer and coordinator: dr. Saverio D'Auria, dr. Koichi Nagai, dr. Luca Luisa, dr. Cecile Deterre, dr. Alex Madsen, dr. Wyne, mr. Jacek Pieron, dr. Josh Moss, dr. Irena Dolenc, dr. Jochen Hartert, dr. Matthew Fisher, dr. Josh Moss.

My contribution would not be possible without the support from the Institute of Nuclear Physics Polish Academy of Sciences. My warm thanks go to prof. Piotr Malecki and prof. Barbara Wosiek for accepting me to the Krakow ATLAS group. I owe my deepest gratitude to prof. Piotr Malecki for very valuable advice and meritorious discussions. Advice and comments given by Prof. Władysław Dąbrowski have been a great help in understanding radiation effects in silicon detectors. Special thanks to Prof. Janusz Chwastowski for proofreading of this monograph.

Last but not least, I would like to express my appreciation to the whole Krakow ATLAS group for creating a friendly and inspiring working environment.

List of Figures

Appendix A

.1 Final State Machine hierarchy

The FSM framework tools are used in ATLAS to provide abstract modelling of the complicated experimental infrastructure. In addition, they deliver intuitive user interfaces and allow quick access down to the smallest system detail. To reduce the system complexity, functionally connected objects are grouped into the SMI++ domains. In the domain objects are organised in a tree-like structure that forms a subsystem control. A schematic illustration of the generic hierarchy of controls, the FSM tree, is shown in Figure 1.

The ATLAS experiment is ultimately operated by a small team of people with only one DCS operator. For this reason, the detector modelling at the top level of the FSM hierarchy must be very abstract and intuitive. In the solution adopted by ATLAS FSM framework component the information about the control tree is handled by means of two different types of SMI++ objects: state and status. These objects work in parallel and provide information about the behaviour of a given node (Control Unit, Logical Unit or Device Unit) in the hierarchy. The state object describes the operational mode of the nodes. The states at the top level of the FSM nodes corresponding to subdetectors are uniform within ATLAS, and with the following standardised values:

- SHUTDOWN - the subdetector is powered off; no power in the experimental cavern.
- READY - the subdetector is ready for data taking.

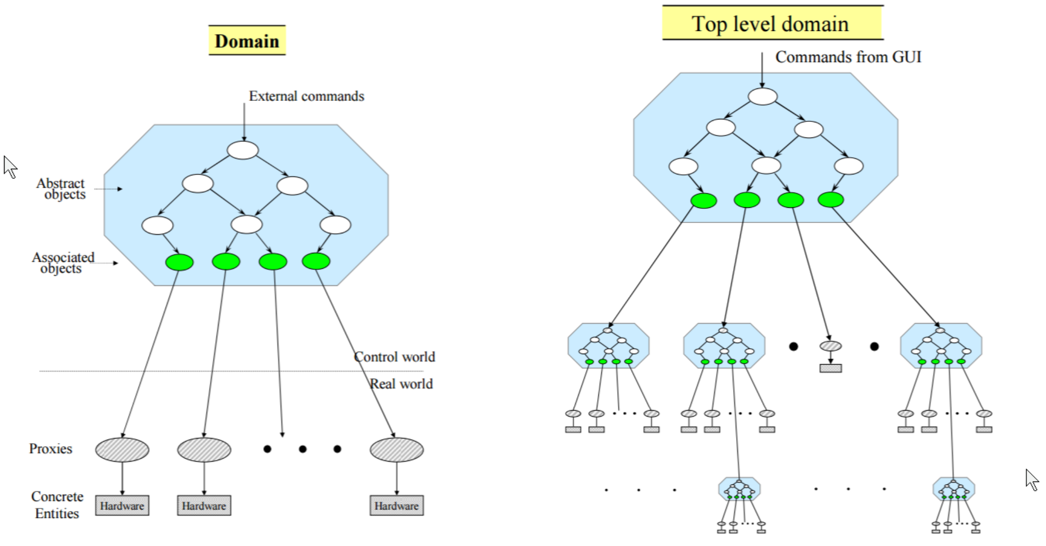

(a)

(b)

Figure 1: (a) The basic concepts of SMI++ : proxies, their associated objects, abstract objects and object grouping into a domain. (b) A typical large control system, objects are organized into a hierarchy of domains [46].

- STANDBY - the subdetector is prepared for transition to READY state, waiting for stable beam condition.
- TRANSITION - optional state indicating that a subdetector is executing a command (eg. ramping the power supplies) to get to another operational state.
- UNKNOWN - denotes that the subdetector states cannot be evaluated, usually due to lack of communication with hardware.
- NOT_READY - a state indicating that the subdetector cannot be classified to any of the above predefined categories.

The transitions between the states can be triggered by a command in the FSM or on change of the monitored device's parameters. The state transition diagram is shown in Figure 2.

The status object provides indication of working conditions of the node. It is typically based on the summary of alarms associated to the node, e.g. a given

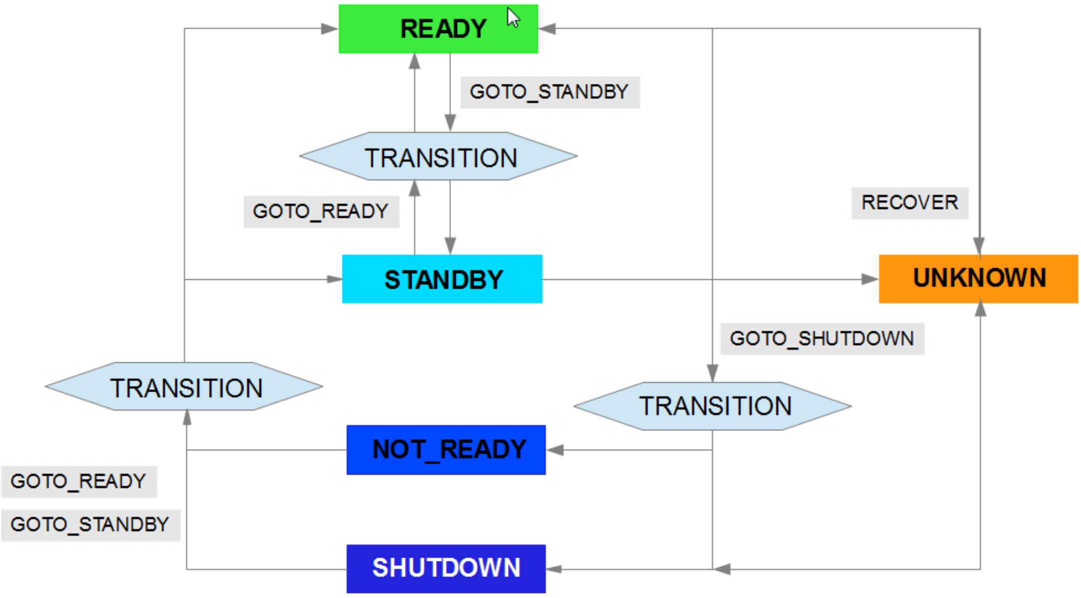

Figure 2: State diagram for ATLAS FSM Subdetector Control Unit.

detector module can be in READY state and at the same time report an over-temperature warning/error which will be reflected in the status. In general the status indicates problems that should be addressed. The values for states are predefined, as shown in Figure 3 and identical for all types of nodes.

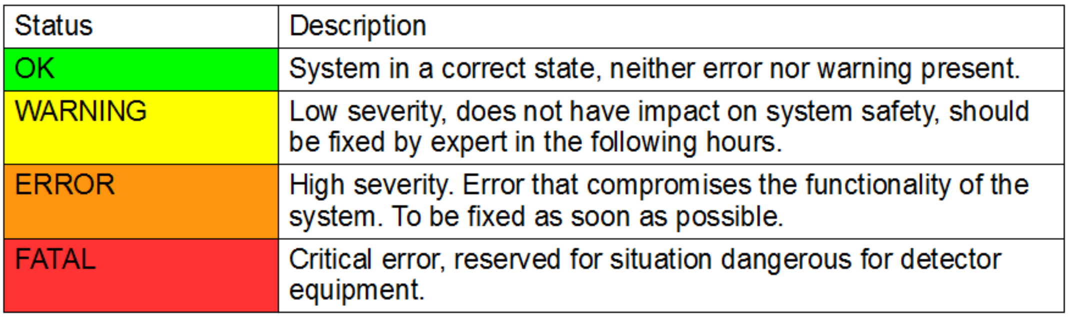

Status	Description
OK	System in a correct state, neither error nor warning present.
WARNING	Low severity, does not have impact on system safety, should be fixed by expert in the following hours.
ERROR	High severity. Error that compromises the functionality of the system. To be fixed as soon as possible.
FATAL	Critical error, reserved for situation dangerous for detector equipment.

Figure 3: Status qualifiers used in ATLAS DCS. Fixed names and colours are assigned according to the severity of the fault.

References

[1] L. Evans. The Large Hadron Collider (LHC). *New J. Phys.*, 9:335, 2007. 2, 8

[2] G. Aad et al. The ATLAS Experiment at the CERN Large Hadron Collider. *JINST*, 3:S08003, 2008. 2, 18, 19, 20, 35, 37, 95, 111

[3] S. Chatrchyan et al. The CMS experiment at the CERN LHC. The Compact Muon Solenoid experiment. *JINST*, 3:S08004. 361 p, 2008. Also published by CERN Geneva in 2010. 2

[4] ALICE Collaboration. The ALICE experiment at the CERN LHC. *JINST*, 3(08):S08002, 2008. 2

[5] LHCb Collaboration. The LHCb Detector at the LHC. *JINST*, 3(08):S08005, 2008. 2

[6] S. Haywood, L. Rossi, R. Nickerson, and A. Romaniouk. ATLAS Inner Detector: Technical Design Report, 2. Technical report, CERN, Geneva, 1997. 2, 39, 87

[7] ATLAS Collaboration. ATLAS Fact Sheets. `https://atlasexperiment.org/fact_sheets.html`. (Visited on 2017-03-20). 2

[8] M. Cadabeschi, V. Cindro, B. Demirkoz, D. Dobos, I. Dolenc, H. Frais-Kolbl, A. Gorisek, E. Griesmayer, J. Hartert, E. Jankowski, H. Kagan, G. Kramberger, K. Lantzsch, B. Macek, I. Mandic, E. Margan, M. Mikuz, J. Moss, M. Niegl, H. Pernegger, E. Stanecka, S. Smith, C. Spatharakis,

D. Tardif, W. Trischuk, and M. Zavrtanik. Commissioning and First operation of the pCVD diamond ATLAS Beam Conditions Monitor. Technical Report ATL-COM-INDET-2010-032, CERN, Geneva, Apr 2009. 5

[9] G. Aad et al. The ATLAS Inner Detector commissioning and calibration. *Eur. Phys. J.*, C70:787–821, 2010. 5

[10] E. Stanecka. Performance and operation experience of the ATLAS Semiconductor Tracker and Pixel Detector at the LHC. *PoS*, Vertex2013:001, 2013. 5

[11] Heater Pad System technical documentation webpage. `https://twiki.cern.ch/twiki/bin/viewauth/Atlas/HeaterPadSystem`. (Visited on 2017-03-20). 6

[12] Heater Pad Control Card Design Review meeting. `https://indico.cern.ch/event/65570/`, 2009. (Visited on 2017-03-20). 6

[13] E. Stanecka. ATLAS Inner Tracker Performance at the Beginning of the LHC Run 2. *Acta Phys. Polon.*, B47:1739–1744, 2016. 6

[14] E. Stanecka. The ATLAS Inner Detector operation, data quality and tracking performance. In *Proceedings, 32nd International Symposium on Physics in Collision (PIC 2012): Strbske Pleso, Slovakia, September 12-15, 2012*, pages 383–388, 2013. 6

[15] E. Stanecka. Recent results on soft QCD topics, and jet, V+jet and photon production from ATLAS. Technical Report ATL-PHYS-PROC-2016-194, CERN, Geneva, Nov 2016. 6

[16] ATLAS Awards Long Shutdown 1 Achievements. `https://atlas.cern/updates/atlas-news/atlas-awards-long-shutdown-1-achievements`. (Visited on 2017-03-20). 7

[17] The Joint COntrols Project (JCOP) Workshop. `https://indico.cern.ch/event/406103/`. (Visited on 2017-03-20). 7

[18] I. M. Gregor et al. Technical Design Report for the ATLAS ITk- Strips Detector: Draft for the ATLAS Circulation . Technical Report ATL-COM-UPGRADE-2016-035, CERN, Geneva, Nov 2016. 7

[19] The HL-LHC Project CERN. Project Schedule. `https://project-hl-lhc-industry.web.cern.ch/content/project-schedule`. (Visited on 2017-03-20). 9, 111

[20] ATLAS Collaboration. Computer generated image of the whole ATLAS detector. `https://cds.cern.ch/record/1095924?ln=pl`. (Visited on 2017-03-20). 10, 111

[21] *ATLAS inner detector: Technical Design Report, 1.* Technical Design Report ATLAS. CERN, Geneva, 1997. 11

[22] K. Potamianos. The upgraded Pixel detector and the commissioning of the Inner Detector tracking of the ATLAS experiment for Run-2 at the Large Hadron Collider. *PoS*, EPS-HEP2015:261, 2015. 13, 111

[23] G. Aad et al. ATLAS pixel detector electronics and sensors. *JINST*, 3:P07007, 2008. 12, 38

[24] M. Capeans, G. Darbo, K. Einsweiller, M. Elsing, T. Flick, M. Garcia-Sciveres, C. Gemme, H. Pernegger, O. Rohne, and R. Vuillermet. ATLAS Insertable B-Layer Technical Design Report. Technical Report CERN-LHCC-2010-013. ATLAS-TDR-19, CERN, Sep 2010. 13

[25] A. Ahmad et al. The Silicon microstrip sensors of the ATLAS semiconductor tracker. *Nucl. Instrum. Meth.*, A578:98–118, 2007. 14, 38

[26] F. Campabadal et al. Design and performance of the ABCD3TA ASIC for readout of silicon strip detectors in the ATLAS semiconductor tracker. *Nucl. Instrum. Meth.*, A552:292–328, 2005. 14

[27] E. Abat et al. The ATLAS Transition Radiation Tracker (TRT) proportional drift tube: Design and performance. *JINST*, 3:P02013, 2008. 15

[28] Bartosz Mindur. ATLAS Transition Radiation Tracker (TRT): Straw tubes for tracking and particle identification at the Large Hadron Collider. *Nucl. Instrum. Meth.*, A845:257–261, 2017. 15

[29] E. Aad et al. Readiness of the ATLAS Liquid Argon Calorimeter for LHC Collisions. *Eur. Phys. J. C*, 70(arXiv:0912.2642. CERN-PH-EP-2010-041):723–753. 31 p, May 2010. Comments: 31 pages, 34 figures, accepted in EPJC. 16

[30] E. Aad et al. Readiness of the ATLAS Tile Calorimeter for LHC collisions. *Eur. Phys. J. C*, 70(arXiv:1007.5423. CERN-PH-EP-2010-024):1193–1236. 64 p, Jul 2010. Comments: Submitted for publication in EPJC. 16

[31] E. Aad et al. Commissioning of the ATLAS Muon Spectrometer with Cosmic Rays. *Eur. Phys. J. C*, 70(arXiv:1006.4384. CERN-PH-EP-2010-045):875–916. 58 p, Aug 2010. 17

[32] ATLAS Collaboration. ATLAS high-level trigger, data acquisition and controls: Technical Design Report. Technical report, CERN, 2003. 19, 20

[33] ATLAS Collaboration. *ATLAS Computing: Technical Design Report*. Technical Design Report ATLAS. CERN, Geneva, 2005. 20

[34] I. Bird et al. Update of the Computing Models of the WLCG and the LHC Experiments. Technical Report CERN-LHCC-2014-014. LCG-TDR-002, CERN, Apr 2014. 20

[35] K. Lantzsch et al. The ATLAS detector control system. *J. Phys.: Conf. Ser.*, 396:012028. 5 p, 2012. 22, 31

[36] S. Schlenker et al. The ATLAS Detector Control System. *Conf. Proc.*, C111010:MOBAUST02. 4 p, 2011. 22, 32, 111

[37] Alex Barriuso-Poy, H J Burckhart, and E Llobet-Valero. *Hierarchical Control of the ATLAS Experiment*. PhD thesis, Rovira i Virgili U., Tarragona, 2007. Presented on 14 May 2007. 22

[38] O. Beltramello, H. J. Burckhart, S. Franz, M. Jaekel, , G. Morpurgo, F. dos Santos Pedrosa, K. Pommes, and H. Sandaker. The Detector Safety System of the ATLAS experiment. *JINST*, 4:P09012, 2009. 22

[39] S. Schmeling. Common tools for large experiment controls: A common approach for deployment, maintenance, and support. *IEEE Trans. Nucl. Sci.*, 53:970–973. 4 p, 2006. 23, 24

[40] Siemens AG 1996-2017. Scada system simatic wincc open architecture. `http://w3.siemens.com/mcms/human-machine-interface/en/visualization-software/simatic-wincc-open-architecture/pages/default.aspx`. (Visited on 2017-03-20). 23

[41] Controller Area Network - Wikipedia page. `https://en.wikipedia.org/wiki/CAN_bus`. (Visited on 2017-03-20). 25

[42] OPC Foundation. OPC Foundation Webpage. `https://opcfoundation.org/`. (Visited on 2017-03-20). 26

[43] H. Boterenbrood. Elmb 128 software recources. `http://www.nikhef.nl/pub/departments/ct/po/html/ELMB/ELMBresources.html`. (Visited on 2017-03-20). 26

[44] F Varela-Rodriguez and H J Burckhart. *The Detector Control System of the ATLAS experiment at CERN: An application to the calibration of the modules of the Tile Hadron Calorimeter*. PhD thesis, Santiago de Compostela U., Geneva, 2002. Presented on 30 Apr 2002. 26

[45] C. Gaspar and B. Franek. Tools for the automation of large distributed control systems. *IEEE Trans. Nucl. Sci.*, 53:974–979, 2006. 28

[46] B. Franek and C. Gaspar. SMI++ object oriented framework used for automation and error recovery in the LHC experiments. *J. Phys.: Conf. Ser.*, 219:022031. 10 p, 2010. 28, 116, 118

[47] M. L. Valsan et al. Role based access control system in the ATLAS experiment. *J. Phys.: Conf. Ser.*, 331:022042, 2011. 31

[48] Distributed information management system webpage. `http://dim.web.cern.ch/dim/`. (Visited on 2017-03-20). 31

[49] LHC Data exchange protocol. `http://lhc-commissioning.web.cern.ch/lhc-commissioning/systems/data-exchange/data-exchange.htm`. (Visited on 2017-03-20). 33

[50] Personal communication with Jolanta Olszowska, the TRT DCS coordinator. 35

[51] M. Oclese. Specifications for the power supply system of the ID heaters. Technical report, CERN, 1997. 38

[52] D. Attree et al. The evaporative cooling system for the ATLAS inner detector. *JINST*, 3:P07003, 2008. 38, 41, 42, 111

[53] Personal communication with Prof. WÅĆadysÅĆaw DÄĚbrowski, TRT DCS coordinator. 40

[54] M. Battistin et al. The Thermosiphon Cooling System of the ATLAS Experiment at the CERN Large Hadron Collider. *Int. J. Chem. React. Eng.*, 13(4):511–521, 2015. 42, 64

[55] S. Stapnes and R. Hawkings. ID environmental gas engineering documents. `https://edms.cern.ch/document/249791/1`. (Visited on 2017-03-20). 43

[56] P. A. Coe, D. F. Howell, and R. B. Nickerson. Frequency scanning interferometry in ATLAS: Remote, multiple, simultaneous and precise distance measurements in a hostile environment. *Measur. Sci. Tech.*, 15:2175–2187, 2004. 43

[57] H. Sandaker. ID DCS - Environmental Sensors. `https://edms.cern.ch/document/696626/1`. (Visited on 2017-03-20). 44

[58] M. Alhroob et al. Custom real-time ultrasonic instrumentation for simultaneous mixture and flow analysis of binary gases in the CERN ATLAS experiment. *Nucl. Instrum. Meth.*, A845:273–277, 2017. 45, 72

[59] M. Alhroob et al. Custom real-time ultrasonic instrumentation for simultaneous mixture and flow analysis of binary gases in the CERN ATLAS experiment. *Nucl. Instrum. Meth.*, A845:273–277, 2017. 47, 71, 72, 73, 112, 113

[60] R. Schmidt. Introduction to Machine Protection. In *Proceedings, 2014 Joint International Accelerator School: Beam Loss and Accelerator Protection: Newport Beach, CA, USA, November 5-14, 2014*, pages 1–20, 2016. 47

[61] R. Schmidt and J. Wenninger. Machine Protection Issues and Strategies for the LHC. In *9th European Particle Accelerator Conference (EPAC 2004) Lucerne, Switzerland, July 5-9, 2004*, 2004. 48

[62] R. Schmidt. Machine Protection and Interlock Systems for Circular Machines - Example for LHC. In *Proceedings, 2014 Joint International Accelerator School: Beam Loss and Accelerator Protection: Newport Beach, CA, USA, November 5-14, 2014*, pages 319–341, 2016. 48

[63] D. Bocian. Accidental Beam Losses during Injection in the Interaction Region IRI. Technical Report LHC-PROJECT-NOTE-335, CERN, Geneva, Jan 2004. 48

[64] I. Dolenc-Kittelmann, V. Cindro, and M. Mikuz. *Development of Beam Conditions Monitor for the ATLAS experiment.* PhD thesis, Ljubljana U., Ljubljana, 2008. Presented 18 Sep 2008. 48, 49, 50, 51, 52, 112

[65] V. Cindro et al. The ATLAS beam conditions monitor. *JINST*, 3:P02004, 2008. 50

[66] A. Gorisek et al. ATLAS diamond beam condition monitor. *Nucl. Instrum. Meth.*, A572:67–69, 2007. 51

[67] B. Macek. *Measurement of Luminosity in ATLAS Spectrometer with Beam Conditions Monitor.* PhD thesis, Jozef Stefan Institute Slovenia, 2011. 51, 52, 77

[68] F. Anghinolfi, P. Jarron, A. N. Martemyanov, E. Usenko, H. Wenninger, M. C. S. Williams, and A. Zichichi. Nino: an ultra-fast and low-power front-end amplifier/discriminator {ASIC} designed for the multigap resistive plate chamber. *Nucl. Instrum. Meth.*, A533:183–187, 2004. 51

[69] I. Dawson and C. Buttar. The radiation environment in the ATLAS inner detector. *Nucl. Instrum. Meth.*, A453:461–467, 2000. 53

[70] S Baranov, M Bosman, I Dawson, V Hedberg, A Nisati, and M Shupe. Estimation of Radiation Background, Impact on Detectors, Activation and Shielding Optimization in ATLAS. Technical Report ATL-GEN-2005-001. ATL-COM-GEN-2005-001. CERN-ATL-GEN-2005-001, CERN, Geneva, Jan 2005. 53

[71] I. Mandic, V. Cindro, A. Gorisek, G. Kramberger, and M. Mikuz. Online integrating radiation monitoring system for the ATLAS detector at the Large Hadron Collider. *IEEE Trans. Nucl. Sci.*, 54:1143–1150, 2007. 53, 73

[72] J. Hartert et al. The atlas radiation dose measurement system and its extension to slhc experiments. 2008. 53

[73] P. Borgeaud et al. DMILL: A Mixed analog - digital radiation hard technology for high-energy physics electronics: Status report Project RD-29. 1993. 53

[74] M. Dentan et al. DMILL (Durci Mixte sur Isolant Logico-Lineaire): A mixed analog-digital radiation hard technology for high-energy physics electronics. *Nucl. Phys. Proc. Suppl.*, 32:530–534, 1998. 53

[75] G. Cranberger et al. Functional specification of atlas radiation monitor. `https://edms.cern.ch/document/498365/1.0`. (Visited on 2017-03-20). 54, 56, 112

[76] A. Holmes-Siedle and L. Adams. Radfet: A review of the use of metal-oxide-silicon devices as integrating dosimeters. *International Journal of Radiation*

Applications and Instrumentation. Part C. Radiation Physics and Chemistry, 28(2):235 – 244, 1986. 54

[77] G. Sarrabayrouse and V. Polischuk. {MOS} ionizing radiation dosimeters: from low to high dose measurement. *Radiation Physics and Chemistry*, 61(3 - 6):511 – 513, 2001. 8th International Symposium on Radiation Physics - {ISRP8}. 54

[78] Radiation Experiments and Monitors. Radiation Experiments and Monitors (REM) Webpage. `http://www.radfet.com`. (Visited on 2017-03-20). 54

[79] F. Ravotti, M. Glaser, and M. Moll. Sensor catalogue data compilation of solid-state sensors for radiation monitoring. Technical Report CERN-TS-Note-2005-002. TS-Note-2005-002, CERN, Geneva, May 2005. 55

[80] OSRAM Opto-Semiconductors. BPW34 photodiode datasheet. `http://www.osram-os.com`. (Visited on 2017-03-20). 55

[81] CiS Institut fur Mikrosensorik gGmbH, Erfurt, Germany. CiS Institut fur Mikrosensorik gGmbH Webpage. `http://www.cismst.de`. (Visited on 2017-03-20). 55

[82] I. Mandic. Radiation effects in the readout chip for the ATLAS semiconductor tracker. *IEEE Trans. Nucl. Sci.*, 49:2888–2894, 2002. 55

[83] L. Luisa. Description of the detector control system for the inner detector evaporative cooling. `https://edms.cern.ch/document/894453/1`. (Visited on 2017-03-20). 59

[84] S. Berry. Functional analysis for pixel & sct evaporative cooling system. Technical report, CERN, 2008. 59

[85] K. Folwer. Environmental control system. `https://twiki.cern.ch/twiki/bin/viewfile/Main/AtlasEdinburghGroup?rev=1;filename=ENV_Documentation.pdf`. (Visited on 2017-03-20). 65

[86] R. Bates et al. Implementation of ultrasonic sensing for high resolution measurement of binary gas mixture fractions. *Sensors*, 14(6):11260–11276, 2014. 71

[87] E. Lemmon, M. Huber, and M. McLinden. Refprop standard reference database 23. national institute of standards and technology. Technical report, NIST, 1997. 72

[88] J. Kuijt. `https://www.nikhef.nl/pub/departments/ct/po/html/ELMB/DAC10.pdf`. (Visited on 2017-03-20). 72

[89] G. Aad et al. Operation and performance of the ATLAS semiconductor tracker. *JINST*, 9:P08009, 2014. 75, 86, 91, 96, 113

[90] Iseg spezialelektronik gmg, hd-01454 radeberg/ot rossendorf germany. 74

[91] Power Supply FDR and tender documents. `https://edms.cern.ch/document/373595/1`, 2007. (Visited on 2017-03-20). 74

[92] content@ipv6.com. Udp protocol overview. `http://ipv6.com/articles/general/User-Datagram-Protocol.htm`. (Visited on 2017-03-20). 74

[93] B. Todd. *A beam interlock system for CERN high energy accelerators*. PhD thesis, Brunel U., 2006. 77

[94] D. Calcoen, S. Gabourin, and A. Siemko. CERN Beam Interlock Redundant Dump Trigger Module Performance during LHC Run 2. In *Proceedings, 7th International Particle Accelerator Conference (IPAC 2016): Busan, Korea, May 8-13, 2016*, page THPOY041, 2016. 77

[95] R. Alemany, M. Lamont, and K. Kostro. LHC-Experiments Handshake Protocol Over DIP. Technical report, CERN, Geneva, Feb 2011. (Visited on 2017-03-20). 79

[96] ATLAS Collaboration. Characterisation and mitigation of beam-induced backgrounds observed in the ATLAS detector during the 2011 proton-proton run. *JINST*, 8:P07004, 2013. 80

[97] ATLAS Collaboration. Beam-induced and cosmic-ray backgrounds observed in the ATLAS detector during the LHC 2012 proton-proton running period. *JINST*, 11(05):P05013, 2016. 81

[98] A. Gorisek et al. ATLAS diamond beam condition monitor. *Nucl. Instrum. Meth.*, A572:67–69, 2007. 83

[99] ATLAS Collaboration. The atlas luminosity public results run-1. `https://twiki.cern.ch/twiki/bin/view/AtlasPublic/LuminosityPublicResults`. (Visited on 2017-03-20). 84, 87, 88, 114

[100] ATLAS Collaboration. The atlas luminosity public results run-2. `https://twiki.cern.ch/twiki/bin/view/AtlasPublic/LuminosityPublicResultsRun2`. (Visited on 2017-03-20). 84, 88, 114

[101] ATLAS Collaboration. The atlas data quality public results run-2. `https://twiki.cern.ch/twiki/bin/view/AtlasPublic/RunStatsPublicResults`. (Visited on 2017-03-20). 85, 113

[102] C. Cuenca Almenar, A. Corso-Radu, H. Hadavand, Y. Ilchenko, S. Kolos, K. Slagle, and A. Taffard. ATLAS online data quality monitoring. *Nucl. Phys. Proc. Suppl.*, 215:304–306, 2011. 85

[103] J. Adelman et al. ATLAS offline data quality monitoring. *J. Phys.: Conf. Ser.*, 219:042018, 2010. 85

[104] S Kolos, A Corso-Radu, H Hadavand, M Hauschild, and R Kehoe. A software framework for data quality monitoring in atlas. *J. Phys.: Conf. Ser.*, 119:022033, 2008. 85

[105] A. Valassi et al. COOL, LCG conditions database for the LHC experiments: Development and deployment status. In *Proceedings, 2008 IEEE Nuclear Science Symposium, Medical Imaging Conference and 16th International Workshop on Room-Temperature Semiconductor X-Ray and Gamma-Ray*

Detectors (NSS/MIC 2008 / RTSD 2008): Dresden, Germany, October 19-25, 2008, pages 3021–3028, 2008. 86

[106] K. A. Kastanas, A. Lipniacka, H. Sandaker, and P. Wells. *Monitoring and Measurements with the ATLAS Inner Detector and Search for Supersymmetry using ATLAS data.* PhD thesis, Bergen U., Oct 2014. Presented 12 Dec 2014. 87, 113

[107] M. Lamont. Status of the LHC. *J. Phys.: Conf. Ser.*, 455:012001, 2013. 86

[108] ATLAS Collaboration. The atlas public event displays. `https://twiki.cern.ch/twiki/bin/view/AtlasPublic/EventDisplayRun2Physics`. (Visited on 2017-03-20). 88, 89, 114

[109] E. Stanecka. Performance and operation experience of the ATLAS Semiconductor Tracker and Pixel Detector at the LHC. *PoS*, Vertex2013:001, 2013. 88

[110] ATLAS Collaboration. Cosmics and calibration approved pixel plots. `https://twiki.cern.ch/twiki/bin/view/AtlasPublic/ApprovedPlotsPixel`, 2013. (Visited on 2017-03-20). 90, 114

[111] Didier Ferrere and ATLAS Collaboration. The Upgraded Pixel Detector of the ATLAS Experiment for Run-2. Feb 2016. 90

[112] ATLAS Collaboration. ATLAS Insertable B-Layer Technical Design Report Addendum. Technical Report CERN-LHCC-2012-009. ATLAS-TDR-19-ADD-1, CERN, May 2012. Addendum to CERN-LHCC-2010-013, ATLAS-TDR-019. 91

[113] ATLAS Collaboration. Ibl installation into the inner detector of the atlas experiment side c. `https://cds.cern.ch/record/1702006?ln=pl`. (Visited on 2017-03-20). 92, 114

[114] D. Robinson. ATLAS Tracker and Pixel Operational Experience. Technical Report ATL-INDET-PROC-2016-011, CERN, Geneva, Nov 2016. 93

[115] ATLAS Collaboration. Public sct plots for collision data. `https://twiki.cern.ch/twiki/bin/view/AtlasPublic/SCTPublicResults`. (Visited on 2017-03-20). 93, 94, 97, 98, 114, 115

[116] P. Nikiel, B. Farnham, V. Filimonov, and S. Schlenker. Generic OPC UA Server Framework. *J. Phys.: Conf. Ser.*, 664(8):082039, 2015. 94

[117] SYS TEC electronic GmbH, Heinsdorfergrund, Germany. Sys tec electronic gmbh webpage. `http://www.systec-electronic.com/en/products/industrial-communication/interfaces-and-gateways/usb-can-interface-usb-canmodul16Webpage`. (Visited on 2017-03-20). 94

[118] ATLAS Collaboration. Atlas run-2 detector status. `https://twiki.cern.ch/twiki/bin/view/AtlasPublic/ApprovedPlotsATLASDetector`. (Visited on 2017-03-20). 95

[119] I. Dawson. Radiation background simulation and verification at the LHC: Examples from the ATLAS experiment and its upgrades. *PoS*, Vertex2012:015, 2013. 96

[120] P. Malecki et al. Multiprocessor system controlling power supply distribution for the ATLAS SCT. In S. Claude, editor, *Tenth workshop on electronics for LHC and future experiments, Boston, USA, 13-17 Sep 2004: Proceedings*, pages 210–213. ACM Press, Sep 2004. 96

[121] A. Chilingarov. Temperature dependence of the current generated in si bulk. *JINST*, 8(10):P10003, 2013. 96

[122] M. Moll. *Radiation damage in silicon particle detectors: Microscopic defects and macroscopic properties*. PhD thesis, Hamburg U., 1999. 96

[123] O. Krasel. *Charge Collection in Irradiated Silicon-Detectors*. PhD thesis, Dortmund University, 2004. 96

[124] T. Cornelissen, M. Elsing, S. Fleischmann, W. Liebig, and E. Moyse. Concepts, Design and Implementation of the ATLAS New Tracking (NEWT). 2007. 98

[125] P. F. Akesson et al. ATLAS Tracking Event Data Model. Technical Report ATL-SOFT-PUB-2006-004. ATL-COM-SOFT-2006-005. CERN-ATL-COM-SOFT-2006-005, CERN, Geneva, Jul 2006. 99

[126] ATLAS Collaboration. Impact parameter resolution. `https://atlas.web.cern.ch/Atlas/GROUPS/PHYSICS/PLOTS/IDTR-2015-007/`. (Visited on 2017-03-20). 100, 101, 115

[127] G. Borissov, D. Casper, K. Grimm, S. Pagan Griso, L. Egholm Pedersen, K. Prokofiev, M. Rudolph, and A. Wharton. ATLAS strategy for primary vertex reconstruction during Run-2 of the LHC. *J. Phys. Conf. Ser.*, 664(7):072041, 2015. 100

[128] E. Bouhova-Thacker, T. Koffas, V. Kostyukhin, W. Liebig, M. Limper, G. Piacquadio, Kirill Prokofiev, C. Weiser, and A. Wildauer. A framework for vertex reconstruction in the ATLAS experiment at LHC. *J. Phys. Conf. Ser.*, 219:032019, 2010. 100

[129] G. Piacquadio, Kirill Prokofiev, and A. Wildauer. Primary vertex reconstruction in the ATLAS experiment at LHC. *J. Phys. Conf. Ser.*, 119:032033, 2008. 100

[130] M. Aaboud et al. Reconstruction of primary vertices at the ATLAS experiment in Run 1 proton-proton collisions at the LHC. 2016. 100

[131] R. Fruhwirth, W. Waltenberger, and P. Vanlaer. Adaptive vertex fitting. *J. Phys.*, G34:N343, 2007. 100

[132] R. Fruhwirth, W. Waltenberger, Kirill Prokofiev, T. Speer, and P. Vanlaer. New developments in vertex reconstruction for CMS. *Nucl. Instrum. Meth.*, A502:699–701, 2003. 101

[133] ATLAS Collaboration. Vertex reconstruction performance of the atlas detector at $\sqrt{s} = 13$ TeV. Technical Report ATL-PHYS-PUB-2015-026, CERN, Geneva, Jul 2015. 101

[134] ATLAS Collaboration. 2016 primary vertex performance plots. `https://atlas.web.cern.ch/Atlas/GROUPS/PHYSICS/PLOTS/IDTR-2016-007/`. (Visited on 2017-03-20). 102, 115

[135] ATLAS Collaboration. Studies of the ATLAS Inner Detector material using $\sqrt{s}$ =13 TeV *pp* collision data. Technical Report ATL-PHYS-PUB-2015-050, CERN, Geneva, Nov 2015. 102, 103, 115

[136] ATLAS Collaboration. Technical Design Report for the ATLAS ITk Strip Detector. Technical Report ATL-COM-UPGRADE-2017-006, CERN, Geneva, Mar 2017. 109